"A Gravimetric Study of Adsorption
on a Mixed Oxide Catalyst"

submitted by

Rajesh Thaker

for the degree of

Ph. D

at

The City University
Department of Industrial Chemistry

February 1982

Contents

Tables

Figures

Plates

Graphs

Dedication

To my family

Acknowledgements

I would like to thank the following people for their invaluable help, [redacted] (whose help in providing laboratory space enabled the completion of the project) and my typist [redacted].

In particular my thanks to Dr. J. Cartlidge who, as my supervisor, gave me every possible assistance.

Abstract

Adsorption studies were carried out in a gravimetric adsorption apparatus, a quartz spring balance being used instead of a more sensitive vacuum microbalance (due to lack of finance). This was connected to gas reservoirs and a vacuum pump. Low pressures (< 1torr) were indicated on Pirani and Penning vacu m gauges, higher pressures were measured on a silicone oil U-tube manometer.

To test the balance BET measurements using nitrogen were made on a Sn-Sb oxide catalyst and carbon-black powder. The physisorption study was satisfactory.

Chemisorption of propene, 1-butene and oxygen was studied on Sn-Sb oxide catalyst. The chemisorption work allowed the calculation of isosteric heats of adsorption from a Clapeyron-Clausius type of equation which were found to decrease in complex ways from 28.08, 95.09 and 66.65 kJ/mol to less than 1 kJ/mol for oxygen, propene and 1-butene respectively. Entropies of adsorption were also calculated and were found to vary in a complex fashion with coverage indicating the importance of lattice oxygen, surface complexes and the complex nature of the mechanism of adsorption.

Data was fitted to various models, the best fit being an empirically modified Langmuir isotherm to some of the olefin data. No satisfactory fit was attained with the oxygen data.

Notations

A, A_0	Constants	
B, b, b_1	Constants	
b	Langmuirs Constant	
C, C	Constants	
d	Molecular diameter	$\mathring{A}$
E	Potential energy	kJ mol^{-1}
E	Characteristic energy	kJ mol^{-1}
E_a	Activation energy	kJ mol^{-1}
G	Gibbs free energy	J
H	Enthalpy	J
h	Planck constant	6.626×10^{-34} Js
K, K_1	Constants	
K_e	Equilibrium constant	
k_0	Proportionality constant	
k	Boltzmann constant	1.381×10^{-23} JK^{-1}
L, N	Avogadro constant	6.023×10^{23} mol^{-1}
M	Molecular weight	g, Kg
m	Mass of a molecule	g
P	Pressure	
P_1	Pressure	cm. oil
P_2	Pressure	mm. Hg
P_3	Pressure	Atmos.
q_p	Heat of physisorption	kJ mol^{-1}
q_c	Heat of chemisorption	kJ mol^{-1}
q_{st}	Isosteric heat of adsorption	kJ mol^{-1}
q_d	Differential heat of adsorption	kJ mol^{-1}
R	Universal gas constant	8.314 J $K^{-1}mol^{-1}$
S	Specific surface area	m^2g^{-1}
S	Entropy	J K^{-1}

$\bar{s}_s$	Differential molar entropy	J $K^{-1}mol^{-1}$
s	Molar entropy	J $K^{-1}mol^{-1}$
U	Mean speed	m s^{-1}
U	Intrinsic energy	J
x	Mass adsorbed	g
x_m	Monolayer capacity	g
V	Volume	cm^3
Z	Modulus of rigidity	

Greek

η	Viscosity	$g^{-1}s^{-1}cm^{-1}$
Δ	Spring extension	cm
θ	Surface coverage	
λ	Mean free path	$\overset{o}{A}$
μ	Rate of condensation	molecules $cm^{-2}s^{-1}$
μ_x	Chemical potential	J mol^{-1}
ν	Rate of evaporation	molecules $cm^{-2}s^{-1}$
τ	Time	s^{-1}
χ	Site energy	J
σ	Cross-section of interaction	$\overset{o}{A}^2$
σ	Variance	
σ_e	Experimental variance	
α	Condensation coefficient	
Ω_v	Collision integral	

1. Introduction Section

1.0 General Introduction

In addition to using oil as an energy source its distillates, which consist mainly of hydrocarbons, are of great importance as starting materials in the petrochemical industry. The most important hydrocarbons used as starting materials are those containing one or more functional groups, which are used in the manufacture of plastics, synthetic fibres, dyestuffs and pharmaceuticals. Propene and isobutene are two such hydrocarbons leading to the production of such intermediates as acrylonitrile, acrolein, acrylic acid, propylene oxide and methacrolein.

One of the main keys to the production of starting materials for the petrochemical industry is oxidation, which may be carried out homogeneously or heterogeneously. However, the large variety of products is the main disadvantage of using homogeneous oxidation leading to complex seperation and purification stages. On the other hand heterogeneous oxidation of hydrocarbons is highly selective towards the desired products.

The most favoured catalyst systems for heterogeneous hydrocarbon oxidation are a) noble metals and b) metal oxides or mixtures of metal oxides.

Noble metals usually cause complete oxidation of hydrocarbons to carbon dioxide and water, an exception being silver which converts ethylene to ethylene oxide.

The limitations of partial hydrocarbon oxidation over noble metals led to the use of metal oxides - particularly of

transition metals, as single compounds or mixtures. Ethylene, for example, was oxidised to acetaldehyde and formaldehyde by chromium oxide and vanadium pentoxide, propene to acrolein by cuprous oxide, and more recently by a mixture of tin-antimony oxides, and iso-butene to methacrolein by bismuth-molybdate.

Despite extensive research, the intermediates involved in olefin oxidation over these oxide catalysts have not been positively identified. The precise nature of the active sites is not known and the relationship of catalyst structure with activity and selectivity is uncertain. Some of this uncertainty is due to the difficulty of comparing different studies because of the use of ill-defined catalysts or different catalytic systems[1,2].

In spite of a great number of experimental data from gas adsorption, good correlation between theory and experiment has not, in general, been found. This has led to questioning of the validity of the first generally accepted theory Langmuir's equation (for monolayer adsorption) and its extension the BET (for multilayer adsorption). Unfortunately, proposed extensions and new approaches frequently lead to equations that are so cumbersome and complicated that their use is restricted[3]. Due to these facts, sixty years after its appearance the Langmuir theory still appears to be the generally used and accepted theory of monolayer adsorption.

Research has been carried out in this laboratory on the kinetics of olefin oxidation over tin-antimony and bismuth-molybdate catalysts using solid-gas stirred reactors[4].

The line of the present study was designed to compliment the previous work.

1.1 Introduction

Adsorption is a process in which atoms or molecules of one material (the adsorbate) become attached to the surface of another (the adsorbent) or, in a more general sense, become concentrated at an interface. There are five types of interfaces: gas-solid, liquid-solid, gas-liquid, liquid-liquid and gas-gas. The main concern in the work to be described is the combination of gas and solid, which is common to many systems in heterogeneous catalysts.

1.1.1 Energetics of Adsorption

A number of quite different types of forces can be responsible for bonding the adsorbate to the adsorbent. In principle the forces are the same as those operating between two atoms or molecules. However, the theoretical treatment of adsorption in the present case is made more difficult by the adsorbent atom being incorporated in a solid.

The following forces may be identified:

(1) Dispersion forces[5], which originate through the rapidly changing electron density in one atom which induces a corresponding electrical moment in a near neighbour and so leads to attraction between the two atoms. The resultant force has a relatively long range, over five to six molecular diameters.

(2) The overlap or repulsion forces. They appear when the two atoms approach closely so that their electron charge

clouds cause a repulsive effect.

If the adsorbate and adsorbent are composed of non-polar molecules, then the above forces are the only ones which must be taken into account. If the molecules are polar there are other forces which have to be recognised.

(3) Dipole interactions. These forces occur whenever a polar adsorbate is adsorbed on a non-polar or polar adsorbent, e.g. an ionic solid, or whenever a non-polar adsorbate is adsorbed on a polar adsorbent.

(4) Valency forces, which like the repulsive forces, occur at sufficiently close distances. They are due to the transfer of electrons between the adsorbent and adsorbate, giving a chemical bond.

(5) Interaction forces between the atoms or molecules of the bound adsorbate themselves. These forces must be considered in both physisorption and chemisorption when the coverage of adsorbate on the adsorbent is such that the seperating distances between adsorbate molecules are small.

As previously stated physisorption is basically the combination of attractive and repulsive forces. Based on work by London[5], Kirkwood[6] and Muller[7], the Lennard-Jones expression may be used,

$$E = \frac{b_1}{r^{12}} - \frac{c}{r^6} \qquad (1.1)$$

where,

b_1 and c are constants

E - potential energy (kJ/mole)

r - distance between adsorbate and adsorbent.

A typical energy plot is given in Fig. 1.1 for the physisorption of a molecule S_2 on the surface of a solid A. The depth of the minimum represents the heat of adsorption(q_p).

The chemisorbed state is a much more complex situation. A simplified theoretical scheme is represented in Fig. 1.2. Curves (1) and (11) represent the potential curves for surface coverages θ of $\theta \to 0$ and $\theta = 0.8$ respectively. The potential energy curve (111) represents the physisorption of a gaseous molecule S_2. The heats of physisorption and chemisorption are q_p and q_c respectively. E_a represents the activation energy. Curves (1) and (11) represent the situations where θ is small; hence more active sites will be preferentially occupied, and high θ; where only the less active sites will be available, respectively.

As S_2 approaches the surface, it will be physisorbed with a heat of adsorption q_p. As the molecule nears the surface the energetics depart from curve (111) and follow curves (1) and (11). If the point of intersection of the chemisorption and physisorption curves is below the line of zero potential, then no activation energy is required for chemisorption. This is represented by point A in Fig. 1.2, for low surface coverages. If, however, the intersection is above the zero potential, as shown for high surface coverages, an activation energy is required for chemisorption to take place, E_a kJ/mole in the example. It should be noted that other simple schemes[8,9] exist, of which this is only one.

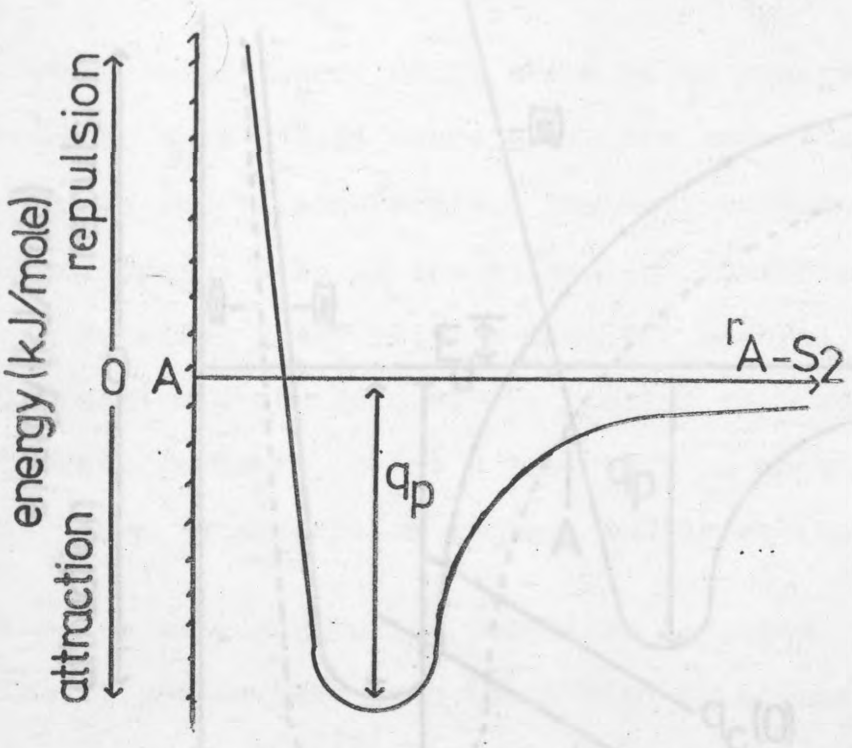

q_p - heat of adsorption

r_{A-S_2} - distance between adsorbent A and adsorbate S_2

Fig. 1.1

Energetics of physisorption

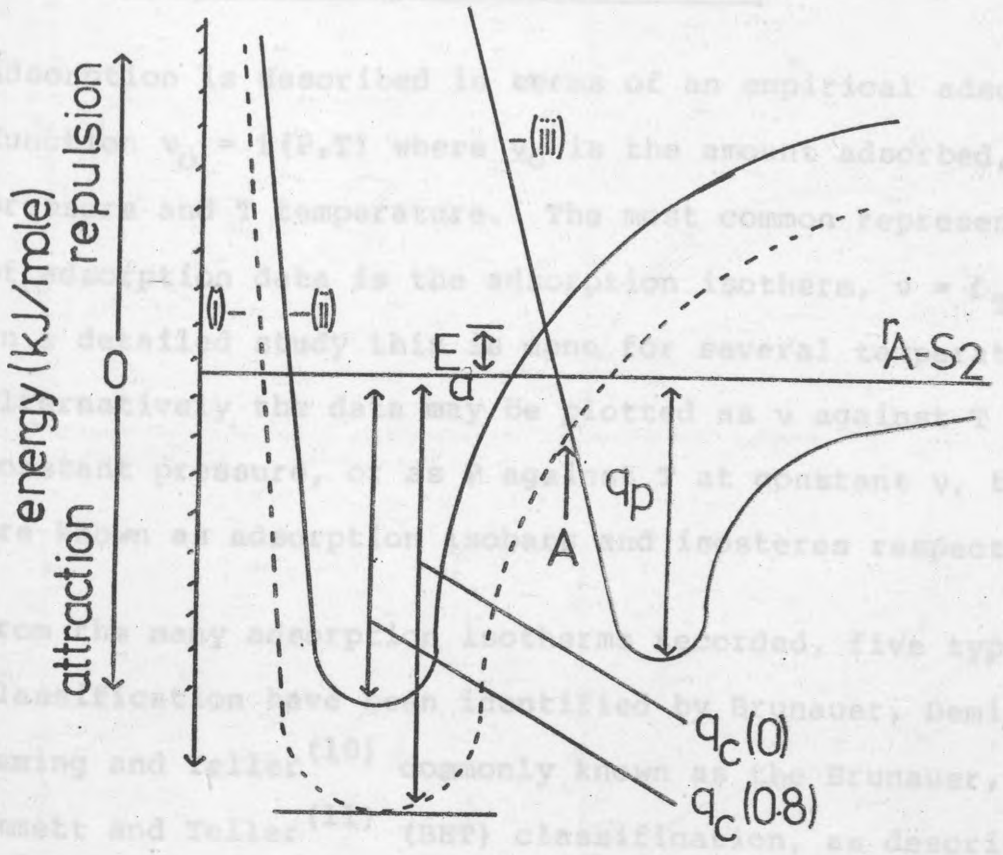

q_p - heat of physisorption

$q_c(0)$ - heat of chemisorption at zero coverage

$q_c(0.8)$ - heat of chemisorption at 0.8 coverage

E_a - activation energy

Fig.1.2

Energetics of chemisorption

1.1.2 Representation of Adsorption Data

Adsorption is described in terms of an empirical adsorption function $v_o = f(P,T)$ where v_o is the amount adsorbed, P pressure and T temperature. The most common representation of adsorption data is the adsorption isotherm, $v = f_T(P)$; in a detailed study this is done for several temperatures. Alternatively the data may be plotted as v against T at constant pressure, or as P against T at constant v, these are known as adsorption isobars and isosteres respectively.

From the many adsorption isotherms recorded, five types of classification have been identified by Brunauer, Deming, Deming and Teller[10] commonly known as the Brunauer, Emmett and Teller[11] (BET) classification, as described in Fig. 1.3.

The Type I isotherm indicates chemisorption, the others physisorption. Type IV shows a hysterisis loop where the desorption path is different to the adsorption path (due to e.g. capillary condensation). Other Types also show this effect. In general it is possible to use isotherms of Type II and IV to calculate the specific surface area of an adsorbent (see later) and Type IV to estimate pore size distribution, with Types III and IV neither of these estimates are possible.

It should be noted that the above is a generalisation and there are a number of isotherms which are either borderline cases or difficult to fit into the classification at all.

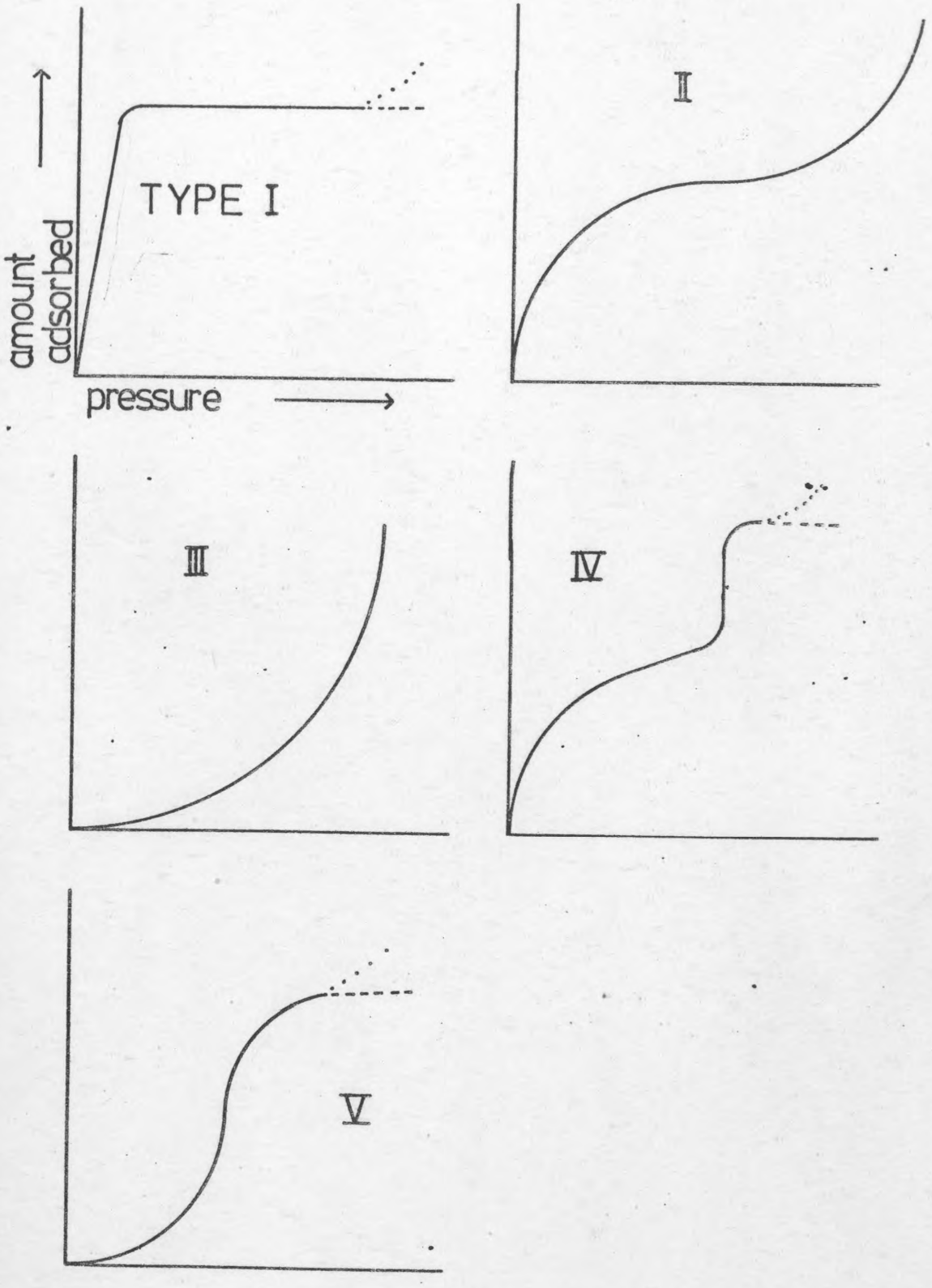

Fig.1.3

BET classification

1.1.3 Characteristics of Chemisorption

Chemisorption, as mentioned above, is said to describe a situation where the adsorbate-adsorbent bond approaches a chemical bond in strength. The distinction between physisorption and chemisorption is blurred and many principles of physisorption apply to chemisorption. However, there are a number of experimental criteria which help to distinguish between the two.

The best criterion is that of heat of adsorption (see later) which is much greater for chemisorption than for physisorption. The heat of physisorption being comparable to the heat of condensation. Adsorption work with carbon monoxide and hydrogen[11,12] seemed to support this, where the heats of chemisorption were found to exceed 80 and 60 kJ/mole respectively. The heats of physisorption were always less than 24 and 8 kJ/mole[13,14]. Although the distinction in general is valid, the opposite has also been found[15].

Chemisorption is more specific than physisorption. Chemisorption needs a clean surface but not all surfaces, even when clean can chemisorb. Physisorption takes place on all surfaces under the correct conditions of temperature and pressure.

Temperature range is another criterion that may be used to differentiate between physisorption and chemisorption. As physisorption and condensation are related, the former occurs only at temperatures near or below the boiling point of the adsorbate at the prevailing pressure. Chemisorption can usually take place at temperatures far above the boiling

point, however, as with heats of adsorption this is not always the case.

Chemisorption ceases when the adsorbate can no longer make direct contact with the surface, and therefore results in a monolayer, i.e. a Type I isotherm in Fig. 1.3. Physisorption has no such limitation and under suitable conditions of temperature and pressure may result in layers many molecules thick.

Finally being a chemical reaction, chemisorption may have an appreciable activation energy. If so, it will only proceed at a reasonable rate above a certain minimum temperature. Physisorption has no activation energy and so occurs rapidly at all temperatures below the boiling point of the adsorbate. Taylor[16] first suggested that chemisorption involved an activation energy and this has been used to interpret adsorptive and catalytic phenomena. Energies of activation have been calculated from rates of adsorption at different temperatures. In some cases, particularly on oxide surfaces, relatively high activation energies are found[4].

The activation energy needed for chemisorption explains a variety of observations. For example, heats of adsorption are frequently found to be small at low temperatures and large at higher ones. This is due to physisorption predominating at the lower temperatures where chemisorption is very slow. At higher temperatures, chemisorption predominates. Rates of adsorption have been found to decrease as the temperature was raised. At lower temperatures there was rapid physisorption while at higher

temperatures it was the slower chemisorption.

1.2 Isotherms

Research in adsorption has been guided by early work from Langmuir, Freundlich and Polanyi. (The latter will not be discussed as it deals exclusively with physisorption.)

The Langmuir equation is perhaps the most important single equation in the field of adsorption. Although other isotherms have been derived that fit experimental data and do not obey the Langmuir equation, invariably the basis of such isotherms is the Langmuir equation. The kinetic derivation is given below. However, other derivations have also been carried out, the thermodynamic derivation by Volmer[17] and the statistical derivation by Fowler[18].

1.2.1 Langmuir's Isotherm[19]

The collisions occurring between the molecules of the adsorbate and the surface of the adsorbent may be elastic or inelastic. Normally the collisions are inelastic and the molecules remain in contact with the surface for a certain period of time (very rarely are the collisions elastic), after which they return to the gas phase. This period according to Langmuir is responsible for adsorption; the period being short for physisorption and long for chemisorption.

If μ represents the rate of condensation of molecules on the surface and ν the rate of evaporation then the net rate of adsorption is

$$\frac{ds}{dt} = \alpha\mu - \nu \qquad (1.2)$$

where,

s - surface concentration (number of molecules adsorbed per unit area of surface)

α - condensation coefficient (ratio of molecules remaining on the surface to those striking the surface)

α is close to unity as elastic collisions are infrequent. At equilibrium $\frac{ds}{dt} = 0$ and $\alpha\mu = \nu$. From the kinetic theory of gases, μ for a unit area of surface is represented by (see Appendix X)

$$\mu = \frac{p}{(2\pi mkT)^{\frac{1}{2}}} \qquad (1.3)$$

where,

m - mass of molecule

k - Boltzmanns constant

T - absolute temperature

p - pressure

If q is the heat given out when a molecule is adsorbed from statistical considerations the number of molecules acquiring a quantity of energy equal to or greater than q will be proportional to $e^{-q/kT}$ consequently

$$\nu = k_0 e^{-q/kT} \qquad (1.4)$$

where,

k_0 - proportionality constant

It is now possible using Langmuir's assumptions to derive the explicit form of $\alpha\mu = \nu$.

α, μ and ν are functions of p, T and s. θ is now used in

place of surface concentration

$$\theta = \frac{s}{s_1} \qquad (1.5)$$

where,

s_1 - surface concentration to complete a monolayer

Langmuir introduced two assumptions into his derivation. The first is that the probability of evaporation of a molecule from the surface is the same whether neighbouring positions on the surface are occupied or not, implying that the forces of interaction between the adsorbed molecules are negligible. The expression to describe this situation is

$$\nu = \nu_1\theta \qquad (1.6)$$

where,

ν_1 = rate of evaporation from a completely covered surface

The above equation also implies a uniform heat of adsorption over the entire surface, i.e. a homogeneous surface.

The second simplifying assumption is that only those molecules that strike the bare surface will condense, this is expressed as

$$\alpha\mu = \alpha_0(1 - \theta)\mu \qquad (1.7)$$

where,

α_0 - condensation coefficient on the bare surface

$1 - \theta$ - fraction of the surface that is bare

The value of α_0 is always close to unity. Substituting (1.7) and (1.6) into $\alpha\mu - \nu$ and solving for θ, the Langmuir isotherm equation is produced

$$\theta = \frac{\alpha_0/\nu_1 \cdot \mu}{1 + \alpha_0/\nu_1 \cdot \mu} \qquad (1.8)$$

This is more commonly written as

$$\theta = \frac{bp}{1 + bp} \qquad (1.9)$$

where,

b - adsorption coefficient (function of temperature only)

The value of b can be obtained by manipulation of (1.2), (1.3), (1.7), (1.8) and $\alpha\mu = \nu$ and is found to be

$$b = \frac{\alpha_0 \, e^{q/kT}}{k_0 (2\pi mkT)^{\frac{1}{2}}} \qquad (1.10)$$

The Langmuir isotherm equation for single site adsorption may be linearized as:

$$p/\theta = 1/b + p \qquad (1.11)$$

This should have unit slope at all temperatures.

Alternatively, the Langmuir equation may be expressed as

$$\theta = bp(1 - \theta) \qquad (1.12)$$

Taking logarithems and transposing

$$\ln \theta/p = \ln b + \ln(1 - \theta) \qquad (1.13)$$

since $(1 - \theta) < 1$

$$\ln(1-\theta) = -(\theta + \tfrac{1}{2}\theta^2 + 1/3\theta^3 \ldots.) \qquad (1.14)$$

This simplifies to $\ln(1 - \theta) = -\theta$ except when $\theta \to 1$, consequently (1.13) simplifies to

$$\ln \theta/p = \ln b - \theta \qquad (1.15)$$

Data which fits the Langmuir equation should give a linear relationship between θ/p and θ.

θ may not always be known and may be replaced by x/x_m or v/v_m where x represents the mass adsorbed and x_m the mass of a monolayer and v represents the volumetric equivalents.

Hence, if x/x_m is substituted for θ in equation (1.11) we have the following relationship

$$p/x = 1/b.x_m + \frac{1}{x_m} p \qquad (1.16)$$

which should still be linear for p/x v p.

The simple Langmuir isotherm gives two limiting types of behaviour. At very low pressures where $bp \ll 1$ the isotherm reduces to $\theta = bp$, whilst at high pressures, where $bp \gg 1$, $\theta \rightarrow 1$.

The basic assumptions made during the derivation of the Langmuir isotherm and then to its extension in the BET model (see later) are open to criticism[8,20].

The model assumes that the surface is energetically uniform i.e. that all adsorption sites are exactly equivalent, but there is much evidence (e.g. from variation of heat of adsorption with coverage) that the surface of most solids

is energetically heterogeneous.

A further criticism of the model is that it neglects "horizontal" interactions between the molecules of the adsorbed layer. The horizontal forces between the adsorbate molecules cannot remain negligible because at higher coverages the average seperation is much less than a single molecular diameter.

It should be emphasized, however, that a fit to the algebraic form of the Langmuir isotherm may be fortuitous. The heat of adsorption may be found to be independent of surface coverage due to the internal compensation of several opposing effects, such as attractive lateral interaction (leading to an increase in the heat of adsorption with coverage) and surface non-uniformity (leading to a decrease of heat of adsorption with coverage).

The isotherm derived thermodynamically by William[21] and kinetically by Henry[22] is based on the Langmuir model, modified by the stipulation that each adsorbed molecule occupies n adjacent sites. The rate at which molecules are adsorbed is now $\alpha\mu(1 - \theta)^n$. Linearizing by taking logarithems leads to the Williams-Henry isotherm

$$\ln {}^{\nu}/p = \ln \nu_m\, b - {}^{n\nu}/\nu_m \qquad (1.17)$$

If on adsorption each molecule dissociates into two atoms (or ions) and each atom or ion occupies one site, e.g. O_2, the isotherm equation becomes

$$\theta = \frac{bp^{\frac{1}{2}}}{1 + bp^{\frac{1}{2}}} \qquad (1.18)$$

The more general equation

$$\theta = \frac{bp^{1/n}}{1 + bp^{1/n}} \qquad (1.19)$$

has been derived[23]. It reduces to the Freundlich isotherm at low pressures and gives the Langmuir plateau at high pressures.

Another empirical relationship showing these properties is

$$\theta = \left(\frac{bp}{1 + bp}\right)^{1/n} \qquad (1.20)$$

1.2.2 Adsorption with Lateral Interaction

The model is an ideal localized monolayer with the further assumption that each adsorbed molecule interacts with its nearest neighbours. The total energy of interaction can be expressed as the sum of the contributions of nearest neighbour pairs. Each site has Z nearest neighbour sites and the interaction of Z adsorbed molecules on nearest neighbour sites is V.

The problem is most simply treated using the Bragg-Williams approximation[24], in which the distribution of adsorbed molecules is assumed to be random. In other words lateral interaction is neglected for the purpose of computing the number of nearest neighbour pairs, this result then being used to calculate the total interaction energy. Rushbrooke[25] then derived thermodynamically

$$bp = \frac{\theta}{1 - \theta} e^{\theta ZV/kT} \qquad (1.21)$$

1.2.3 Adsorption on Non-Uniform Surfaces

The idea of irregularities being a general property of solid surfaces has long existed. The surface of a real solid is liable to contain various kinds of imperfections which will make it energetically heterogeneous. These include cleavage steps, dislocations and point defects.

The existence of cleavage steps has been shown by the electron microscope and is illustrated in Fig. 1.4. The step heights such as h_1 and h_2 may vary from one to hundreds of atomic diameters.

The dislocation is also an important surface imperfection shown by the electron microscope and illustrated in Fig. 1.6. A dislocation is a region of misfit of atomic dimensions within the crystal. The two important dislocations are the edge and screw dislocations (see diagram).

Finally, there are the point defects, as illustrated in Fig. 1.5. A point defect may be a vacancy where one or more ions are missing completely. An interstitial defect which is an ion, normally a cation, in an interstitial position rather than in the lattice. An impurity defect where an ion has been replaced by a foreign ion.

In addition to this general non-ideality of surfaces, many consist of more than one crystal face. Even on a perfect crystal the adsorption potential on an edge or corner is different from that on the main surface[19]. A further complication arises if the properties of the solid surface change with time.

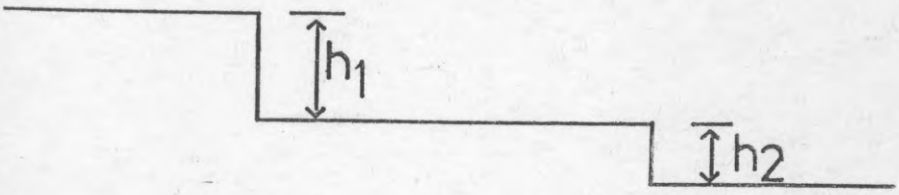

Fig.1.4

Representation of cleavage steps on the surface of a solid

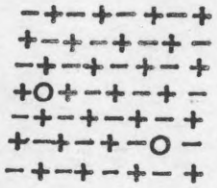

a) Vacancies
(Schottky defects)

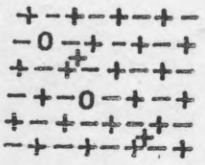

b) Displacement to interstitial sites
(Frenkel defects)

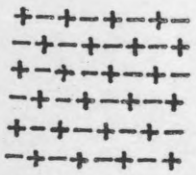

c) Ideal crystal

o - vacancy

Fig.15 Point defects

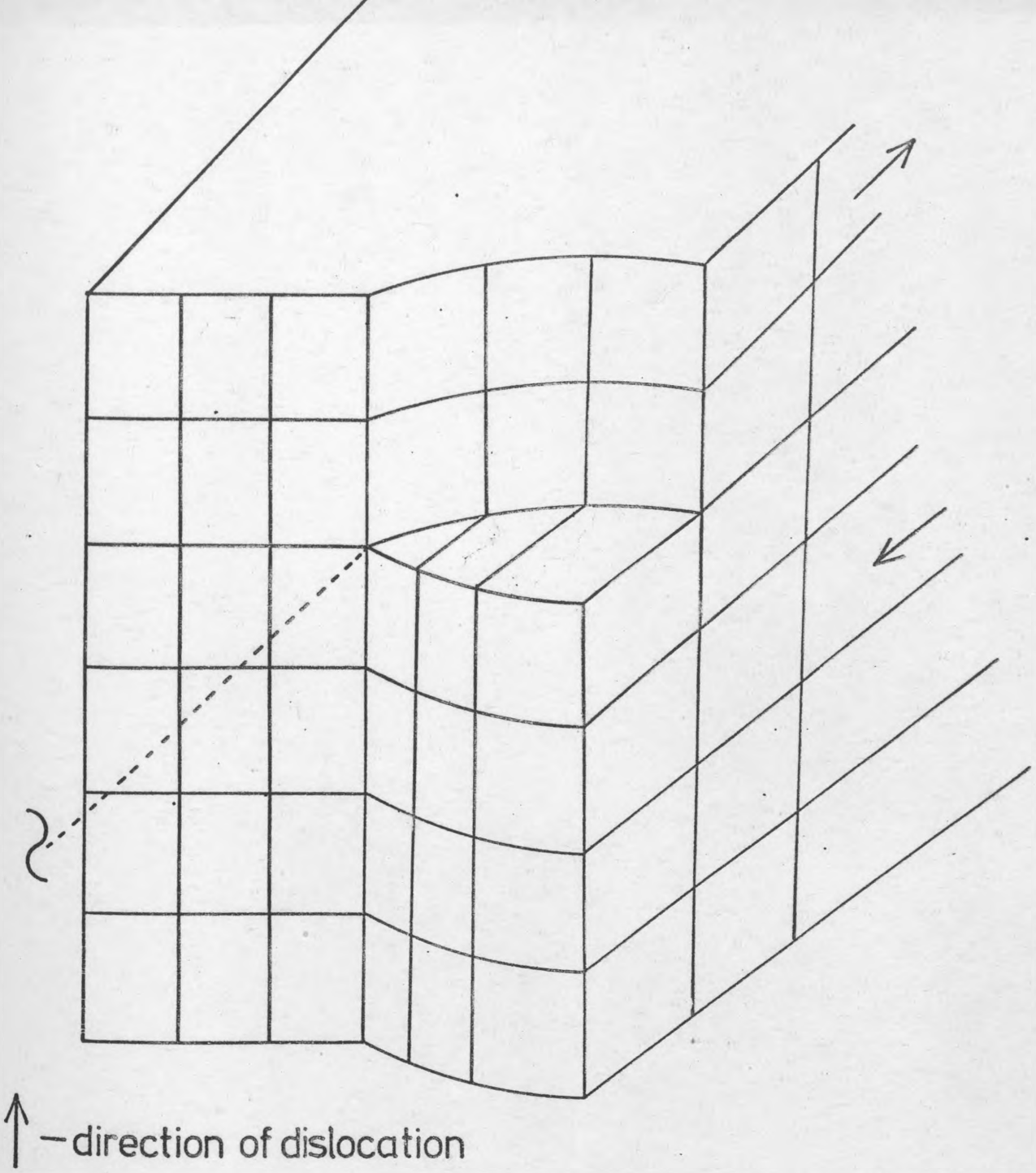

Fig. 1.6

Screw dislocation

One of the earliest attempts to formulate a theory of adsorption on a non-uniform surface was due to Langmuir[19] (see earlier), who suggested the extension of the simple adsorption isotherm to polycrystalline and amorphous surfaces. In the former case, the surface was assumed to be composed of a finite number of patches of sites with equal energy, the isotherm being

$$\nu = \sum \frac{\nu_{mi}\ b_i\ p}{1 + b_i\ p} \qquad (1.22)$$

where,

i indicates the i^{th} patch .

For the latter case the summation may be replaced by an integral.

Frumkin and Slyqin[26,27] assumed a linear decrease between site energies and represented this by replacing q, the heat of adsorption in the Langmuir equation by $q_0(1 - \alpha_0\Theta)$, leading to an equation of the form

$$\Theta = \frac{RT}{q\alpha_0} \ln A_0 p \qquad (1.23)$$

A_0, α_0 being constants.

In 1938 Cremer and Flugge[28] pointed out that at low pressure since the Langmuir isotherm reduces to Henry's Law the isotherm being linearized by taking logs of both sides giving unit slope. Deviation from the theoretically expected slope can be explained on the assumption that adsorption takes place on sites of progressively decreasing activity.

An approximate method for deriving the adsorption isotherm from the distribution function and vice-versa, making use

of Langmuir's isotherm, has been given by Roginskii[29-31]. The simple distribution

$$N_\chi = K_1(\chi_{max} - \chi)^\beta \, \partial\chi \qquad (1.24)$$

where,

N_χ - number of sites with energy between χ and $\chi + \partial\chi$

K_1, β - constants

was shown to lead to the isotherm

$$\ln \nu \cong (\beta + 1) \ln \ln P + C \qquad (1.25)$$

where,

c - constant

If β has a value of zero then (1.25) simplifies to

$$\nu \cong A \ln P \qquad (1.26)$$

which is comparable to the Temkin equation. If the experimental distrubition is assumed

$$N_\chi = K \, e^{-\alpha\chi} \partial\chi \qquad (1.27)$$

it leads to the Freundlich isotherm

$$\nu = Bp^{1/n} \qquad (1.28)$$

The first rigorous treatment of adsorption on a non-uniform surface was made by Halsey and Taylor[32]. The fractional coverage of sites having energy χ is given by the Langmuir equation as

$$\theta_\chi = \left(\frac{a}{p} \cdot e^{-\chi/kT} + 1 \right)^{-1} \qquad (1.29)$$

The total surface coverage, assuming a continuous range of χ values, may be written as

$$\theta = \int_{-\infty}^{\infty} \frac{N_\chi \partial\chi}{\frac{a}{p} \cdot e^{-\chi/kT} + 1} \qquad (1.30)$$

where N_χ is the distribution function usually normalized to

$$\int N_\chi \partial\chi = 1 \qquad (1.31)$$

Two distributions are considered

i) N_χ = constant (1.32)

This corresponds to the assumption of an adsorbing surface consisting of a number of uniform (i.e. Langmuir) patches of equal area. The solution, which is made possible by the further assumptions that at low coverage the least active sites are bare, and at high pressure the most active sites are covered, takes the form

$$\ln p = \frac{1-\theta}{mkT} + \ln p_0 \qquad (1.33)$$

where,

$p_0 = ae^{-\chi/kT}$

m - constant

ii) Assuming an exponential distribution

$$N_\chi = Ce^{-\chi/\chi_m} \qquad (1.34)$$

and integrating (1.30) from $-\infty$ to $+\infty$ Halsey and Taylor arrived at an equation, identical in form with the Freundlich isotherm

$$\ln \theta = \frac{kT}{\chi_m} \ln p + \text{constant} \qquad (1.35)$$

where χ_m is a constant at a constant temperature T.

The treatment due to Sips[33,34] is essentially the reverse of that of Halsey and Taylor. He considered a combination of the Langmuir and Freundlich isotherms

$$\theta = \frac{Ap^{1/n}}{1 + Ap^{1/n}} \qquad (1.36)$$

which has the proper limits for monolayer adsorption, yet reduces to $\theta = Ap^{1/n}$ at low pressure.

Adsorption with lateral interaction on a heterogeneous surface on which sites of equal energy are grouped in patches has been examined by Halsey[35]. On such patches co-operative adsorption takes place. Two-dimensional condensation will begin at

$$P/P_0 = e^{-\Delta q/RT} \qquad (1.37)$$

If the surface is characterized by a distribution function of co-operative adsorption energies $N_{\Delta q}$, the isotherm is given by

$$\theta = \int_{\Delta q}^{\infty} N_{\Delta q} dq = \int_{-RT\ln P/P0}^{\infty} N_{\Delta q} dq \qquad (1.38)$$

The use of an exponential distribution of the form

$$N_{\Delta q} = Ce^{(-\Delta q/\Delta q_m)} \qquad (1.39)$$

leads to the co-operative analogue of the Freundlich isotherm

$$\theta = C'(P/P_0)^{RT/\Delta q_m} \qquad (1.40)$$

A more recent modification of the Langmuir model is that carried out by Jovanovic[36,37]. The principle innovation in Jovanovic's approach is the attempt at a detailed consideration of collisions between the bulk gas phase molecules and the molecules in the process of desorbing from the surface. The equation derived by Jovanovic for monolayer coverage was as follows

$$\theta = 1 - \exp(-ax) \qquad (1.41)$$

where

$$a = \frac{\sigma \tau p_0}{(2\pi mkT)^{\frac{1}{2}}} \qquad (1.42)$$

x - relative equilibrium pressure

τ - average time spent on the surface by a molecule

σ - cross-section of interaction

m - mass of a molecule

k - Boltzmanns Constant

A simpler derivation than the original is given by Budrugeac[38]. Misra[39] has generated both the Jovanovic and Langmuir isotherms by integrating the differential equation $\frac{d\theta}{dp} = C(1-\theta)^K$, C and K being constants for K = 1 and 2 respectively. However, no models, kinetic or statistical, have yet been found for isotherms with K values other than 1 or 2.

1.2.4 General Equation of Adsorption

Attempts have been made to determine the energy distribution from experimental data, the form of the energy distribution depending on the choice of local isotherm. However, it has been shown[40] that various local isotherms with corresponding distribution functions fit the data equally well, consequently it is not possible to identify the true local isotherm as well as the true energy distribution. What is in fact required is a general adsorption equation, over all pressures. Such an equation would give standard parameters which could be used to characterise adsorption systems.

Such an equation has been put forward[3,41] and is known as the Maxwell-Boltzmann-Langmuir (MBL) isotherm. The starting

point is the definition of two functions, they are:

i) The function between the adsorption energy and the number of sites possessing the given adsorption energy,

ii) The function between the fraction of sites of a given energy covered by adsorbate and the bulk phase concentration of the adsorbate.

The above may be generalised by the following equation

$$\theta(p, T) = \int_{B_{min}}^{B_{max}} \theta_L(p, T)\, f(q)dq \qquad (1.43)$$

where

$\theta_L(p, T)$ - local isotherm

$f(q)$ - distribution function

The isotherm is based on the Maxwell-Boltzmann distribution (usually found in descriptions of molecular velocities and kinetic energies) of site energies combined with the Langmuir local isotherm to give the following expression

$$\theta = \frac{2}{\sqrt{\pi}(RT_f)^{3/2}} \int_0^{\infty} \frac{(q)^{\frac{1}{2}} \exp(-q/RT_f)dq}{1 + (\frac{LRT}{p})\exp(-q/RT)} \qquad (1.44)$$

where,

T_f - frozen temperature (the heterogeneity parameter)

L - related to the Langmuir constant

by $L \exp(-q/RT) = (K_L)^{-1}$

However, though good correlation was found between theory and experiment at low pressures, at ultra high vacuums the predicted and actual did not agree. The equation (1.44) was thus modified by using the following argument. The integration interval $(0, \infty)$ is not physically correct since the true distribution of adsorption energies must cover some finite interval with an upper limit q_{max}. Equation

(1.44) works when the region of the integral from q_{max} to infinity is negligible in relation to the interval from zero to q_{max} (the region of moderate adsorbate pressures). The lower the adsorbate pressure the greater the adsorption on highly energetic patches of the surface. Hence, the relative importance of the interval from q_{max} to infinity is greater under these conditions and must be taken into account in the formulation. The modified form is now[42]

$$\theta = \frac{1}{\mu}\int_{o}^{q_{max}} \frac{q^{\frac{1}{2}}\exp^{(-q/RT_f)}}{1 + \frac{LRT}{p}\exp(^{-q}/RT)}\, dq \qquad (1.45)$$

where,

$$\mu = \frac{\pi^{\frac{1}{2}}\,(RT_f)^{3/2}}{2}\left(1 - \exp(^{-q_{max}}/_{RT_f})\right)$$

Recent studies have extended the above to multilayer adsorption[42].

Much work has been done in deriving equations to describe multilayer adsorption (physisorption). The only relevant multilayer adsorption equation is the Brunauer, Emmet and Teller[43] (BET) extension of the Langmuir isotherm, the theory of which follows. This extension when used in conjunction with (1.46) enables the specific surface area of a sample to be estimated.

$$S = \frac{x_m.N.\,A_m}{M} \times 10^{-20} \qquad (1.46)$$

where,

S - surface area (m^2g^{-1})

x_m - monolayer capacity (g-adsorbate per g-adsorbent)

A_m - area occupied by molecule of adsorbate ($\mathring{A}^2$)

N - Avogadros number

1.2.5 Brunauer, Emmet and Teller (BET) Equation

The assumptions made in the BET approach are:-

(i) Localised adsorption, i.e. adsorption occurs at fixed sites on the surface, so that, as in the Langmuir approach, lateral interactions are ignored.

(ii) Adsorption onto a higher layer can only occur on a molecule already adsorbed.

(iii) Surface homogeneity.

Brunauer, Emmet and Teller approached the problem kinetically, extending Langmuirs equation to multilayer adsorption, within each layer of which dynamic equilibrium is assumed to occur.

Let S_o', S_1' .... S_i' be the areas of the surface covered by 0, 1 .....i layers of molecules. Then the total surface area SA is given by

$$SA = \sum_{0}^{i} Si \qquad (1.47)$$

The total volume of adsorbate will be

$$V = t \sum_{0}^{i} iS_i \qquad (1.48)$$

where,

t - monolayer thickness

But the monolayer volume $V_m = t(SA)$, therefore

$$\theta = \frac{V}{Vm} = \frac{\sum_{o}^{i} i S_i'}{\sum_{o}^{i} S_i'} \qquad (1.49)$$

Since there is an equilibrium, the rate of condensation on the bare surface must be equal to the rate of evaporation from the first layer, that is

$$a_1 \, p \, s_o' = b_1 \, s_1' \, e^{-q_1/RT} \qquad (1.50)$$

where,

a_1, b_1 - constants

q_1 - heat of desorption of the first layer

This is essentially the Langmuir equation for unimolecular coverage. For the second layer we have

$$a_2 . p . s_1' = b_2 . s_2' . e^{-q_2/RT} \qquad (1.51)$$

Consequently for the i^{th} layer

$$a_i . p . s_{i-1}' = b_i . s_i' . e^{-q_i/RT} \qquad (1.52)$$

Further simplifying assumptions now have to be made

(i) The ratio a_i/b_i is taken as constant for all layers after the first

(ii) The energy q_1 is assumed to be equal to $-\Delta H_{ads}$. The second and subsequent layers are considered to be adsorbed with an energy equal to the latent heat of condensation q_L of the bulk adsorbate.

(1.52) now becomes

$$S_i' = x . S_{i-1}' \qquad (1.53)$$

where,

$$x = \frac{a_i}{b_i} . p . e^{q_L/RT} \qquad (1.54)$$

This does not hold for i=1, in this case the relationship

will be

$$S_1' = \frac{a_1}{b_1}.p.e^{q_1/RT}.S_o' \qquad (1.55)$$

or

$$S_1' = YS_o' \qquad (1.56)$$

where,

$$Y = \frac{a_1}{b_1}.p.e^{q_1/RT} \qquad (1.57)$$

From (1.48) we have

$$S_{i-1}' = xS_{i-2}' \qquad (1.58)$$

In general

$$S_i' = xS_{i-1}' = x^2S_{i-2}' \ldots = x^{i-1}S_1' \qquad (1.59)$$

or

$$S_i' = c.x^iS_o' \qquad (1.60)$$

where,

$$c = Y/x \qquad (1.61)$$

Substituting (1.61) into (1.49) we have

$$\frac{V}{Vm} = \frac{c \sum_{i=1}^{i=\infty} ix^i}{1 + c \sum_{i=1}^{i=\infty} x^i} \qquad (1.62)$$

The summation represented by the denominator is the sum of an infinite geometric progression and is equal to $\frac{x}{1-x}$. The summation of the numerator may be represented as

$$\sum_{i=1}^{i=\infty} ix^i = x \frac{d}{dx} \sum_{i=1}^{i=\infty} x^i = \frac{x}{(1-x)^2} \qquad (1.63)$$

Substituting into (1.62) and rearranging

$$\frac{V}{Vm} = \frac{cx}{(1-x)(1-x+cx)} \qquad (1.64)$$

If the adsorption takes place on a free surface then at p_o, the saturation pressure of the adsorbate, an infinite

number of layers can build up on the adsorbent. Hence for $V = \infty$ when $p = p_o$, x must be equal to unity in (1.64). From (1.54)

$$\frac{a_i}{b_i}.p_o.e^{q_L/RT} = 1 \qquad (1.65)$$

It follows that $x = {}^{p}/_{p_o}$. Substituting into (1.64) and by manipulation the BET isotherm is obtained as a linear equation

$$\frac{p}{V(p_o-p)} = \frac{1}{V_m c} + \frac{c-1}{V_m c}.{}^{p}/_{p_o} \qquad (1.66)$$

This is the most commonly used form of the BET equation. ${}^{p}/_{V(p_o-p)}$ against ${}^{p}/_{p_o}$ should be linear with a slope $S = \frac{c-1}{V_m c}$ and intercept $i = \frac{1}{x_m c}$. The solution of the two simultaneous equations leads to $x_m = \frac{1}{S+i}$, which in conjunction with (1.46) leads to the evaluation of the specific surface area of the sample.

While the BET model is still the most often used in the field of multilayer physisorption, it is open to criticism [20], and refinements have been undertaken by Huttig and Frankel-Halsey-Hill to name but a few.

1.2.6 Freundlich Isotherm

The Freundlich isotherm [44] is described by the equation

$$V = Kp^{1/n} \qquad (1.67)$$

where,

V - volume adsorbate

p - pressure of gas

K,n - constants (n>1)

It deals most successfully with adsorption at intermediate pressures.

Although initially an empirical relationship, it may be derived theoretically[45-47] if certain assumptions are made concerning the nature of the surface and the mechanism of adsorption.

Data which fits should give a linear relationship between ln V and ln p.

1.3 Thermodynamic and Kinetic Considerations

1.3.1 Heats of Adsorption (Appendix IX)

When a Clasius-Clapeyron type of equation is applied to a set of isotherms at a fixed coverage, isosteric heats of adsorption (q_{st}) are obtained. If the heats of adsorption are measured isothermally at particular θ values, in such a way that no external work is done during adsorption, the differential heat of adsorption (q_d) is obtained. It is possible to show, by the use of thermodynamics that $q_{st} = q_d + RT$.

It is uncertain which heat is measured in a calorimeter (the most commonly used method for measuring heats of adsorption) when small quantities of gas are admitted and adsorbed. In such an experiment, external work is done, but it is not certain how much of this work is transferred to the calorimeter as heat. If none is transferred, q_d is obtained, while if all is transferred, q_{st} is obtained. It is very likely that in practice the "calorimetric differential heat" is intermediate between q_{st} and q_d.

Strictly, when comparing heats of adsorption q_{st} should be used because there is no possible variation of these owing

to differences in technique of measurement, as there may be with calorimetric heats. However, with chemisorption the maximum possible error in comparing the two heats of adsorption, namely RT, is less than the normal error of measurement and for most purposes it is possible to neglect the difference between the two heats of adsorption.

Strictly speaking the derivation of the Clapeyron-Clausius equation is not wholly valid for adsorption. A sounder theoretical treatment, which in fact leads to a Clapeyron-Clausius type of equation, is via the Van't Hoff Isochore and is given below.

1.3.1.1 The Clapeyron-Clausius Equation Via the Van't Hoff Isochore

To find a relationship between pressure, temperature and heat of chemisorption start with:-

$$dG = Vdp - SdT \qquad (1.68)$$

from which the following relationships may be obtained

$$\left(\frac{\partial G}{\partial T}\right)_p = -S \qquad (1.69)$$

$$\left(\frac{\partial G}{\partial p}\right)_T = V \qquad (1.70)$$

from the basic definition of the Gibbs function we have the relationship

$$S = (H - G)/T \qquad (1.71)$$

Substituting into (1.69)

$$\left(\frac{\partial G}{\partial T}\right)_p = (G - H)/T \qquad (1.72)$$

Consider the equation

$$\left(\frac{\partial (G/T)}{\partial T}\right)_p = \frac{1}{T}\left(\frac{\partial G}{\partial T}\right)_p + G\left(\partial/\partial T\left(1/T\right)\right)_p$$

$$= \frac{1}{T}\left(\left(\frac{\partial G}{\partial T}\right)_p - \frac{G}{T}\right) \qquad (1.73)$$

Substituting (1.72) into (1.73) and rearranging, the following equation is obtained

$$\left(\frac{\partial (G/T)}{\partial T}\right)_p = -H/T^2 \qquad (1.74)$$

This is the Gibbs-Helmholtz equation which may be applied to a chemical reaction as described by,

initial state (reactants) → final state (products)

i.e. $\Delta G = G_f - G_i$

The Gibbs-Helmholtz equation applies to both G_f and G_i and can be written

$$\left(\frac{\partial (G_f/T - G_i/T)}{\partial T}\right)_p = -\left(\frac{H_f}{T^2} - \frac{H_i}{T^2}\right) \qquad (1.75)$$

or to simplify, at standard state

$$\left(\frac{\partial (\Delta G^\Theta/T)}{\partial T}\right)_p = -\frac{\Delta H^\Theta}{T^2} \qquad (1.76)$$

The relationship $\Delta G^\Theta = -RT\ln Ke$ may now be substituted into (1.76) where Ke is the equilibrium constant. (1.76) now becomes

$$d(\ln Ke) = \frac{\Delta H}{RT^2}.dT \qquad (1.77)$$

The reaction of interest is

$$A + B \underset{}{\overset{Ke}{\rightleftharpoons}} C$$

where,

A - adsorbent

B - adsorbate

C - adsorbed phase

$$Ke = \frac{\text{activity C}}{(\text{activity A})(\text{activity B})}$$

A and C are assumed to be solid, the activity thus becoming

unity. Assuming ideality activity B is replaced by its pressure. (At high pressures the fugacity should be used.) (1.77) now becomes

$$d(\ln p^{-1}) = \frac{\Delta H}{RT^2} dT \qquad (1.78)$$

integrating

$$\ln p = \frac{\Delta H}{RT} + \text{constant of integration} \qquad (1.79)$$

which is a Clapeyron-Clausius type relationship.

1.3.2 Entropies of Adsorption (Appendix VIII)

Three different entropies associated with an adsorbed layer may be distinguished

S_θ - total entropy of the adsorbed layer

s_θ - integral molar entropy

$\bar{s}_\theta$ - differential molar entropy

The relationship being as follows

$$S_\theta = (n_\theta) s_\theta \qquad (1.80)$$

$$\bar{s}_\theta = \left(\frac{\partial S_\theta}{\partial (n_\theta)}\right)_T = \left(\frac{\partial s_\theta}{\partial \theta}\right)_T + s_\theta \qquad (1.81)$$

where n_θ is the number of moles adsorbed at coverage θ.

The molar free energy change ΔG which occurs when an infinitesimal quantity of gas is transferred isothermally at T Kelvin from a reservoir at standard pressure to the adsorbed layer is given by

$$-\Delta G = -(H_g - \bar{H}_\theta) + T(s_g - \bar{s}_\theta) \qquad (1.82)$$

H_g and s_g are, respectively, the integral molar enthalpy and entropy of the gas at 1 atmosphere. $\bar{H}_\theta$ is the differential molar enthalpy of the adsorbed layer. $(H_g - \bar{H}_\theta) = q_{st}$, the isosteric heat of adsorption.

If the adsorbed layer is in equilibrium at a pressure P then, assuming ideal behaviour,

$$\Delta G = -RT\ln P$$

hence

$$\bar{s}_\theta = s_g - R\ln P - {}^{q_{st}}/_{T} \qquad (1.83)$$

If s_θ is required it can be obtained by an integration over all coverages from zero to θ

$$s_\theta = \frac{1}{\theta}\int_0^\theta \bar{s}_\theta d\theta \qquad (1.84)$$

The entropy of the gas[48] can be estimated from the following equation

$$\begin{aligned} s_g = &\text{(entropy due to translational motion) +} \\ &\text{(entropy due to vibrational motion) +} \\ &\text{(entropy due to electronic effect) +} \\ &\text{(entropy due to rotational effect)} \end{aligned} \qquad (1.85)$$

A further discussion is given in Appendix VI.

1.3.3 Kinetics

From general kinetic considerations the rate of impact of molecules on a surface is u (molecules impacted per unit area per second) may be written as follows

$$u = \frac{p}{(2\pi mkT)^{\frac{1}{2}}} \qquad (1.86)$$

S_T the sticking probability (defined as the fraction of these impacts resulting in adsorption) when substituted into (1.86) modifies it to

$$u = \frac{S_T p}{(2\pi mkT)^{\frac{1}{2}}} \qquad (1.87)$$

where u is now the molecules adsorbed per unit area per second.

S_T is rarely equal to unity and the following factors have an influence on lowering the value of S_T.

Activation energy; only those molecules possessing the required amount of energy will be chemisorbed.

Steric factor; even if the molecule possesses the required activation energy, the probability of adsorption may depend on which part of the molecule hits the surface.

If surface heterogeneity is assumed, then this implies a varying activity from site to site. Consequently the sticking probability must be some function of this variation and S_T may be written in the form

$$S_T = \alpha\, f(\theta) e^{-E_a/RT} \qquad (1.88)$$

Where α is the condensation coefficient and is the probability that a molecule will be adsorbed, provided it possesses the necessary activation energy E_a and collides with a vacant surface site, $f(\theta)$ is a function of the surface coverage θ and represents the probability of a collision taking place at an available site, consequently

$$u = \frac{\alpha(\theta)p}{(2\pi mkT)^{\frac{1}{2}}}\, f(\theta)\, e^{-E_a(\theta)/RT} \qquad (1.89)$$

The complexity of the equation is due to possible variations of α and E_a with θ, and $f(\theta)$ becoming complex due to e.g. adsorption with dissociation, etc.

Consequently if u and p can be measured the variation of S_T with θ may be studied or if S_T can be approximated and p measured then the variation of u with θ may be studied, the former is found to be easier.

Either of these studies will give the activation energy.

1.4 Catalysis[49]

Many chemical reactions that are carried out in the laboratory and most industrial chemical processes are catalytic. Due to the difficulty of discovering effective catalysts the fraction of the possible spontaneous reactions known is larger than the fraction of catalytic reactions.

Catalysis can be divided into three categories; homogeneous, heterogeneous and enzymic.

In homogeneous catalysis, all the reactants and the catalyst are dispersed as molecules in one phase. In heterogeneous catalysis, the catalyst constitutes a separate phase. Normally, the catalyst is a solid and the reactants and products are gases or liquids. The catalytic reaction occurs at the surface of the solid and in the absence of physical constraints the reaction rate is proportional to the area of the catalyst. Enzyme catalysts are macromolecules small enough to be molecularly dispersed with reactants and products in one phase, but large enough so that one may speak of active sites at the surface of the enzyme molecule.

1.4.1 Catalysts

Catalysts come in a variety of forms, e.g. wires, pellets and powders. In principle the catalytic activity should be proportional to the area of the catalyst (stated previously), thus it would seem logical to use as fine a powder as is

obtainable. However, the material would be unusable in flow reactors, as even at large pressure drops flow through a bed of such fine particles would be very slow. Even in a batch reactor, in spite of a reasonable reaction rate, the recovery of the catalyst may prove to be difficult. Another associated problem is that, in the bed of the flow reactor, such fine catalyst particles could adhere to each other and sinter with the subsequent loss of surface area.

A possible way round these problems is to deposit the catalyst on an inert porous support such as alumina or silica, the texture of which resembles a loose gravel bed. However, even doing this has its disadvantages as the rates of transport of heat, reactants and products in and out of the catalyst granules or pellets are restricted.

In spite of mass and heat transport problems supported catalysts are widely used. However, other forms of catalysts are used, e.g. platinum and nickel powders in the hydrogenation of ethene, pelletized tin-antimony oxide powders in the oxidation of propene and platinum-rhodium alloy gauze used in the high temperature oxidation of ammonia to nitric acid.

A fundamental problem in catalysis is due to foreign compounds which strongly adsorb onto the surface, known as poisons, which can reduce the rate of a catalytic reaction. If the poison is adsorbed strongly onto the catalyst surface so that it cannot be removed by eliminating the poison from the gas (or liquid) phase it is described as a permanent poison. If it can be removed it is described as a temporary poison. If the poison is adsorbed as strongly

as the reactants it is termed a competitive inhibitor.

The surface of a metal is soft in the classification of Pearson[50]. Thus the effective poisons for metallic catalysts are soft such as carbon monoxide, hydrogen sulphide and hydrogen cyanide. In oxide catalysis, where the catalytic site is an unsaturated coordinated ion at the surface (e.g. Al_2O_3 or Cr_2O_3) the most effective poisons are hard bases such as water or amines.

Even in the absence of poisons, deactivation of a catalyst may be noticed at high temperatures. This may be due to sintering causing a loss of surface area of the catalyst or, as in the case of reactions involving hydrocarbons, due to deposition on the catalyst surface of slowly reacting hydrocarbon residues.

In general, an overall heterogeneous catalytic reaction can be divided into the following five processes:

(i) The diffusion of the reactants from the bulk fluid to the catalytic site.
(ii) Chemisorption of one or all of the reactants.
(iii) The reaction between the adsorbed species (surface reaction) or between a molecule in the fluid phase and the adsorbed species.
(iv) Desorption of the products.
(v) Diffusion of the products to the bulk fluid phase.

Ideally it is desirable to have process (iii) as the rate

limiting step.

1.5 Methods of Measuring Adsorption Isotherms

There are three main methods for the determination of adsorption isotherms. These are the volumetric, gravimetric and dynamic methods, general details of which are given below.

1.5.1 Volumetric Method

This is the most widely used method for adsorption isotherm determination, the underlying principle being as follows[51].

The temperature, pressure and volume of a quantity of adsorbate are measured and the number of moles present calculated, after which it is brought into contact with the adsorbent. When the temperature, pressure and volume readings are constant, i.e. when equilibrium has been attained, the number of moles present in the gas phase is again calculated. The difference between the initial and final number of moles being equal to the amount of gas adsorbed by the adsorbent.

The accurate determination of the number of moles unadsorbed at equilibrium depends on the precise knowledge of the 'dead-space' (i.e. space surrounding the adsorbent) which is normally determined using helium. However, estimation of the free gas may be complicated by parts of the dead-space being at different temperatures, therefore the volume of a particular component must be measured at the correct temperature before assembly.

Not only is it important to have a knowledge of the dead-space but also, in particular at low pressures, it is necessary to take into account a correction for thermal transpiration. The thermal transpiration, or thermolecular flow, appears as a pressure difference between connected parts of an apparatus held at different temperatures. Provided that the bore of the tubing is very much smaller than the mean free path of the gaseous molecules, the pressure above the adsorbent (p_A) at a temperature T_A is given by[52]

$$p_A = p_m(T_A/T_m)^{\frac{1}{2}}$$

where p_m and T_m represent the pressure and temperature respectively of the manometer.

When the mean free path of the gas molecules is very much smaller than the diameter of the tubing, i.e. when Poiseuille's Law is applicable, the pressure throughout the apparatus is equal. In the region between the two extremes of Knudson and Poiseuille flow the effect is a complex function of the temperature, pressure and bore of the tubing.

1.5.2 Gravimetric Method

The sorption balance introduced by McBain and Bakr[53] was until recently the most used gravimetric technique. It essentially consists of a helical spring usually of fused quartz (but copper-beryllium alloy springs have been reported[54,55]), suspended from a hook inside a glass tube with a light bucket containing the adsorbent attached to the other end. The balance case is connected to a gas storage reservoir, manometer and vacuum system. The amount

of gas taken up by the adsorbent is measured by noting the extension of the previously calibrated spring by means of a cathetometer.

Although the spring balance does away with the need for a dead-space calculation, it is necessary to carry out a buoyancy correction, particularly at high pressures. Further details are given in the experimental section.

Greater sensitivity (to a microgramme) can be obtained by using vacuum microbalances, which are based on the principles of the beam balance, and well documented in the literature[56-59].

1.5.3 Dynamic Method

Early dynamic methods included the passing of a stream of air saturated with benzene over u-tubes containing silica-gel, and following the course of the adsorption by weighing the tubes at frequent intervals[60]. Another method[61] consisted of saturating the adsorbent with the vapour at a definite temperature and pressure, then passing dry air through the system at a known rate, noting the decrease in weight of the adsorbent. With the sophistication of vacuum microbalances it is now possible to follow an adsorption on chart recorders.

The recent trend in dynamic methods is to use gas chromatographic techniques, the most popular of which is the continuous flow method[62] used to measure nitrogen adsorption at -196°C and hence determine surface areas.

Attempts have been made to employ flow methods in chemisor-

ption studies and hence determine specific surface areas. An example is the method developed by Gruber[3] which uses the specific, irreversible adsorption of carbon monoxide on a metal surface at room temperature. A pulse of carbon monoxide and its carrier gas is passed through the reference side of a conductivity cell, then through the catalyst bed and finally into the sample side of the conductivity cell. The recorder trace shows two peaks, the areas of which corresponds to the amount of carbon monoxide present before and after adsorption, from the difference in areas the amount of carbon monoxide adsorbed may be calculated.

2. Apparatus and Experimental

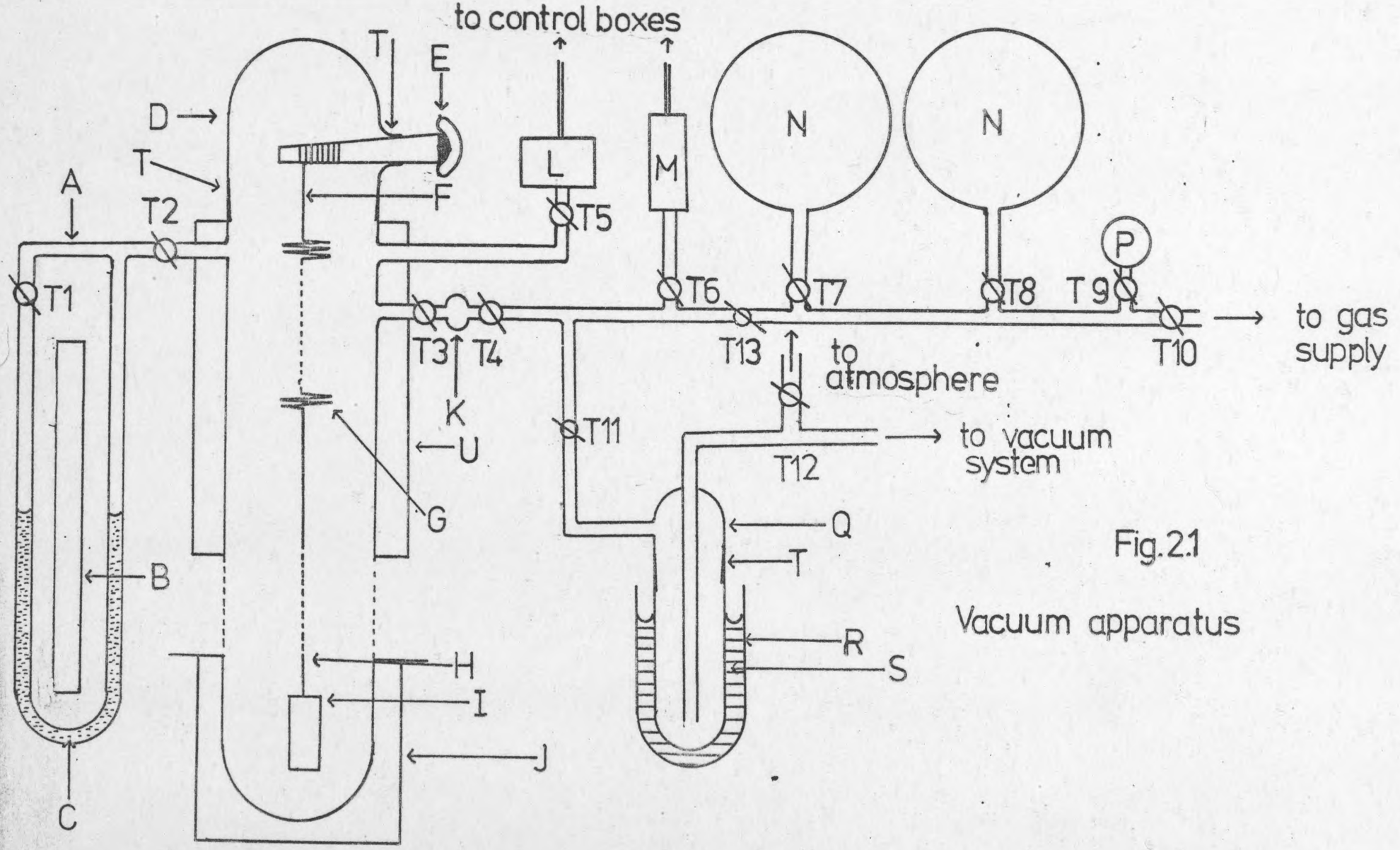

Fig. 2.1

Vacuum apparatus

Key to Fig. 2.1

A Manometer
B Manometer scale (cm.)
C Manometer fluid
D Balance case
E Rotating key
F Terylene thread
G Fused quartz spring
H Glass-fibre 'hangdown'
I Catalyst boat or basket
J Precision oven
K Doser
L Penning gauge
M Pirani gauge
N Gas reservoirs
P Pressure gauge
Q Cold trap
R Dewar
S Liquid nitrogen coolant
T Greased joints
T1, T2 etc. Greased vacuum taps
U Air thermostat

2.1 Vacuum System

A 'CRENCO HYVAC' two stage rotary oil pump in conjunction with an 'EDWARDS' E203D oil vapour diffusion pump gave a vacuum of 10^{-5}torr($\approx 1/760$ Pa) to 10^{-6}torr. An oil vapour diffusion pump was used in preference to a mercury vapour one because of the potential hazard of mercury vapour as well as the possibility of contamination of the samples used.

The working fluid of the rotary pump was 'EDWARDS' high vacuum oil, that of the vapour diffusion pump was 'DOW CORNING' silicone 702 fluid, its stated vapour pressure being 10^{-8}torr.

To prevent backstreaming occuring, i.e. when a small percentage of molecules of the working fluid, in the vapour diffusion pump, suffer collisions in the jet region causing migration into the vacuum apparatus, an 'EDWARDS' 2L1B baffle and isolation valve was used.

Because of the sensitive quartz spring it was vital that the rotary pump was mounted so that vibrations would not be transmitted to the apparatus. The mounting was in fact a wooden board on a metal frame, the frame being cut to prevent contact with the work bench. The use of thick rubber tubing from the rotary pump to the air admittance valve (vacuum tight seals being maintained by use of jubilee clips) also helped to minimise the transmission of vibrations.

In addition it was necessary to use a liquid nitrogen cold trap to remove condensible vapours, such as water vapour,

and also any oil vapour that may still have escaped from the pumping system.

Valves D, E and F in Fig. 2.2 were muff-coupled 'EDWARDS' S.C.10 speedivalves used in conjunction with 'VITON' (silicone rubber) o-rings. "Muff-coupling" produced vacuum tight seals by compressing the greased o-ring between a compression sleeve and the valve. Valve H, like all the other taps in the vacuum apparatus, was glass and the grease used was 'DOW CORNING' high vacuum grease.

To allow high pumping speeds it was essential to use large bore tubing (≈1.5cm diameter) in preference to narrow bore tubing, with appropriate large bore taps. Large bore tubing also enabled the thermal transpiration effect (see earlier) to be ignored, as the mean free path λ at the lowest pressure used was smaller than the smallest bore tube diameter (see Section 3).

2.1.1 Working Principles

2.1.1.1 Rotary Pump

A sketch of the two stage rotary pump is given in Fig. 2.3. The two rotors are mounted on a common shaft and set at 90° to each other, the whole being immersed in a single oil bath. The gas is trapped between the blades and swept out through the exhaust valve.

The oil functions both as a lubricant and sealant between the moving parts.

The gas ballast permits the pumping of condensible vapours through the rotary pump, without condensation and con-

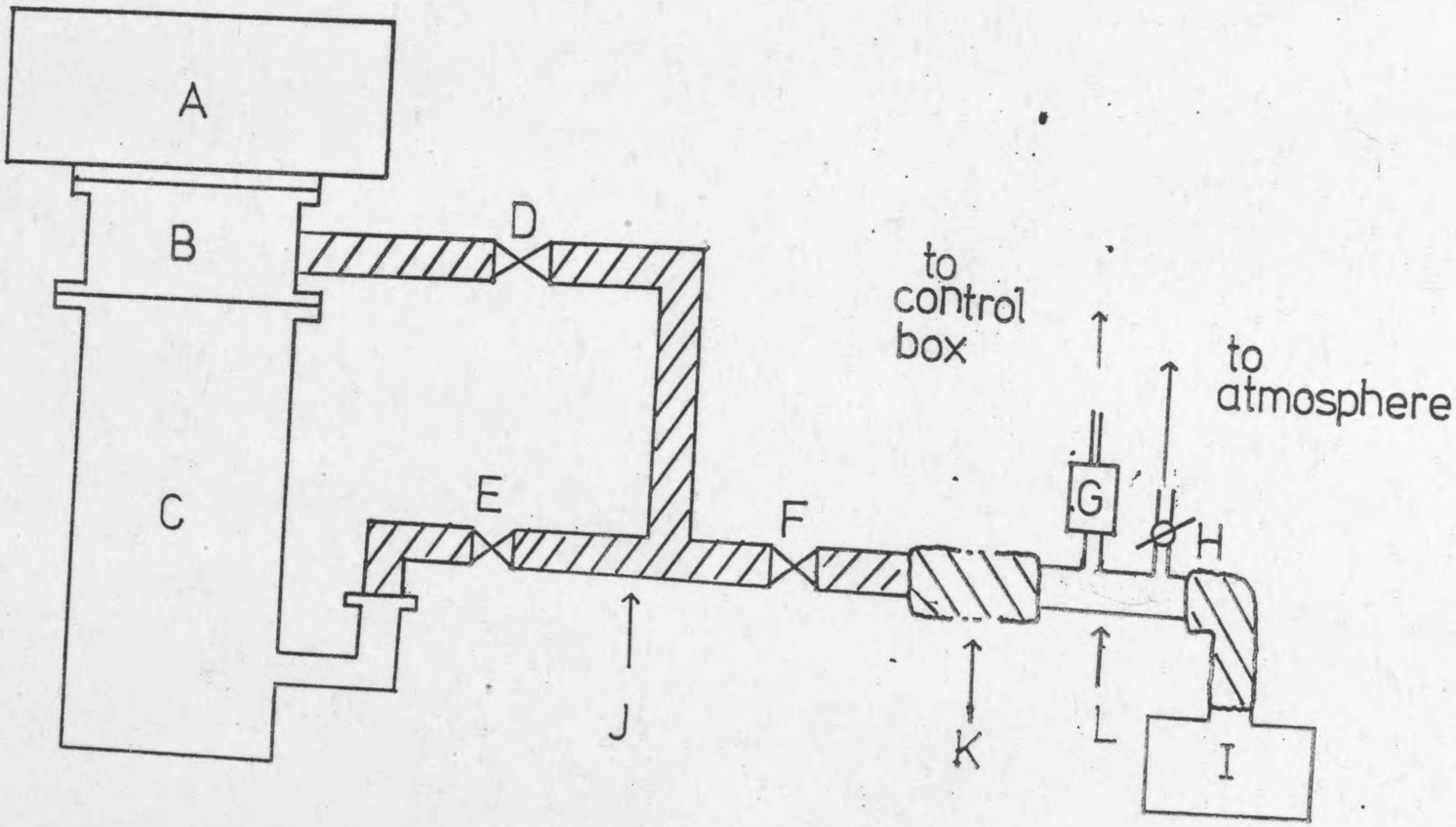

Fig.2.2

Sketch of vacuum producing system

Key to Fig. 2.2

A Vacuum apparatus
B Isolation and baffle valve
C Oil vapour diffusion pump
D Roughing valve
E Backing valve
F Throttle valve (for leak detection)
G Pirani Gauge
H Air admittance valve
I Backing pump
J Copper piping
K Rubber tubing
L Glass tubing

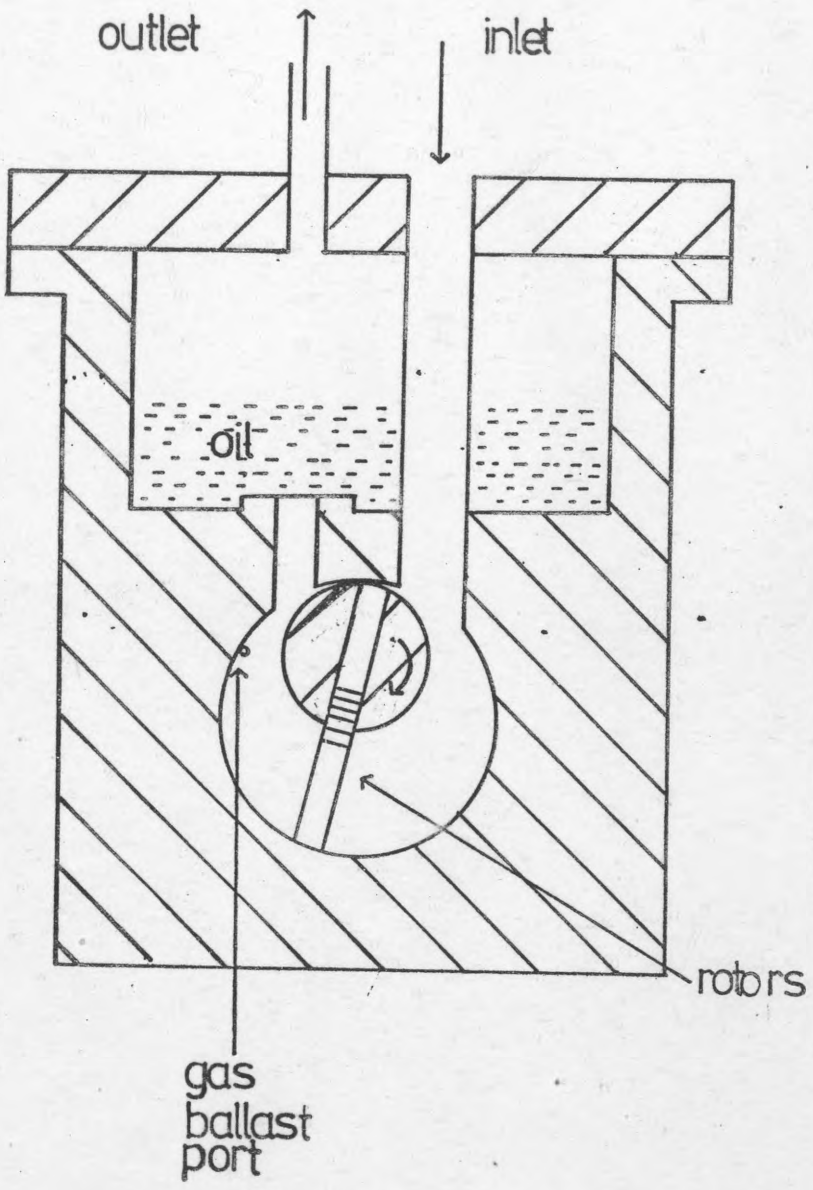

Fig. 2.3

Rotary pump

sequent harmful effects to the pump oil. The pump was not in fact operated in this way due to the cold trap already mentioned.

2.1.1.2 Oil Vapour Diffusion Pump

A sketch of the oil vapour diffusion pump is given in Fig. 2.4. The pump fluid in the boiler is heated to generate a suitable boiler pressure within the jet stream. The resultant vapour passes upward through the jet stages and emerges from the jet nozzles as high velocity vapour streams to impinge and condense on the cooled pump body and subsequently drain to the boiler. Under normal operation, a portion of any gas arriving at the pump inlet (top jet) is trapped, compressed and transferred to the next stage. This process is repeated through the pump jet stages, until the gas is removed by the backing pump via the backing tube and the condenser.

In operating the oil diffusion pump it is absolutely essential to allow the backing rotary pump to reduce the pressure to the working backing pressure of the diffusion pump in order to prevent the silicone oil becoming too hot, so causing decomposition or attack by oxygen.

2.2 Oven

During the course of the study two ovens were used at

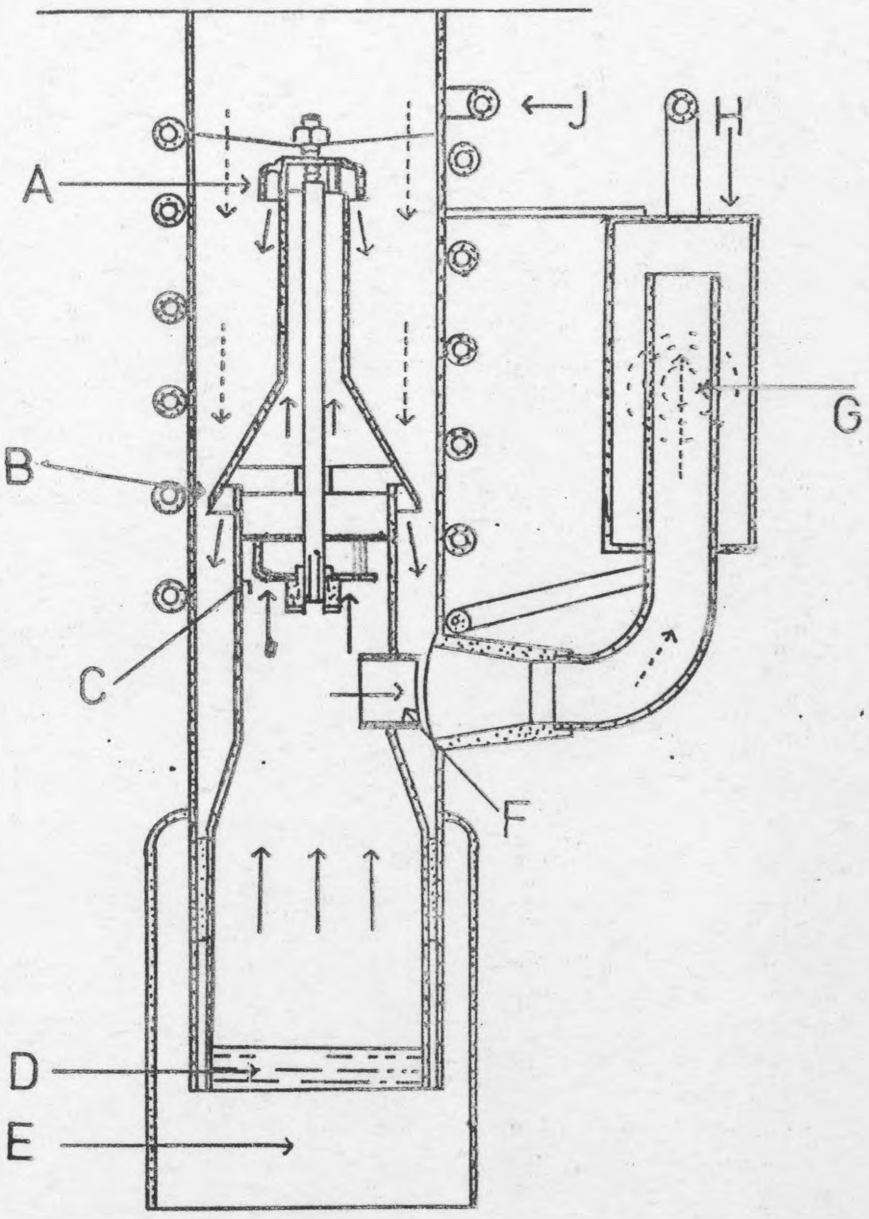

Fig.2.4

Oil vapour diffusion pump

Key to Fig. 2.4

A First stage jet assembly
B Second stage cone
C Splash baffle
D Silicone oil
E Heater
F Ejector jet
G To backing pump
H Baffle valve
J Water cooling tube
↑ Oil vapour
↑ Gas being evacuated

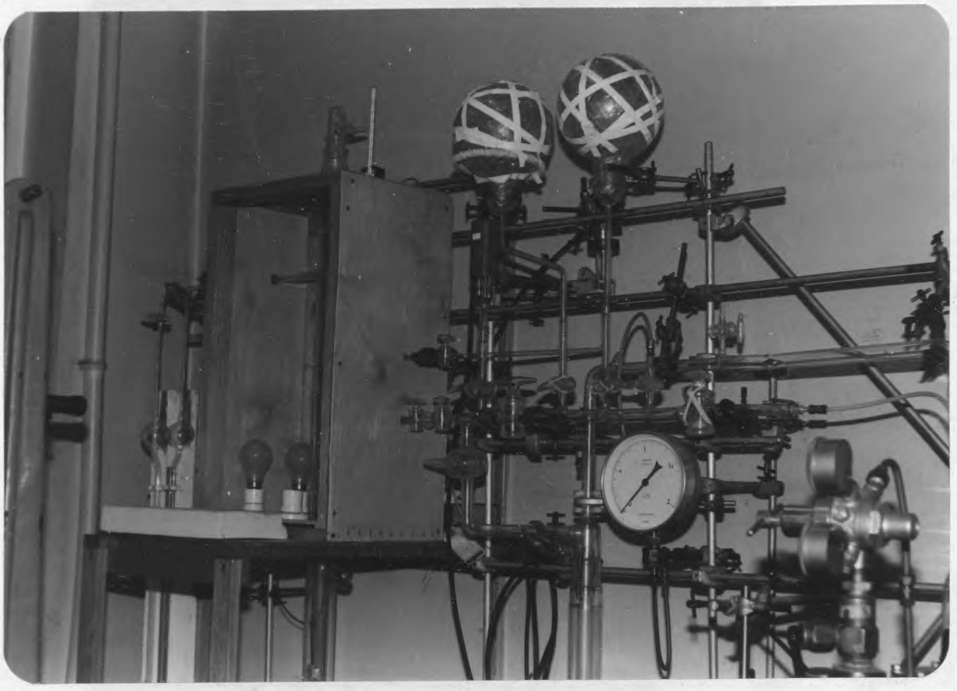

Plate 1
Side view of apparatus

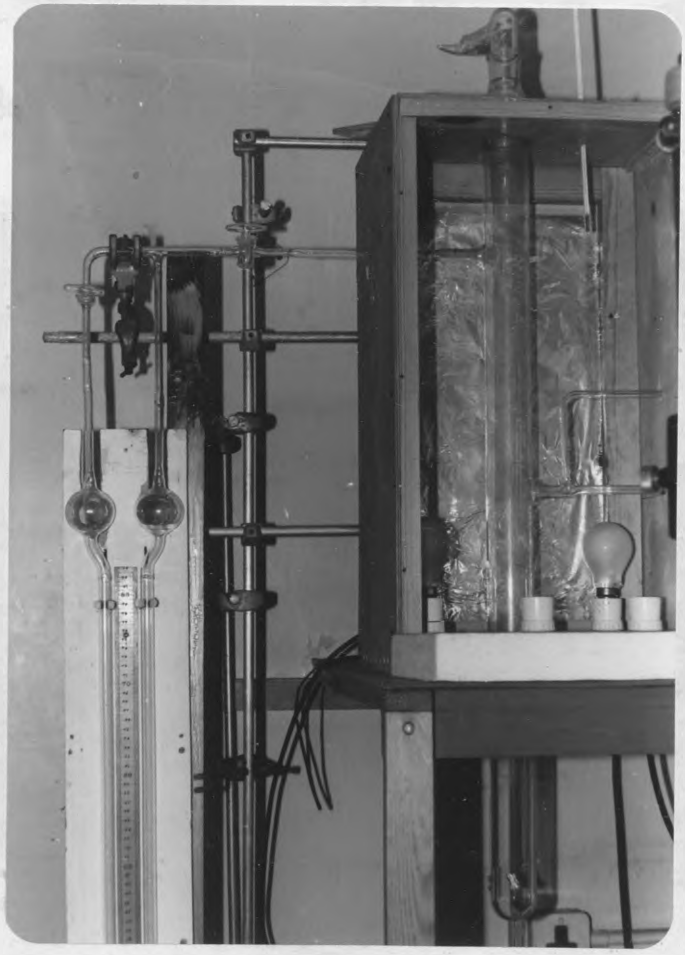

Plate 2
Sorption balance and manometer

Plate 3
Balance case containing spring

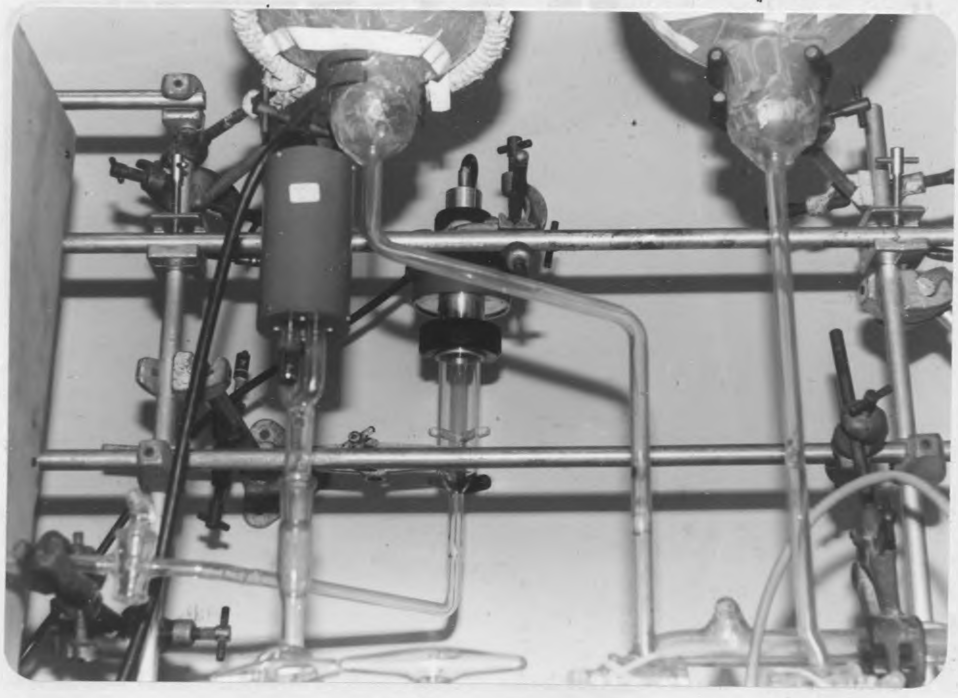

Plate 4
Pirani (foreground) and Penning gauge heads

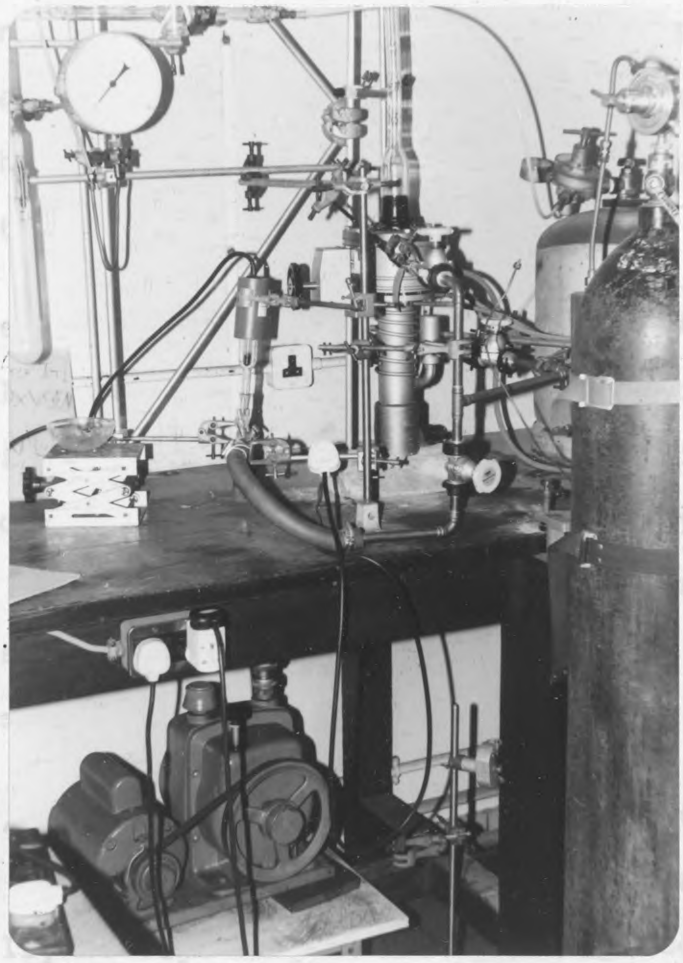

Plate 5
Vacuum pumps

Plate 6
Diffusion pump showing muff-coupled valves

different times to maintain a constant temperature around the catalyst basket during adsorption. They also provided the high temperatures needed for outgassing of the catalysts.

The first was a 'PHILLIPS' 4000 oven and the second a 'PYE' series 104 oven. Both were precision gas chromatography ovens with seperate temperature control units. Gas chromatography ovens were preferred as they allowed precise control of oven temperatures and were comparatively cheap. Heat loss was minimised by surrounding the heated part of the balance with thick asbestos sheets.

However, in spite of good insulation, the oven temperature was not as indicated on the temperature controller, especially at high temperatures. To overcome this problem a chrome-alumel thermocouple was placed at the centre of the oven and connected to a thermocouple potentiometer box which, when used in conjunction with a calibration table, gave an accuracy of ± 0.1 c.

2.3 Pressure Measurement

Three types of pressure measuring devices were used. The working principles of two, the Pirani and Penning gauges, are given below. The Pirani gauge scale recorded pressures between 0.51 torr and 10^{-3} torr. Lower pressures, down to 10^{-6} torr, were indicated on a Penning gauge.

Higher pressure measurements were carried out by a manometer, the manometer fluid being silicone oil. This was preferred to the conventional mercury manometer due to the fourteen fold increase in sensitivity obtained, and also

eliminating contamination of the catalysts by mercury vapour.

2.3.1 Working Principles

2.3.1.1 Pirani Vacuum Gauge

A Pirani gauge depends on the thermal conductivity of a gas, at low pressures, being proportional to its pressure and that a heated wire suspended in a gas will lose part of its energy by impact of 'cold' molecules on its surface.

A hot wire loses energy by conduction through the gas and the ends of the wire. There is also loss by radiation, especially with polyatomic molecules. By making the wire sufficiently long and thin, the end losses may be practically eliminated.

Pirani gauges are operated in Wheatstone bridge circuits, where the voltage is kept constant and the change of current is observed as a function of pressure[63].

The practical advantage of Pirani gauges is that they may be used with gases and vapours, corrosive or otherwise. Also, backing line Pirani gauges are useful when checking for leaks in vacuum systems when the compression produced by a diffusion pump permits small leaks to be detected.

2.3.1.2 Penning Vacuum Gauge

The action of a working Penning gauge is as follows. An anode rod passes through a circular cathode. When a voltage is applied between the two, electrons are drawn from the cathode and accelerate towards the anode, as in a

thermionic diode. However, a magnetic field deflects the electrons so that they follow a complex spiral path which is very much longer than the spacing between the electrodes. Collisions with the gas molecules ionize the gas, producing positive ions and additional electrons, both of which cause further ionization.

The sum of the positive ion current to the cathode and the electron current to the anode constitutes the gauge head current which is measured by the associated control unit. The current is approximately proportional to the gas pressure up to about 10^{-4} torr, at higher pressures the current rises at a diminishing rate until it reaches a maximum at about one torr.

Penning gauges tend to 'age' due to the production of electrical leakage paths and conducting or insulating layers caused by the dissociation of hydrocarbons or silicone vapours. Such contamination can lead to erroneous or unstable indications of pressure, so that the Penning gauge reading can rarely be regarded as a precise measurement of pressure.

2.4 Sorption Balance

The essential part of the sorption balance, similar to that first introduced by McBain and Bakr[53], was a transparent fused quartz spring (particulars of which are given in Fig. 2.5) supplied by 'THERMAL SYNDICATE LTD.' The advantage that the fused quartz spring had over the other spring types was that its extension was perfectly elastic, consequently there was no elastic hysterisis

FRONT ELEVATION

SIDE ELEVATION

SPRING	d	D	N	W	E	ME
II	·2	15	61	1·0	33	40
I	·2	15	46	1·0	25	30

d - dia. of fibre (mm)
D - dia. of coil (mm)
N - number of turns
W - max. load (gm)
E - sensitivity (cm/gm)
ME - max. extension (cm)

Fig. 2.5

Fused quartz spring

occuring.

The upper hook of the spring was attached by thread to a glass key which, when turned, raised or lowered the spring.

The lower hook of the spring was attached to an aluminium foil catalyst basket by means of a glass fibre 'hand-down'.

As shown in Fig. 2.1 the sorption balance was placed in a vertical glass cylinder, or balance 'case', of length 100cm. and diameter 5cm. which was connected to the vacuum system.

The lower half of the balance 'case', containing the catalyst basket, was placed centrally in the oven, to ensure the catalyst was kept at the temperature required.

As quartz has a small but definite temperature coefficient [64, 65], it was necessary to thermostat the part of the balance 'case' containing the spring. This was done by using electric light bulbs as heaters in an enclosed box with holes for ventilation. The supply to the bulbs was controlled with a 'FISONS' Fi-monitor fixed to a mercury thermometer to hold the temperature at a constant 25°C. The Fi-monitor sensed the position of the mercury thread.

A travelling microscope (cathetometer) was used to measure any displacement of the spring caused by uptake of adsorbate. It consisted of a low power telescope, mounted on a rigid bed, which was focused on a reference point on the glass fibre 'hang-down'. The vernier scale of the cathetometer allowed measurements of 0.001cm.(10μm) to be made.

To eliminate any errors in measurements due to vibrations

the cathetometer was placed on a solid concrete block, and the whole system built onto a vibration-free outside wall built up directly from the foundations.

2.4.1 Working Principle

2.4.1.1 Fused Quartz Spring

Assuming the mass of the spring to be negligible compared to the load, and the helix angle to be small, the extension, Y, can be related to the load, m, by the equation (see Appendix XII),

$$Y = \frac{2lR^2m}{\Pi zr^4} \qquad (2.1)$$

where,

r - radius of silica fibre

l - length of silica fibre

R - coil radius

z - modulus of rigidity of silica.

Taking the mass of the spring into account equation (2.1) will now become,

$$Y = \frac{2lR^2m}{\Pi zr^4} + \frac{r^2\rho l^2}{\Pi zr^4} \qquad (2.2)$$

where,

ρ - density of silica.

At zero load the extension is given by,

$$Y_o = \frac{R^2\rho l^2}{\Pi zr^4} \qquad (2.3)$$

The sensitivity, K, is given by,

$$K = \frac{Y - Y_o}{m} = \frac{2R^2l}{\Pi zr^4} \qquad (2.4)$$

Replacing the fibre length, l, by $2\Pi rn$, where, n, is the number of turns, the sensitivity, K, is now,

$$K = \frac{4R^3n}{zr^4} \qquad (2.5)$$

Hence the sensitivity may be increased by decreasing the radius of the silica fibre, increasing the coil radius and the number of turns.

There is, however, a limit to which these factors can be changed. The limit is set by the mechanical strength and overall length of the spring.

With spring balances a buoyancy correction is required. Assuming an ideal gas the following expression may be used,

$$\partial w = \frac{MV}{RT} .p. \qquad (2.6)$$

where,

∂w - upthrust

p - pressure

T - absolute temperature

M - molecular weight of gas

V - volume of the load

R - universal gas constant.

It is difficult to calculate the volumes of the catalyst basket, the adsorbent and the adsorbed phase. The correction was determined empirically by measuring the apparent weight of the load in the presence of an inert gas (helium) which was assumed to be unadsorbed. This was performed at a series of pressures. It was also assumed that the upthrust from a given adsorbate was proportional

to the ratio of the molecular weight of adsorbate to that of the inert gas.

The above use of an inert gas also allowed for the estimation of the error due to thermal gradients. This effect, caused by the spring and catalyst basket being held at differing temperatures, leads to the production of thermal currents within the gas phase and a thermal gradient along the hang-down fibre which can cause apparent increases or decreases of weight. Another possible effect caused by the apparatus not having a uniform temperature is that of thermal transpiration. However, this may be ignored as wide bore tubing was used (see earlier).

2.5 Evacuation of the Apparatus

Initially the baffle valve and air admittance valve were shut as were all other openings to the atmosphere in the system. The roughing and backing valves (D and E in Fig. 2.2) were opened, the cooling water turned on (at a rate not less than 0.5l/min) and the rotary pump switched on.

Once the backing pressure, as indicated on the Pirani gauge (G), had reached 0.5torr or less the vapour diffusion pump was switched on, and the cold trap was filled with liquid nitrogen. After allowing four or five minutes for the oil to warm, the roughing valve (D) was shut and the baffle valve opened. This allowed the apparatus to be evacuated.

To close down the apparatus safely, the following sequence

was necessary. The baffle valve was closed and the electrical supply to the diffusion pump switched off. The time allowed for the diffusion pump oil to cool was twenty to twenty-five minutes before the backing valve (E) was closed. The air admittance valve was opened and the rotary pump switched off. Also at this point it was important to remove the liquid nitrogen cold trap to prevent oxygen condensing from the atmosphere.

The above procedure ensured that the vapour diffusion pump was left evacuated and prevented the pump from absorbing air. If the oil was not allowed to cool sufficiently, on re-evacuation the oil would superheat and evolve a quantity of vapour which would pass into the backing pump.

Oil suck back into the system could occur if the rotary pump was stopped under vacuum. Consequently the backing pump was never shut down under these conditions.

2.5.1 Leak Testing

The apparatus was initially tested for vacuum tightness by opening all taps, except those to the atmosphere, in Fig. 2.1 and evacuating. A Tesla coil was used to test for any pin-holes that may have occurred due to the glass-blowing work carried out in order to assemble the apparatus.

Opening taps T1 and T2, under vacuum, removed any dissolved gases from the manometer fluid, this procedure was necessary whenever the apparatus had been taken up to pressure using air with tap T2 open.

The best attainable vacuum was found to be 10^{-6} torr. $\approx$ $\frac{1}{7600}$ Pa.

2.6 Equipment Maintenance and Safety

There were three items of equipment requiring regular maintenance during the course of the study. These were the greased taps, oil vapour diffusion pump and the rotary backing pump.

2.6.1 Taps

Constant regreasing of the taps was found to be necessary because of the 'streaking' of the vacuum grease due to cold, heat or excessive use. This effect led to the production of a poorer ultimate vacuum than would normally be expected.

The best way to regrease was first to remove all traces of grease from the key and socket using a solvent such as chloroform. Then regrease the key with 'DOW CORNING' high vacuum grease and place it into the warmed socket. The key was then 'worked-in' so that all streaks were removed.

2.6.2 Oil Vapour Diffusion Pump

As previously discussed oil from the diffusion pump may be lost due to super heating or breakdown by oxygen. Both will lead to a progressively worsening ultimate vacuum, which can only be improved by replacing the used oil.

To do this the diffusion pump and baffle valve had to be completely isolated from the system. As taps D and E in Fig. 2.2 were muff-coupled it was relatively easy to

isolate the diffusion pump and baffle valve from the rotary pump. The vacuum apparatus was isolated by cutting the glass tubing above the baffle valve. Once isolated the diffusion pump was seperated from the baffle valve by removing the four holding bolts.

The pump could now be tilted and the used oil poured out. It was replaced with a new 50ml. charge of silicone oil. The system was then re-connected.

2.6.3 Rotary Backing Pump

Due to the breakdown of the rotary pump oil, regular replacement was necessary to maintain the optimum ultimate vacuum and also to prevent damage to the pump.

The pump was easily isolated by unscrewing the coupling at the inlet. The oil was poured out by removing the wing nut at the base of the pump. After all the used oil had drained out, the nut was replaced and a new charge of oil poured in through the inlet pipe. The pump was then re-connected to the system.

2.6.4 Safety

Whenever the apparatus was being pressurised or evacuated there was a possibility of implosion; due to rapid evacuation, or explosion; due to excessively swift pressure build up. In both cases shards of glass would be ejected from the apparatus and would cause extensive facial damage - in particular to the eyes. To prevent such injuries it was found necessary to wear some sort of facial protection when near the apparatus in the form of a face

visor, or at the very minimum, a pair of safety spectacles.

In the handling of the liquid nitrogen it was found necessary to wear protective gloves for two reasons. It was found the the dewar used to transport the liquid nitrogen to the apparatus could unaccountably break, cutting the unprotected hand of the handler. Also spurting of the liquid nitrogen, due to excessive boiling, could cause cold burns on the back of unprotected hands.

Finally, as flammable gases were used such as oxygen, it was important that there was no naked flames in the laboratory in case of tap or cylinder leaks.

2.7 Sorption Balance Materials

2.7.1 Catalyst Boat

The catalyst boat or basket had to be as light as possible. It was important that it retained its mechanical strength under negative and positive pressures, and also over a large temperature range. It should also not adsorb any of the adsorbates used.

A glass boat was tried but was too heavy (the lightest glass boat weighing in the region of one gramme). The maximum load capacity of the spring, i.e. catalyst boat plus sample, was one gramme. A variety of low density metallic films were found to satisfy all the above mentioned criteria; it was decided to use an inexpensive aluminium foil.

The boat was constructed in the shape of a cylinder, with

one open end, of height 1.5cm. and diameter 1.0cm., with two holes pierced at the top to take the thread.

2.7.2 The Thread

The thread was needed between the rotating key (E in Fig. 2.1) and the top of the quartz spring, and also between the bottom of the spring and the catalyst boat.

A terylene thread was found to be suitable; it was found to be thermally stable up to 225°C. It remained taut without stretching under the weight of the catalyst basket and catalyst, and its weight was appropriately low. A quartz fibre was found to be too stiff.

During the course of the experiment it was found necessary to use temperatures greater than 225°C. Under these conditions the thread disintegrated leading to permanent damage to the sensitive quartz spring. The thread between spring and sample was than replaced by a glass fibre 'hang-down', which had the required properties and withstood high temperatures.

2.7.3 Spring Calibration

The procedure was as follows:
The spring was suspended by means of a terylene thread in a draught free air thermostat. The thermostat temperature was set to 25°C. The bottom 'hook' of the spring served as the reference or datum point. The cathetometer was focussed upon the datum point and the scale reading noted.

The glass-fibre 'hang-down' and catalyst basket were weighed seperately and the change in the datum noted after

each had been connected to the spring.

Known weights were then added to the catalyst basket, up to a total of approximately 0.8g, then the weights were successively removed so checking for hysteresis. The datum position was noted for every change in weight.

The readings are shown in Tables 2.1 and 2.2. For increased accuracy in the estimation of the spring sensitivity, a computed linear regression analysis was used in preference to a graphical analysis.

However a graphical representation is given in Graphs 2.1 and 2.2 and the computed analysis in Tables 2.3 and 2.4.

Blank experiments were performed to check that the materials were suitable for adsorption studies.

Initially the quartz spring (connected to the catalyst basket by means of the glass-fibre hang-down) was suspended in the balance case in the centre of the air thermostat, with the basket in the oven. The balance case was then evacuated.

The blank experiments were carried out using nitrogen, oxygen, propene, butene, argon and helium at various temperatures and over a range of pressures.

No adsorption occurred and the materials were considered suitable for their purpose.

2.8 Catalysts

The samples used during the course of the study were

Weight (g)	Change in Datum (cm)
0	0
0.0966	1.633
0.1708	3.333
0.3069	6.432
0.4317	9.262
0.5734	12.459
0.4991	10.766
0.3662	7.777
0.2391	4.893
0	0

Table 2.1

Spring I Calibration

Weight (g)	Change in Datum (cm)
0	0
0.2488	8.404
0.2809	9.688
0.3188	10.965
0.3567	12.242
0.3946	13.519
0.4536	14.831
0.4902	16.065
0.5675	18.654
0.6796	22.399
0.7446	24.894
0.5184	17.355
0.3288	11.042
0.2488	8.433
0.1147	4.270
0	0

Table 2.2

Spring II Calibration

Observed Value (cm)	Fitted Value (cm)	Difference (%)
1.633	1.651	-1.0730
3.333	3.334	-0.0222
6.432	6.421	0.1686
9.262	9.252	0.1055
12.459	12.466	-0.0616
10.766	10.781	-0.1411
7.777	7.766	0.1367
4.893	4.883	0.2019

Standard Deviation 0.390%
Spring Sensitivity (cm/g) 22.6849

Table 2.3

Computed Analysis of Spring I Calibration

Observed Value (cm)	Fitted Value (cm)	Difference (%)
8.404	8.537	-1.578
9.688	9.576	1.159
10.965	10.802	1.481
12.242	12.029	1.737
13.519	13.256	1.943
14.831	15.166	-2.260
16.065	16.350	-1.780
18.654	18.853	-1.068
22.399	22.481	-0.370
24.894	24.585	1.237
17.355	17.263	0.525
11.042	11.126	-0.763
8.433	8.537	-1.229
4.270	4.196	1.740

Standard Deviation 1.446%
Spring Sensitivity (cm/g) 32.3706

Table 2.4

Computed Analysis of Spring II Calibration

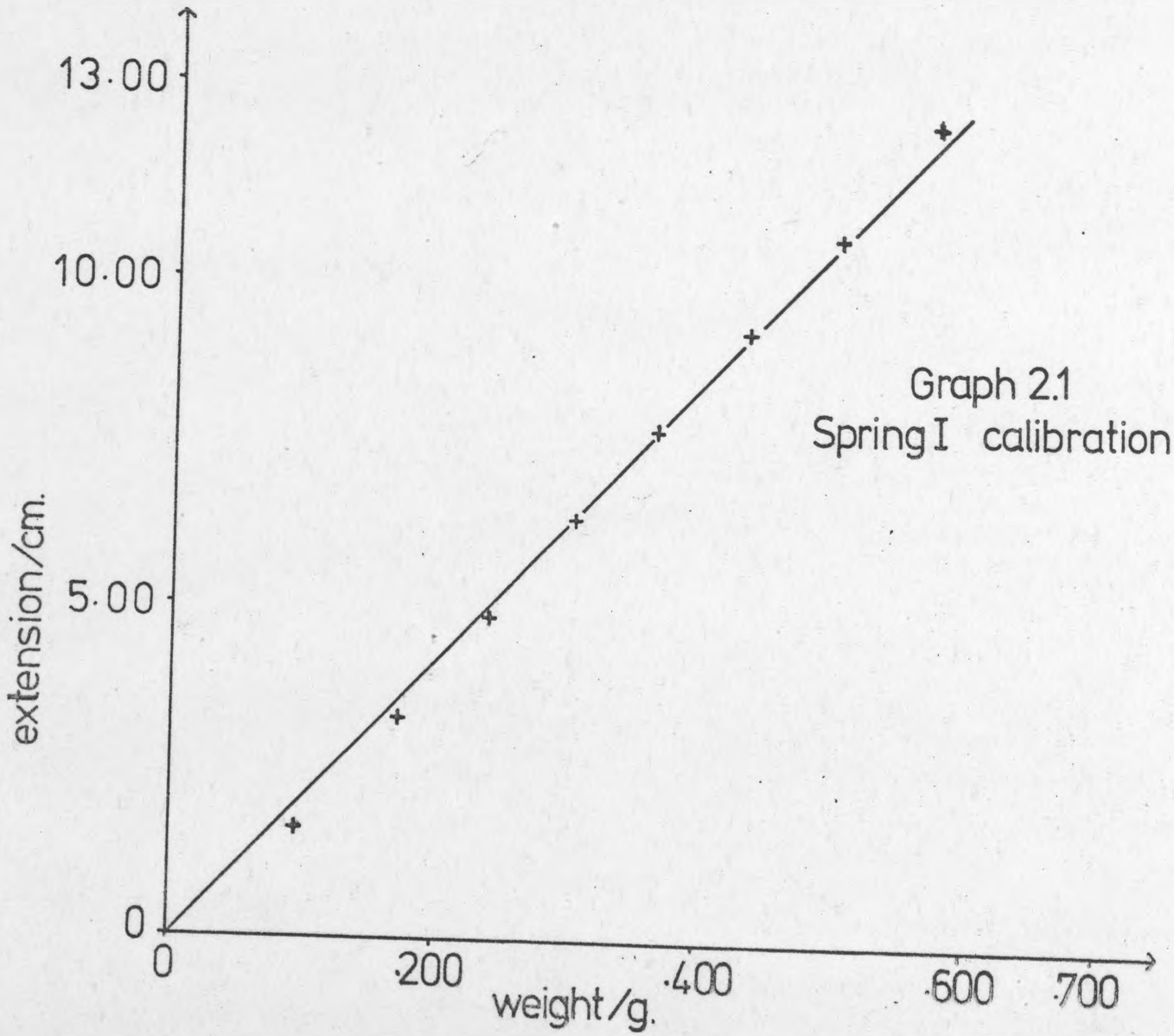

Graph 2.1
Spring I calibration curve

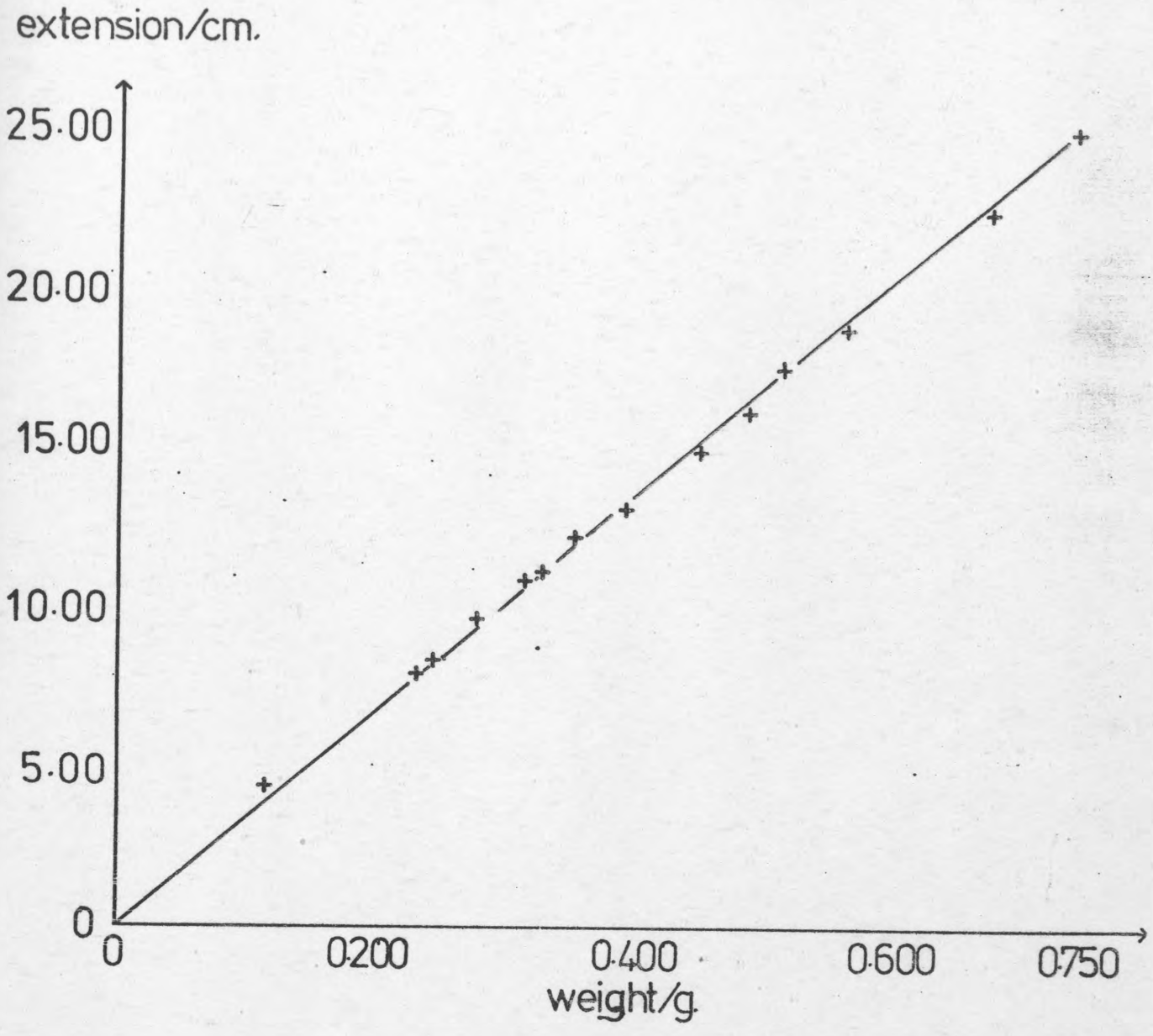

Graph 2.2

Spring II calibration curve

carbon-black as an inert reference material and bismuth-molybdate and tin-antimony catalysts.

The carbon-black was supplied by 'CABOT CARBON LTD' specifically for BET studies to examine the suitability of the sorption balance. The quoted specific surface area being $65.0 \pm 0.5\ m^2g^{-1}$.

The tin-antimony and bismuth-molybdate catalysts were prepared in the laboratory[4] and were pelleted by 'B.P. LTD'. The specific surface areas being quoted by 'B.P. LTD' as 7.40 and 0.25 m^2g^{-1} respectively. The method of preparation being as follows[4, 66].

The tin-antimony catalyst was produced by seperately oxidising the pure metals with nitric acid at about 100°C, and mixing the correct proportion (atomic ratio of tin to antimony being 2:1) of the washed oxides before drying at 110°C. The resulting mixture was heated in air by programmed heating at 20°C per hour to 850°C and then maintained at this temperature for 16 hours.

The bismuth molybdate preparation was as follows. The catalyst was precipitated from a solution of ammonium molybdate mixed with acidified bismuth nitrate and ammonia to give a final P h. of 5.5 and a bismuth to molybdenum atomic ratio of unity. The precipitate then being washed, dried and heated to 450°C.

Both the tin-antimony and bismuth molybdate catalysts were used in the form of pellets of diameter 1/8" by 1/16".

2.8.1 Correction of Catalyst Weight

The sample was weighed carefully and then suspended in its container from the spring. The datum change caused by outgassing and then returning to room temperature was noted.

A buoyancy correction had to be made. This was carried out by noting the datum change compared to vacuum, with the balance case pressurised to one atmosphere with argon.

2.9 Gas Storage

Initially the gas reservoirs (covered with tape to prevent danger from shards of glass in the event of implosion) had to be evacuated to remove any air present. This was carried out by closing taps T4 and T10 with taps T6, T13, T7, T8, T9 and T11 open, and then following the general evacuation procedure as described in section 2.5.

The gas cylinder was connected to T10 by means of plastic tubing.

Once the reservoirs had been evacuated, the gas cylinder was 'cracked open' to allow a flow of gas. T10 and T11 were closed slightly to allow removal of any air in the pipeline. T11 was then shut leading to an increase of pressure in the reservoirs, the pressure being indicated by the precision pressure gauge P. Once the desired pressure had been reached T10 was shut.

The above was repeated twice, before allowing the pressure in the gas reservoirs to reach a value of 1.5 atmospheres,

whereupon T13, T10, T7, T8, T9 as well as the cylinder valve were shut. The reservoirs now contained the gas supply for a particular adsorption experiment.

2.10 Outgassing

Before any adsorption data could be taken it was necessary to prepare the adsorbent surface.

In theory it should be possible to desorb any adhering gases by evacuation alone. In practice the situation is much more complex and it has been found that outgassing is improved by evacuating at high temperatures.

An empirical formula[67] exists which enables a rough estimate to be made of the outgassing time at temperatures between 100 to 400°C with a vacuum of 5×10^{-6} torr or better. The equation is

$$t = 14.4 \times 10^{4} \times T^{-1.77} \qquad (2.7)$$

Frequently evacuation has to take place at very high temperatures to remove any chemisorbed layers.

In order to minimise the time required for outgassing, the temperature should be the maximum consistent with the avoidance of sintering or alteration of the surface. Estimation of this temperature is to a large extent empirical.

One of the great advantages of the gravimetric method of measurement is that outgassing can take place to a constant weight.

For the physisorption of nitrogen on carbon black it is

generally accepted that degassing for several hours at 110°C[8] is sufficient to provide a clean surface for adsorption.

However, for the chemisorption work on the tin-antimony catalyst and the scouting experiments on the bismuth-molybdate catalyst, the time and temperature for outgassing were found by experiment. It was found that the catalysts reached constant weight after outgassing at a temperature of 300°C for 18 hours. The temperature was well below that at which the catalysts were fired and consequently it was assumed that the surface was unchanged.

2.11 Experimental Procedure

2.11.1 Adsorption

First the catalyst was outgassed with the lower end of the balance case maintained at the correct temperature (with the air thermostat on), and with the balance at the best possible vacuum. During this time T1 to T6 were kept open. However, before starting adsorption measurements T1, T3, T5, T6 as well as T11 were closed and T13 opened to admit adsorbate to the system. Careful manipulation of T3 connecting the 'doser' to the balance case allowed small increases in pressure in the balance case. This was shown by the manometer. Adsorption on the catalyst surface was indicated by a change in datum. When taking the manometer scale readings it was important that there were no parallax errors. To minimise such errors the scale reading was taken when a straight edge placed

horizontally at the bottom of the oil meniscus was coincident with its image in the mirror placed behind the manometer arm.

A more sensitive pressure measuring device could have been used, e.g. a tilted manometer or pressure transducer, but the limited spring sensitivity would have nullified such improvement.

The adsorption was carried out in stages up to a point when no change in datum was noticed, in the case of chemisorption, or to a relative pressure of 0.3 in the case of physisorption.

It should be noted that between stages a certain period had to be allowed, so that equilibrium could be attained. This time was short for physisorption (a few minutes) and large for chemisorption (up to several hours).

When a pressure greater than 50cm of oil was required for physisorption then (having reached the maximum difference in oil levels) T1 was opened, admitting gas into the left hand arm of the manometer. With T1 now closed a further dose of gas was admitted into the balance case.

There was found to be a limit beyond which adsorption measurements could not be taken due to continuous undampable spring oscillations. The limit was related to the adsorbate pressure, and temperature difference between the air thermostat and the lower end of the balance case. Fortunately, during the course of this study, this limit was not exceeded.

It was also of great importance to check the spirit level of the cathetometer between readings. If the air bubble was to change position at any time during an adsorption run and was not brought back to its original position, then the cathetometer reading taken would be erroneous. The air bubble position was adjusted by tilting the cathetometer up or down by means of the screw under the barrel of the cathetometer.

2.11.2 Desorption

All openings to the atmosphere were shut and the system evacuated, using the backing pump only, up to T13 and T3. Adsorbate gas was removed in stages, the pressure and datum change noted after every stage. Once the pressure change could not be detected by the oil manometer T5 was opened and the oil vapour diffusion pump brought into operation.

2.12 Experimental Detail

2.12.1 Physisorption Study

This was really an initial trial of the sorption balance. Samples of known specific surface areas were used in BET studies using nitrogen adsorbate at liquid nitrogen temperatures. In conjunction with the above, observations were carried out on the catalysts using argon to enable buoyancy corrections to be made.

2.12.2 Chemisorption Scouting Study

Runs were carried out at various temperatures using tin-

antimony and then bismuth-molybdate catalysts with oxygen, propene and butene adsorbates, to find the optimum temperature ranges for chemisorption work.

2.12.3 Chemisorption Studies

From the chemisorption scouting studies it was found that chemisorption of all adsorbates on the bismuth-molybdate catalyst were too little for the sensitivity of the balance. Attempts to meet the cost of a suitable micro-balance were unsuccessful.

However, measurable quantities of gas were found to be adsorbed on the tin-antimony catalyst. The temperature ranges for the various adsorbates were as follows:

Oxygen	80-100°C
Propene	200-250°C
Butene	130-170°C

Further accurate studies were carried out on these systems.

As in the case of the physisorption studies, buoyancy corrections were made using argon.

3. Results and Calculations

3.1 Mean Free Paths and Molecular Diameters

To determine whether thermomolecular flow corrections had to be made (due to the different temperatures in the apparatus) it was necessary to compare the mean free path λ with the bore of the tubing. The derivation of λ is given in Appendix XI. It can be seen that the molecular diameter d of the gas needs to be known. This may be found from viscosity data, as follows.

The elementary gas model assumes that all molecules are non-interacting rigid spheres of diameter d and mass m moving randomly with a velocity v. Assuming the average speed to be proportional to $(RT/M)^{\frac{1}{2}}$ (see Appendix X) the viscosity relationship may be written as

$$\eta(\mu P) = 26.69 \frac{(MT)^{\frac{1}{2}}}{d^2} \qquad (3.1)$$

A more rigorous treatment, taking into account intermolecular forces is that due to Chapman-Enskog[68] which modifies the above equation to

$$\eta = 26.69 \frac{(MT)^{\frac{1}{2}}}{d^2 \Omega_v} \qquad (3.2)$$

where Ω_v is the collision integral and may be obtained from tables by Reid and Sherwood[68].

Whether a correction was necessary for the dipole moment of the molecule was indicated by the equation

$$\delta = \frac{(\mu p)^2}{2E\sigma^3}$$

where

μp - dipole moment (debyes)

σ - hard-sphere diameter ($\mathring{A}$)

E - characteristic energy (J)

the correction being necessary if $\delta \geqslant 0.05$. Although propene and butene exhibit small dipole moments 0.4 and 0.3 debyes respectively, the δ values of 0.02 and 0.004 were sufficiently small to enable a dipole correction to be ignored.

From the above considerations the molecular diameters used were as follows:

Gas	d ($\mathring{A}$)
Oxygen	3.467
Propene	4.678
1-Butene	5.229

It should be noted Ω_v was found by using the Lennard-Jones potential which applies to non-polar gases.

From Appendix XI

$$\lambda = \frac{3.108 \times 10^{-24} \, T}{d^2 \, p} \qquad (3.3)$$

where

T - Kelvin

p - Nm^{-2}

d - metres

The smallest pressure used was 0.10 cm.oil which corresponds to a pressure of

$$\frac{0.10 \times 1.070}{13.546} \times \frac{1.013 \times 10^5}{76.0} = 10.529 \text{ Nm}^{-2} \text{ or Pa}$$

Equation (3.3) now becomes

$$\lambda = 2.952 \times 10^{-25} \frac{T}{d^2} \qquad (3.4)$$

For oxygen, in the temperature range 80-100°C, λ lies between 9.16 and 8.67×10^{-4}m.

For propene, in the temperature range 200-250°C, λ lies between 7.05 and 6.38×10^{-4}m.

For butene, in the temperature range 130-170°C, λ lies between 3.70 and 3.27×10^{-4}m.

Therefore in all cases λ was rather less than one millimetre, which is very much smaller than the diameter of the narrowest bore tubing used which was 1.01 centimetres.

3.2 Correction of Catalyst Weight

There were two corrections to be made to the apparent catalyst weight.

Firstly, the buoyancy effect. The procedure for this was to carry out adsorption and desorption runs using an inert gas (argon) which would not be adsorbed, and notice the apparent loss in weight with increasing pressure. The amount of argon would be used to calculate the corresponding amount of air and this value plotted against pressure as in Graph 3.1.

The conversion of the upthrust due to argon into the upthrust

due to air at the same temperature and pressure was as follows:-

$$PV = nRT \qquad (3.4)$$

where

P - pressure

V - volume

R - gas constant

n - number of mols

T - temperature

also

$$n = \frac{m}{M} \qquad (3.5)$$

where

m - mass of gas

M - molecular weight

From (3.4) and (3.5)

$$\left(\frac{PV}{RT}\right) = \frac{m}{M} \qquad (3.6)$$

Hence for constant P, V and T

$$\left(\frac{m}{M}\right)_{argon} = \left(\frac{m}{M}\right)_{air} \qquad (3.7)$$

This gives the ratio of the upthrusts at constant pressure and temperature.

The second effect to be accounted for was the loss of weight due to outgassing. This was a straightforward measurement, an example of which is given in Table 3.1.

3.3 Corrected Pressure Readings

When the apparatus was evacuated and tap T1 closed (see Fig. 2.1), the pressure after admitting the adsorbate was shown directly in centimetres of oil.

If, however, a pressure greater than 50cm. of oil was required, then it was necessary to open tap T1 and allow the oil levels to become equal before shutting the tap.

Consequently when more adsorbate was admitted into the balance case the gas between the manometer fluid and T1 was being compressed and a correction had to be made to allow for this.

The correction was made by assuming the ideal gas law relationship

$$P_1V_1 = P_2V_2$$

Sample Calculation

Manometer fluid in both arms level at a scale reading of	32.75 cm.
Volume between T1 and left hand manometer fluid, when fluid levels in both arms level	178.47 cm^3
Radius of manometer arm	0.70 cm.

From raw data Table 1 the first pressure value of 55.90 cm.oil was the actual pressure reading not requiring correction. Therefore when T1 was opened in advance of the next dose of gas the whole balance case was assumed to be at this pressure.

The subsequent dose of adsorbate led to the oil level increasing to 60.05 cm. in the left hand manometer arm.

Therefore,

P_1 = 55.90 cm.oil

V_1 = 178.47 cm^3

P_2 = unknown

$V_2 = 178.47 - (60.05 - 32.75)\pi(0.70)^2$

From the gas law relationship

P_2 = 73.31 cm.oil

The true pressure in the balance case was equal to P_2 plus the difference in the two oil levels, which in this case was equal to 55.10 cm.oil.

The corrected pressure value was therefore 128.41 cm.oil.

In the case of desorption the volume V_2 was greater than V_1, and the difference in the oil levels had to be subtracted from the calculated value of P_2.

The conversion factor from centimetres of silicone oil to millimetres of mercury was simply the ratio of the densities multiplied by ten. At 20°C the oil density was 1.070 $g.cm^{-3}$ and that of mercury 13.546 $g.cm^{-3}$ giving a conversion factor of 0.790.

The amount of adsorbate taken up by the adsorbent was calculated by multiplying the change in datum (Δ) by the spring sensitivity (see Section 2.7.3).

3.4 Sn-Sb/N_2

From Appendix I Table 1

Loss in weight due to removal of adsorbed gases (mg)	1.034
Buoyancy correction (mg)	0.179
Correction value (mg)	0.855
Corrected weight (mg)	0.5782

TABLE 3.1

From Appendix I Table 2

Corrected Pressure (cm.oil)	Relative Pressure (P/P_0)	Apparent Amount of N_2 Adsorbed (mg)
52.70	0.055	0
123.13	0.129	0
223.67	0.232	0
347.37	0.361	0
513.22	0.533	0
725.54	0.754	0.216
1000.17	1.040	0.432
1315.79	1.368	0.649
25.12	0.026	0
87.87	0.091	0
179.23	0.186	0
283.83	0.295	0
412.62	0.429	0
571.90	0.594	0
774.03	0.804	0.216
1031.83	1.072	0.432

TABLE 3.2

ORDINATE Apparent amount N_2 adsorbed / mg

ABSCISSA Relative pressure

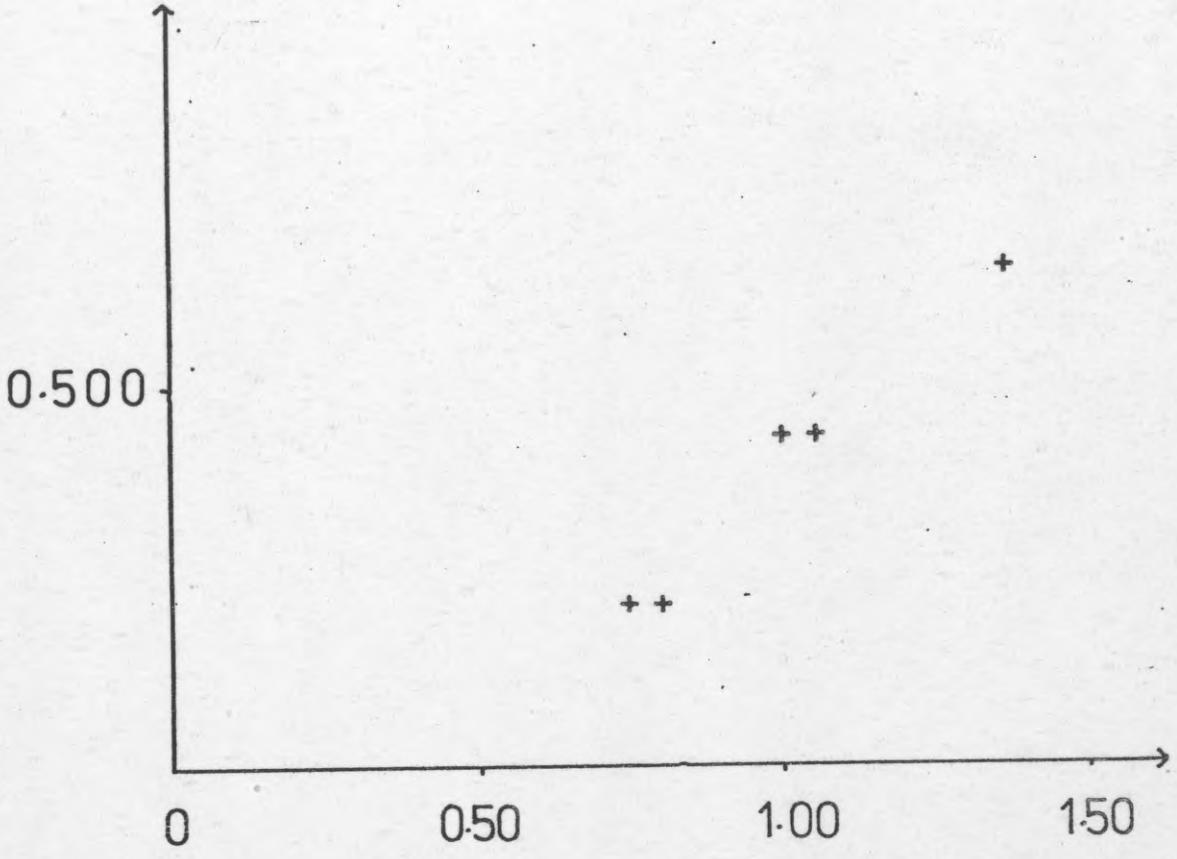

Graph 3.1

Correction curve for Sn-Sb/N_2

From Appendix I Table 3

Corrected Pressure (P)	P/P_0	P_0-P	A (mg)
45.00	0.047	917.15	0.989
108.73	0.113	853.42	1.359
199.43	0.207	762.72	1.483
306.51	0.318	655.64	1.822

A - amount N_2 physisorbed.

TABLE 3.3

For points within valid range

Observed $\frac{P}{(P_0-P)A}$	Fitted $\frac{P}{(P_0-P)A}$	Difference (%)	A (mg.)
49.63	47.61	4.079	0.989
93.73	98.86	-5.473	1.359
176.30	171.80	2.569	1.483
256.50	257.90	-0.556	1.823

Slope	773.759
Intercept	11.419
Monolayer Capacity (x)	0.124×10^{-2} g
C	68.76
S.S.A.	7.67 m^2/g
Standard Deviation	3.654%

TABLE 3.3.1

Corrected Pressure P	P/P_0	P_0-P	A (mg.)
32.80	0.034	929.35	0.679
78.34	0.081	883.81	0.958
144.00	0.150	818.85	1.297
208.84	0.217	753.31	1.421
334.03	0.347	628.12	1.606
421.82	0.438	540.33	1.761
604.92	0.629	357.23	1.946

TABLE 3.4

For points within valid range

Observed $\frac{P}{(P_0-P)A}$	Fitted $\frac{P}{(P_0-P)A}$	Difference (%)	A (mg)
51.93	52.67	-1.419	0.679
92.56	88.87	3.983	0.958
135.60	141.10	-3.994	1.297
195.10	192.60	1.226	1.421

Slope	764.897
Intercept	26.591
Monolayer Capacity (x)	0.126×10^{-2} g
C	29.77
S.S.A.	7.61 m^2/g
Standard Deviation	2.976%

TABLE 3.4.1

For points within and outside valid range

51.93	-5.99	111.50	0.679
92.56	55.71	39.80	0.958
135.60	144.70	-6.66	1.297
195.10	232.60	-19.21	1.421
331.00	402.20	-21.50	1.606
443.30	521.20	-17.56	1.761
870.00	769.30	11.58	1.946

Slope	1303.830
Intercept	-50.445
C	-24.85
Standard Deviation	44.679%

Graphical representation given in Graph 3.2

TABLE 3.4.2

Corrected Pressure P	P/P_0	P_0-P	A (mg)
34.40	0.036	927.75	0.834
82.10	0.085	880.05	1.050
149.80	0.156	812.35	1.328
236.93	0.246	725.22	1.452
360.24	0.374	601.91	1.576
508.42	0.528	453.73	1.700
629.66	0.654	332.49	1.854
445.93	0.463	516.22	1.637
193.47	0.201	768.68	1.328
28.49	0.030	933.66	0.649

TABLE 3.5

For points within valid range

Observed $\frac{P}{(P_0-P)A}$	Fitted $\frac{P}{(P_0-P)A}$	Difference (%)	A (mg)
44.45	47.07	-5.892	0.834
88.82	88.55	0.296	1.050
138.80	147.40	-6.205	1.328
225.00	223.20	0.810	1.452
189.50	185.40	2.144	1.328
47.04	41.93	10.850	0.649

Slope	836.731
Intercept	17.156
Monolayer Capacity (x)	0.117×10^{-2} g
C	49.77
S.S.A.	7.06 m^2/g
Standard Deviation	5.709%

TABLE 3.5.1

For points within and outside valid range

44.45	-11.41	125.700	0.834
88.82	59.07	33.490	1.050
138.80	159.10	-14.620	1.328
225.00	287.90	-27.940	1.452
189.50	223.60	-18.040	1.328
47.04	-20.15	142.800	0.649
379.90	470.10	-23.750	1.576
1059.50	689.00	-4.484	1.699
1022.00	868.20	15.020	1.854
527.60	596.70	-13.100	1.637

Slope	1421.780
Intercept	-62.245
C	-21.84
Standard Deviation	59.153%

See Graph 3.3

TABLE 3.5.2

ORDINATE $P/(P_o-P)A$ / g^{-1}

ABSCISSA P/P_o

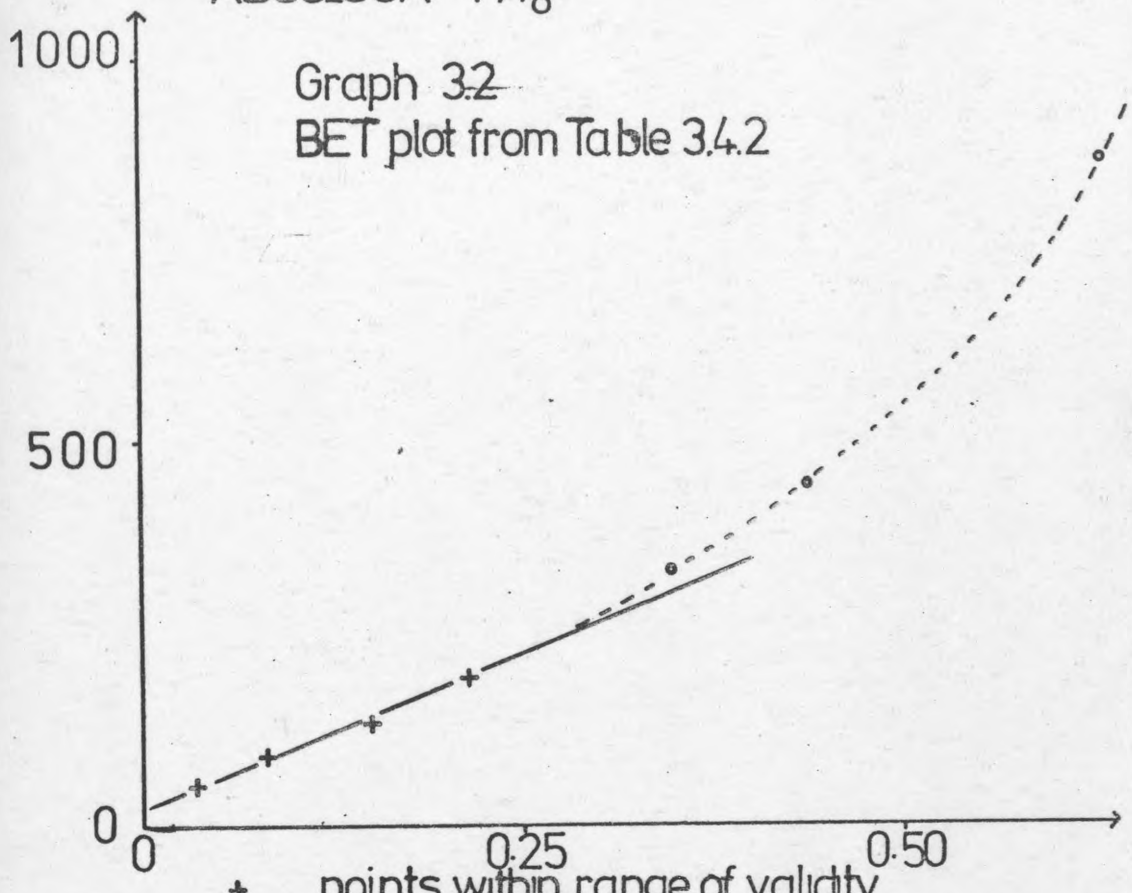

Graph 3.2

BET plot from Table 3.4.2

+ points within range of validity

° points outside range of validity

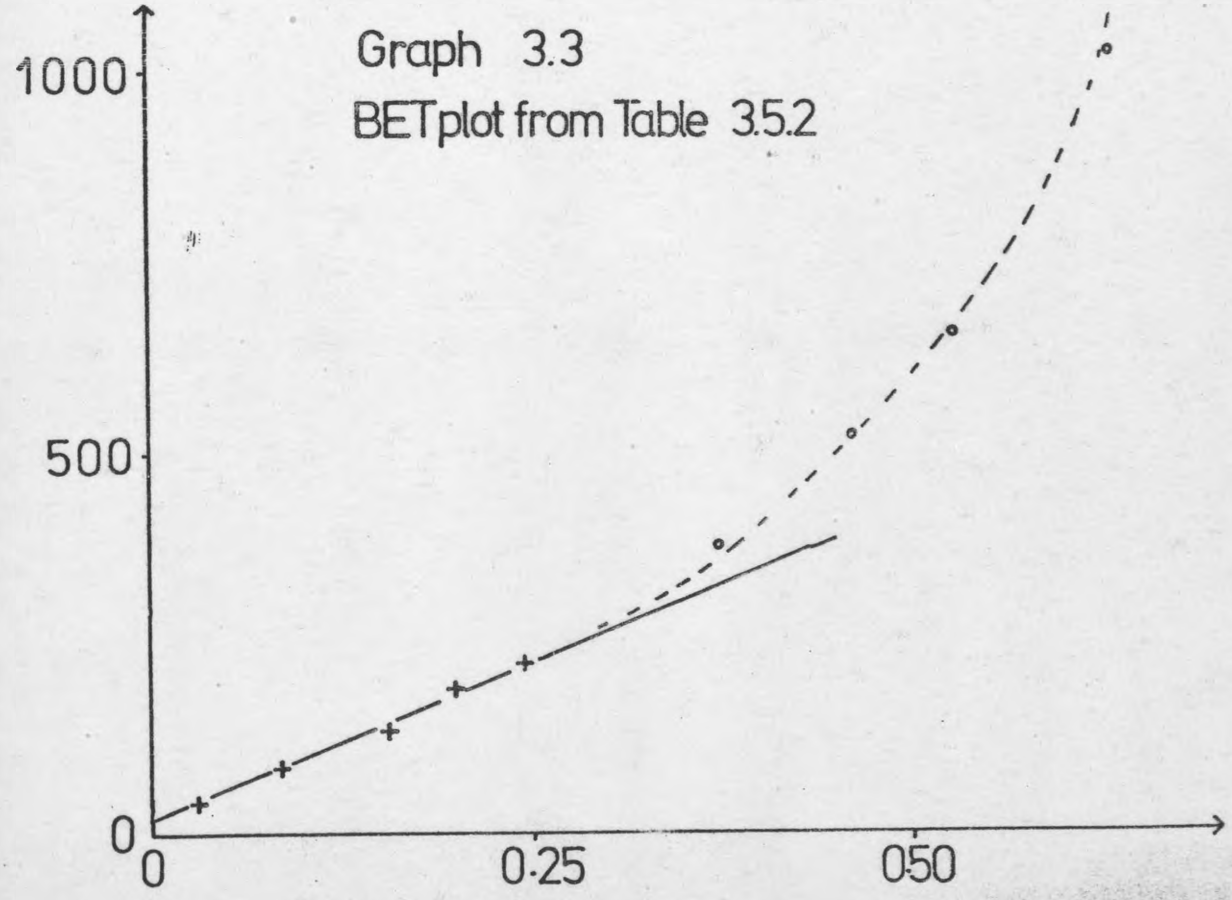

Graph 3.3

BET plot from Table 3.5.2

3.5 Carbon-black/N_2

From Appendix I Table 4

Corrected Carbon Black Weight

Loss in weight due to removal of adsorbed gases (mg)	6.025
Buoyancy correction (mg)	0.243
Correction (mg)	5.782
Corrected weight (g)	0.5259

TABLE 3.6

From Appendix I Table 5

Corrected Pressure P (cm.oil)	P/P_0	P_0-P	A (mg)
13.80	0.014	948.34	8.993
51.60	0.054	910.55	10.007
88.29	0.092	873.86	11.021
133.30	0.138	828.85	11.770
178.26	0.185	783.89	12.431
208.34	0.216	753.81	12.916
132.54	0.138	829.61	11.682
53.47	0.055	908.68	10.024
9.89	0.010	952.26	9.874

TABLE 3.7

For points within valid range

Observed $\frac{P}{(P_0-P)A}$	Fitted $\frac{P}{(P_0-P)A}$	Difference (%)
5.66	5.49	3.267
9.17	9.19	-0.265
13.66	13.75	-0.617
18.29	18.30	-0.035
21.40	21.34	0.252
13.68	13.67	-0.035
5.54	5.67	-2.322
Slope		97.395
Intercept		0.255
Monolayer Capacity (x)		0.102×10^{-1} g
C		383.1
S.S.A.		67.84 m^2/g
Standard Deviation		1.538%

TABLE 3.7.1

For points within and outside valid range

Observed $\frac{P}{(P_0-P)A}$	Fitted $\frac{P}{(P_0-P)A}$	Difference (%)
5.66	5.43	4.139
9.17	9.16	0.069
13.66	13.74	-0.561
18.29	18.31	-0.119
21.40	21.37	0.109
13.68	13.66	0.094
5.54	5.62	-1.447
1.62	1.58	2.168
1.05	1.19	-12.690

Slope	97.889
Intercept	0.179
Monolayer Capacity (x)	0.102×10^{-1}g
C	547.6
S.S.A.	67.56 m^2/g
Standard Deviation	4.445%

A graphical representation is given in Graphs 3.4 and 3.5

TABLE 3.7.2

Corrected Pressure	P/P_0	P_0-P	A (mg)
23.70	0.029	938.45	8.816
44.90	0.047	917.25	10.139
77.25	0.080	884.90	10.492
145.18	0.151	816.97	11.550
192.67	0.200	769.48	12.079

TABLE 3.8

For points within valid range

Observed $\frac{P}{(P_0-P)A}$	Fitted $\frac{P}{(P_0-P)A}$	Difference (%)
2.86	2.69	5.986
4.83	4.94	-2.268
8.32	8.36	-0.501
15.39	15.55	-1.092
20.73	20.58	0.713

Slope	101.866
Intercept	0.184
Monolayer Capacity (x)	0.979×10^{-2}g
C	555.2
S.S.A.	64.92 m^2/g
Standard Deviation	2.875%

TABLE 3.8.1

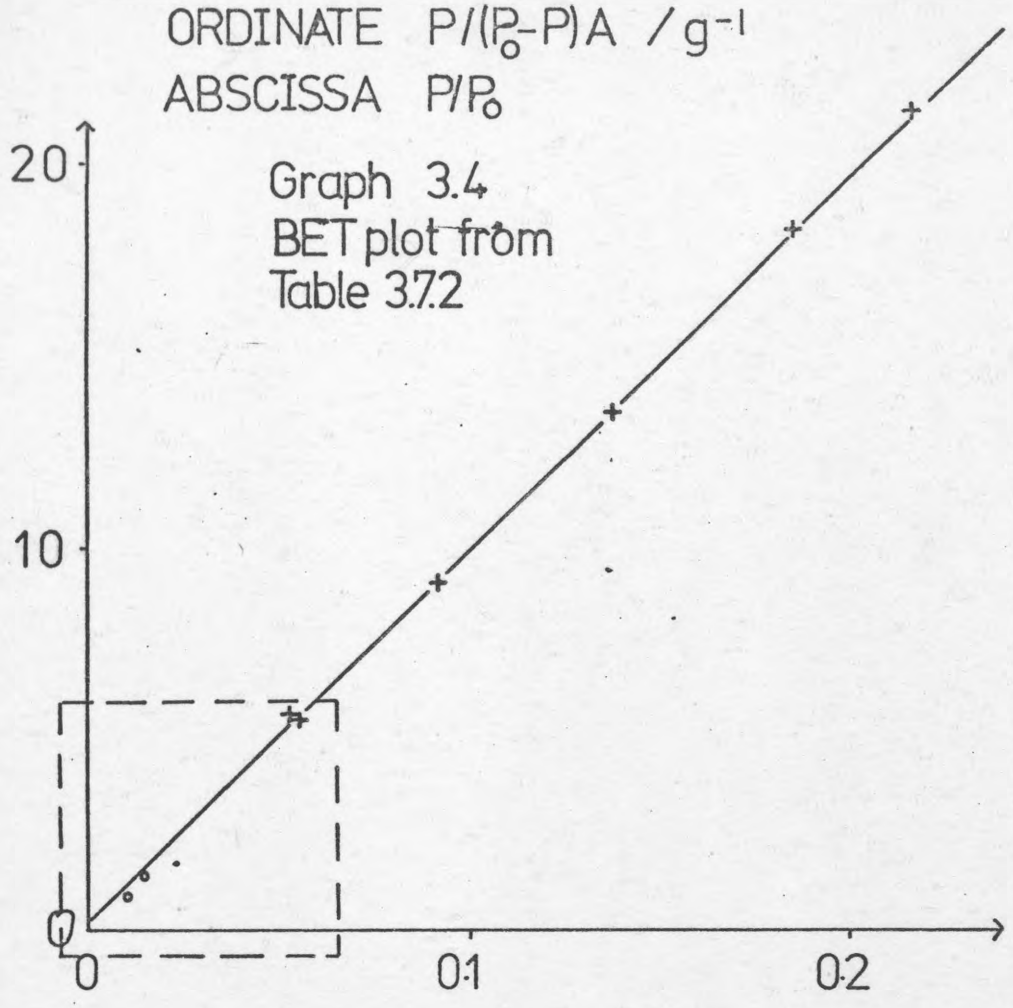

Graph 3.4
BET plot from
Table 3.7.2

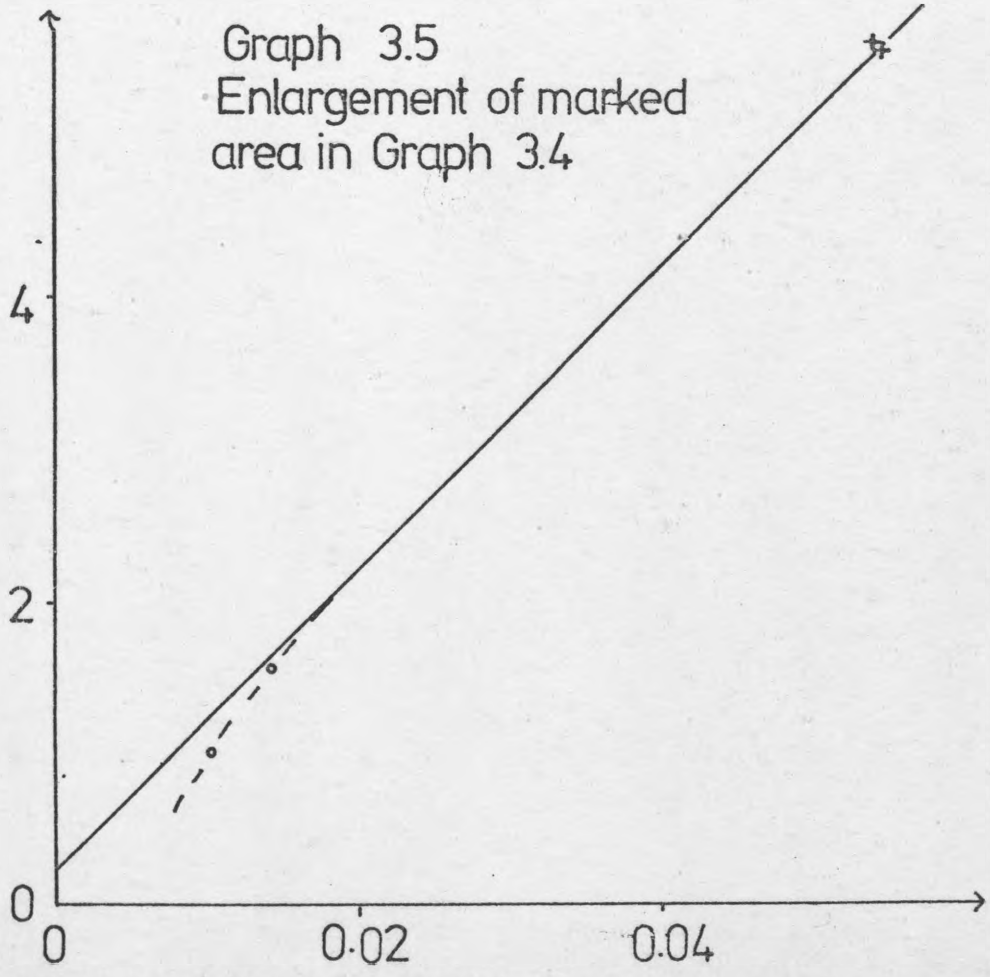

Graph 3.5
Enlargement of marked
area in Graph 3.4

Corrected Pressure	P/P_0	P_0-P	A (mg)
33.10	0.034	929.05	8.993
90.15	0.094	872.00	10.403
152.38	0.158	809.77	11.726
222.70	0.231	739.45	12.608
286.38	0.298	675.77	13.754
180.63	0.188	781.52	12.299
82.02	0.085	880.13	10.712

TABLE 3.9

For points within valid range

Observed	Fitted	Difference
3.96	3.68	7.139
9.94	9.72	2.176
16.05	16.31	-1.645
23.89	23.76	0.538
30.81	30.50	1.001
18.79	19.30	-2.722
8.70	8.86	-1.844

Slope	101.902
Intercept	0.173
Monolayer Capacity (x)	0.979×10^{-2} g
C	588.8
S.S.A.	64.90 m^2/g
Standard Deviation	3.104%

TABLE 3.9.1

3.6 Adsorption Plots for Sn-Sb/0_2 at 80, 90 and 100°C

The buoyancy/thermal convection effect correction was made by using the "apparent" amount of inert argon adsorbed (Appendix III Table 1) to calculate the corresponding amount of oxygen using the relationship described in section 3.1 at temperatures of 80 and 100°C. The results are tabulated below and shown in Graph 3.6.

P cm.oil	Oxygen 'adsorbed' (mg.)	
6.80	0.049	T=80°C
15.80	0.074	
20.50	0.099	
49.30	0.148	
38.70	0.124	
28.90	0.124	
13.00	0.074	
2.10	0.025	

TABLE 3.10

6.80	0.049	T=100°C
19.90	0.099	
28.90	0.124	
44.30	0.148	
32.90	0.124	
11.30	0.074	

TABLE 3.11

The key to the following tables is as follows:

P_1 - pressure in cm.oil

P_2 - pressure in mm.mercury

A - uncorrected amount of oxygen adsorbed (mg)

B - correction value (to be subtracted) (mg)

C - corrected amount of oxygen adsorbed (mg)

D - amount adsorbate adsorbed (mg) per g. of catalyst

E - coverage of sites

The graphical correction curve is required so that the correction value may be read off directly at any pressure used.

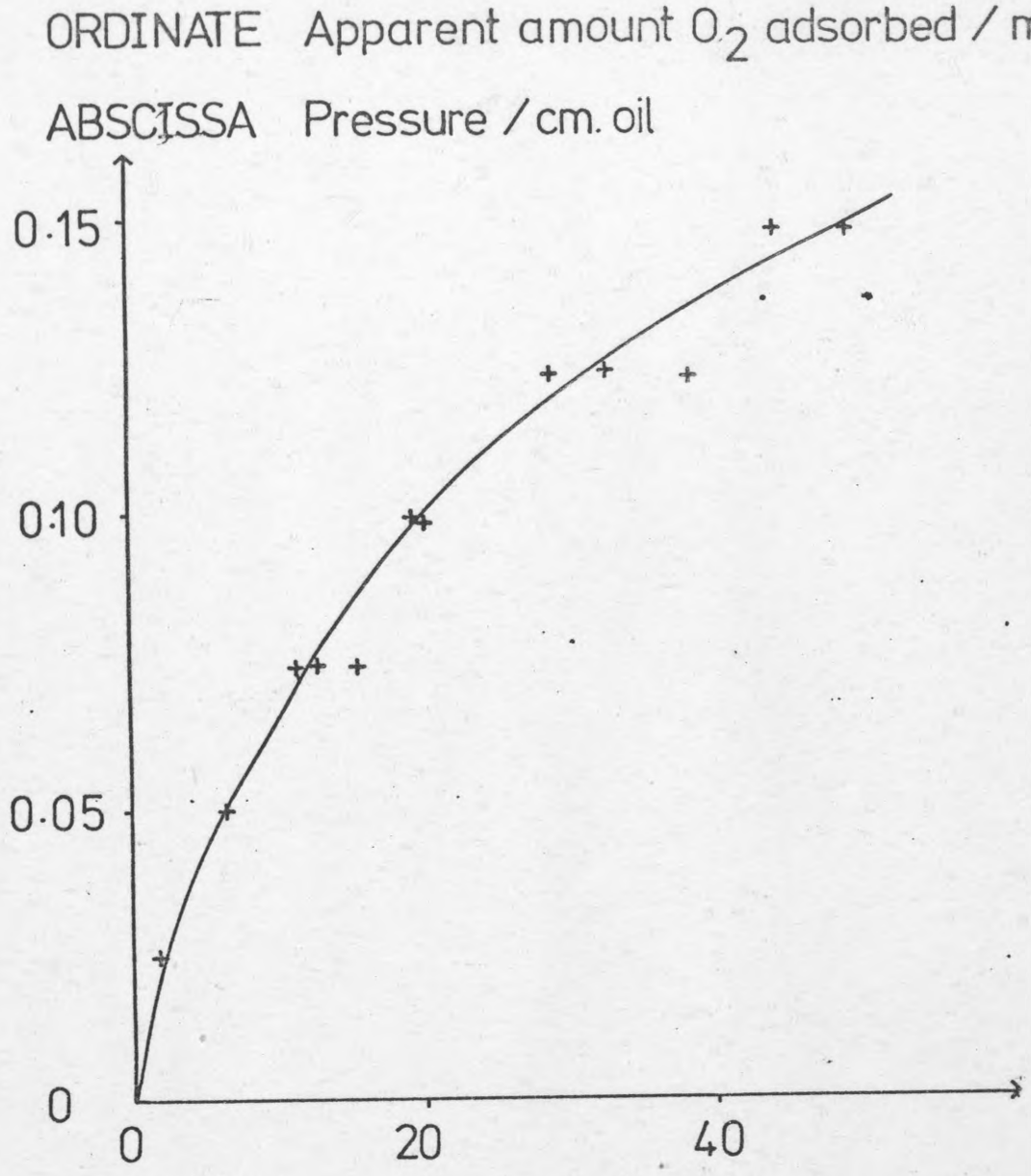

Graph 3.6

Correction curve for Sn–Sb/O_2

Tables 3.12 - 3.20. From Appendix III Tables 2-4.

Corrected Weight of Catalyst 0.5782g.

BLOCK 1 T = 80°C

Run 1

P_1	P_2	A (mg)	B (mg)	C (mg)	D (^{mg}/g-catalyst)	E
0.20	0.158	0.132	0.001	0.131	0.227	0.078
0.40	0.316	0.397	0.003	0.394	0.681	0.236
0.80	0.632	0.793	0.008	0.785	1.358	0.471
1.70	1.343	0.970	0.014	0.956	1.653	0.574
3.50	2.765	1.278	0.027	1.251	2.164	0.751
5.80	4.581	1.587	0.042	1.545	2.672	0.927
7.80	6.161	1.719	0.053	1.666	2.881	1
9.00	7.109	1.719	0.059	1.660	2.871	1

TABLE 3.12

Run 2

0.20	0.158	0.132	0.001	0.131	0.227	0.078
0.50	0.395	0.529	0.004	0.525	0.908	0.315
0.70	0.553	0.617	0.006	0.611	1.057	0.367
1.50	1.185	1.014	0.013	1.001	1.731	0.601
2.60	2.053	1.146	0.021	1.125	1.946	0.675
3.60	2.844	1.322	0.029	1.293	2.236	0.776
4.50	3.555	1.455	0.034	1.421	2.458	0.853
6.60	5.213	1.631	0.047	1.584	2.740	0.950
8.80	6.951	1.719	0.058	1.661	2.873	1
9.00	7.109	1.719	0.059	1.660	2.871	1

TABLE 3.13

Run 3

0.10	0.079	0.088	0.0	0.088	0.152	0.053
0.40	0.316	0.353	0.003	0.350	0.605	0.210
0.90	0.711	0.661	0.009	0.652	1.128	0.391
2.50	1.975	1.058	0.020	1.038	1.795	0.623
4.30	3.397	1.367	0.032	1.335	2.309	0.801
6.70	5.292	1.675	0.047	1.628	2.817	0.977
8.00	6.319	1.719	0.054	1.665	2.880	1
9.00	7.109	1.719	0.059	1.660	2.871	1

TABLE 3.14

BLOCK 2 T = 90°C

Run 1

0.50	0.395	0.485	0.004	0.481	0.832	0.314
1.10	0.869	0.749	0.010	0.739	1.278	0.482
1.50	1.185	0.838	0.013	0.825	1.427	0.539
2.00	1.580	0.882	0.017	0.865	1.496	0.565
3.50	2.765	1.234	0.027	1.207	2.088	0.788
5.80	4.581	1.455	0.042	1.413	2.444	0.922
8.20	6.477	1.587	0.055	1.532	2.650	1
10.20	8.057	1.587	0.065	1.522	2.632	1

TABLE 3.15

Run 2

0.40	0.316	0.353	0.003	0.350	0.605	0.228
0.70	0.553	0.705	0.006	0.699	1.209	0.456
1.80	1.422	0.882	0.015	0.867	1.499	0.566
3.10	2.449	1.102	0.024	1.078	1.864	0.704
4.70	3.713	1.278	0.035	1.243	2.150	0.811
6.40	5.055	1.411	0.046	1.365	2.361	0.891
8.30	6.556	1.587	0.056	1.531	2.648	1
8.70	6.872	1.587	0.059	1.528	2.643	1

TABLE 3.16

Run 3

0.10	0.079	0.132	0.0	0.132	0.228	0.086
0.30	0.237	0.264	0.002	0.262	0.453	0.171
0.70	0.553	0.661	0.006	0.655	1.133	0.428
1.10	0.869	0.793	0.010	0.783	1.354	0.653
2.90	2.291	1.058	0.023	1.035	1.790	0.676
4.70	3.713	1.278	0.035	1.243	2.150	0.811
7.30	5.766	1.499	0.050	1.449	2.506	0.946
9.50	7.504	1.587	0.062	1.525	2.637	1
11.50	9.081	1.587	0.071	1.516	2.622	1

TABLE 3.17

BLOCK 3 T = 100°C

Run 1

0.30	0.237	0.176	0.002	0.174	0.301	0.188
0.70	0.553	0.265	0.006	0.259	0.448	0.281
1.70	1.343	0.397	0.014	0.383	0.662	0.415
3.20	2.528	0.573	0.026	0.547	0.946	0.593
5.00	3.950	0.749	0.037	0.712	1.231	0.772
6.90	5.450	0.970	0.048	0.922	1.595	1
8.90	7.030	0.970	0.059	0.911	1.576	1

TABLE 3.18

Run 2

0.10	0.079	0.132	0.0	0.132	0.228	0.143
0.50	0.395	0.220	0.004	0.216	0.374	0.234
1.80	1.422	0.441	0.015	0.426	0.737	0.462
3.40	2.686	0.661	0.027	0.634	1.097	0.688
5.60	4.423	0.925	0.041	0.884	1.529	0.959
7.10	5.608	0.970	0.049	0.921	1.593	1
9.40	7.425	0.970	0.061	0.909	1.572	1

TABLE 3.19

Run 3

0.30	0.237	0.176	0.002	0.174	0.301	0.189
0.80	0.632	0.265	0.008	0.257	0.444	0.279
1.90	1.501	0.441	0.016	0.425	0.735	0.461
3.40	2.686	0.617	0.027	0.590	1.020	0.640
5.80	4.581	0.882	0.042	0.840	1.453	0.911
7.60	6.003	0.970	0.056	0.914	1.581	1
9.40	7.425	0.970	0.061	0.909	1.572	1

TABLE 3.20

Graphs 3.7 - 3.9 show the amount of gas adsorbed per gramme of catalyst at 80, 90 and 100°C respectively. Graphs 3.10 - 3.12 are plots of coverage (θ) against pressure which will be referred to in the section concerning heats of adsorption.

3.7 Adsorption Plots for Sn-Sb/C_3H_6 at 200, 225 and 250°C

The buoyancy/thermal convection correction was made exactly as described in section 3.5 from data values obtained from Appendix II Table 1 and tabulated below and plotted in Graph 3.13.

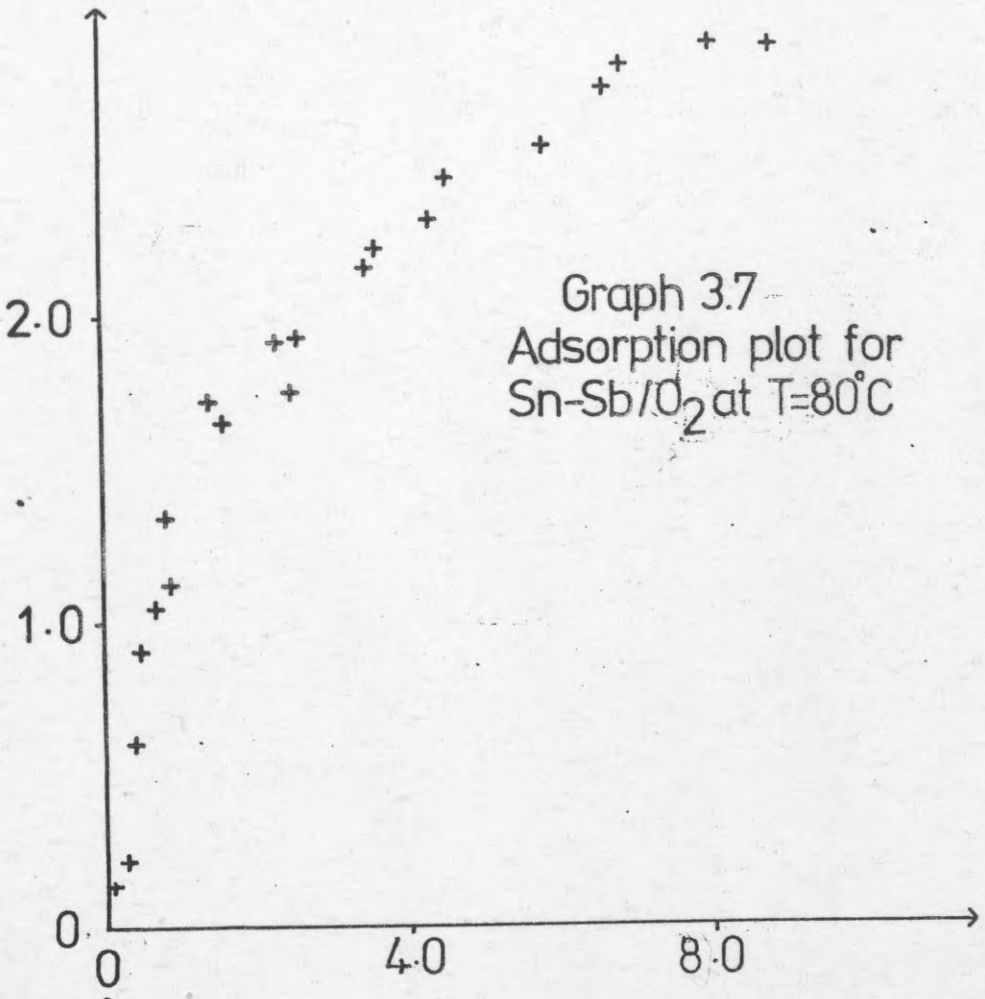

Graph 3.7
Adsorption plot for
Sn-Sb/O_2 at T=80°C

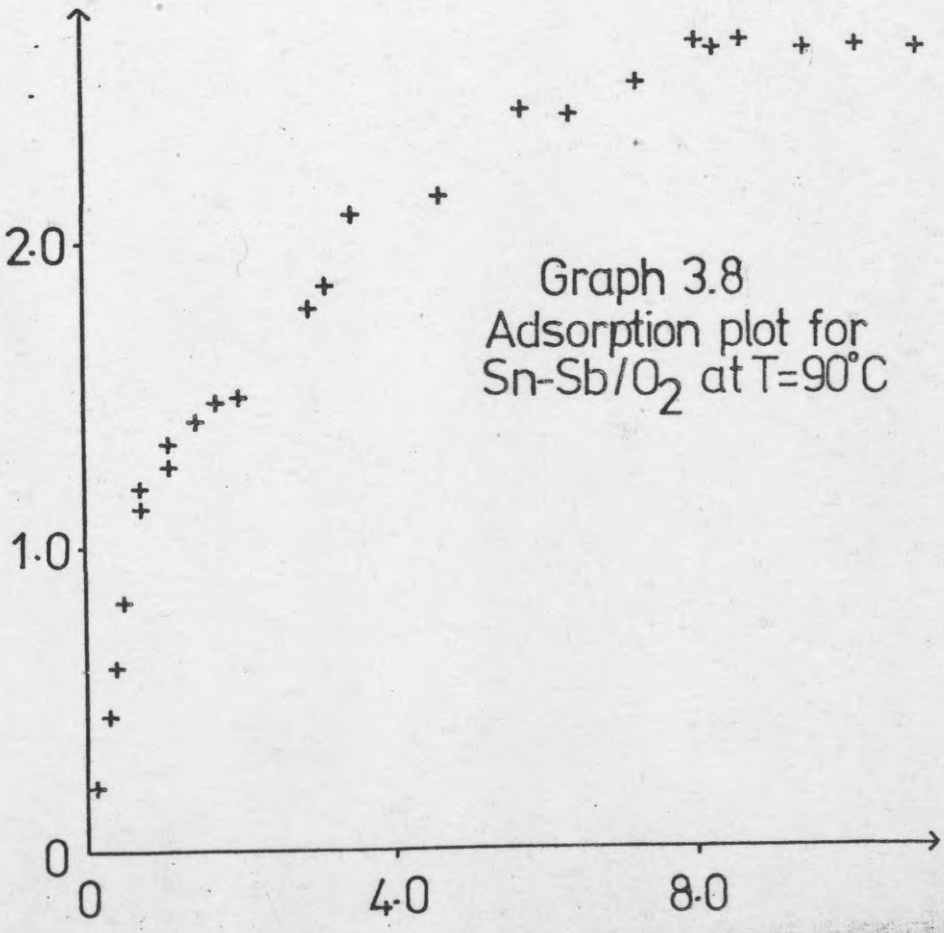

Graph 3.8
Adsorption plot for
Sn-Sb/O_2 at T=90°C

ORDINATE mg adsorbate per g adsorbent
ABSCISSA Pressure / cm. oil

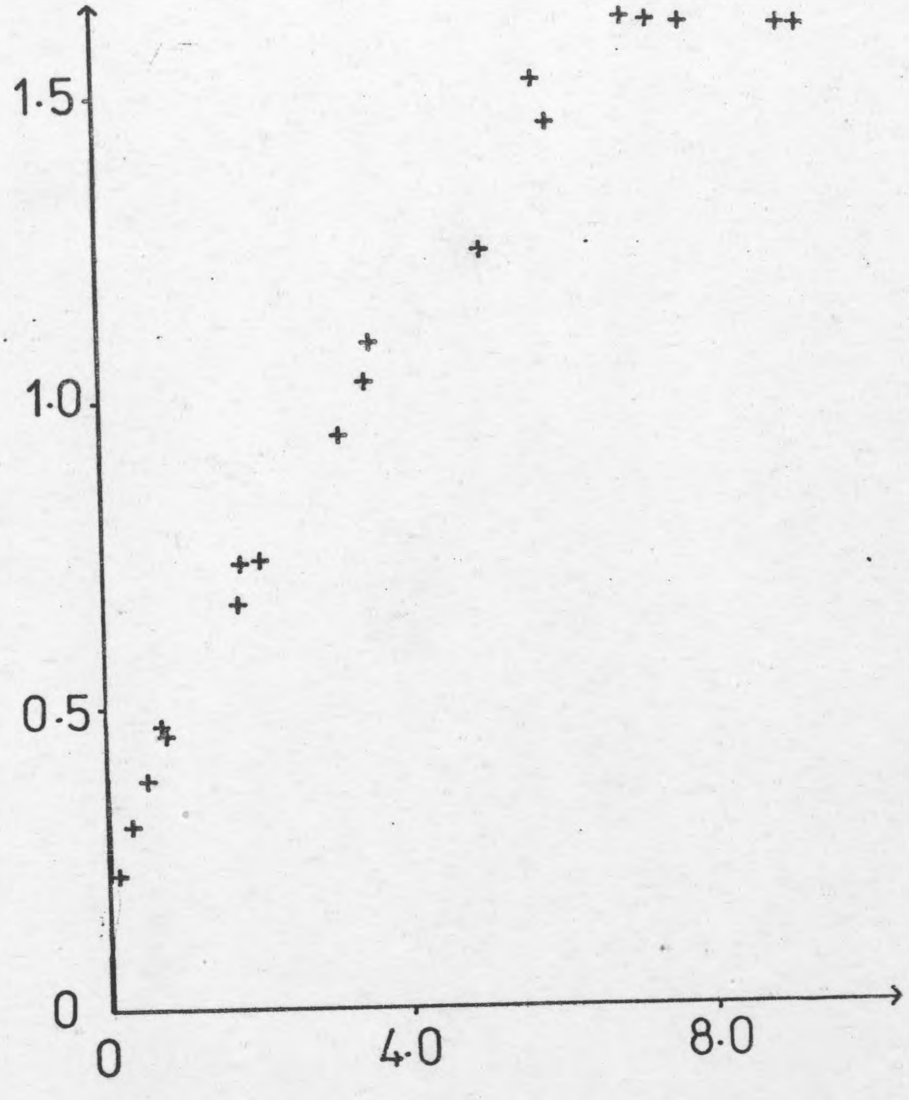

Graph 3.9

Adsorption plot for Sn-Sb at T=100°C

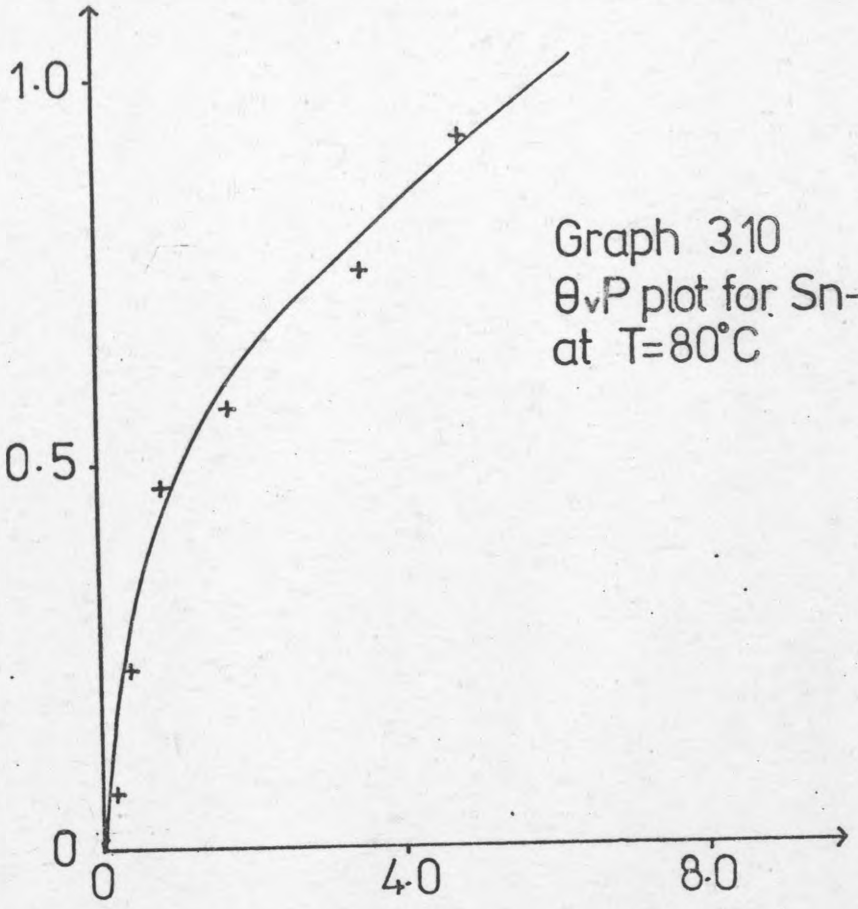

Graph 3.10
θ v P plot for Sn-Sb/O_2
at T=80°C

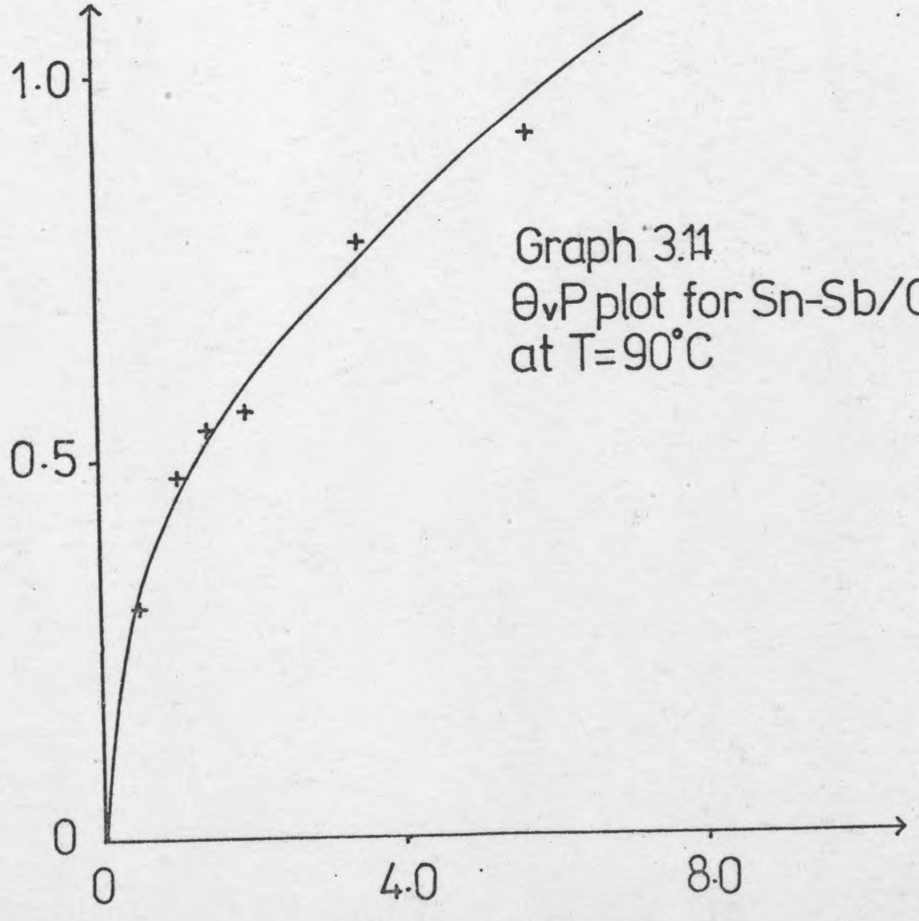

Graph 3.11
θ v P plot for Sn-Sb/O_2
at T=90°C

ORDINATE Coverage θ
ABSCISSA Pressure/cm. oil

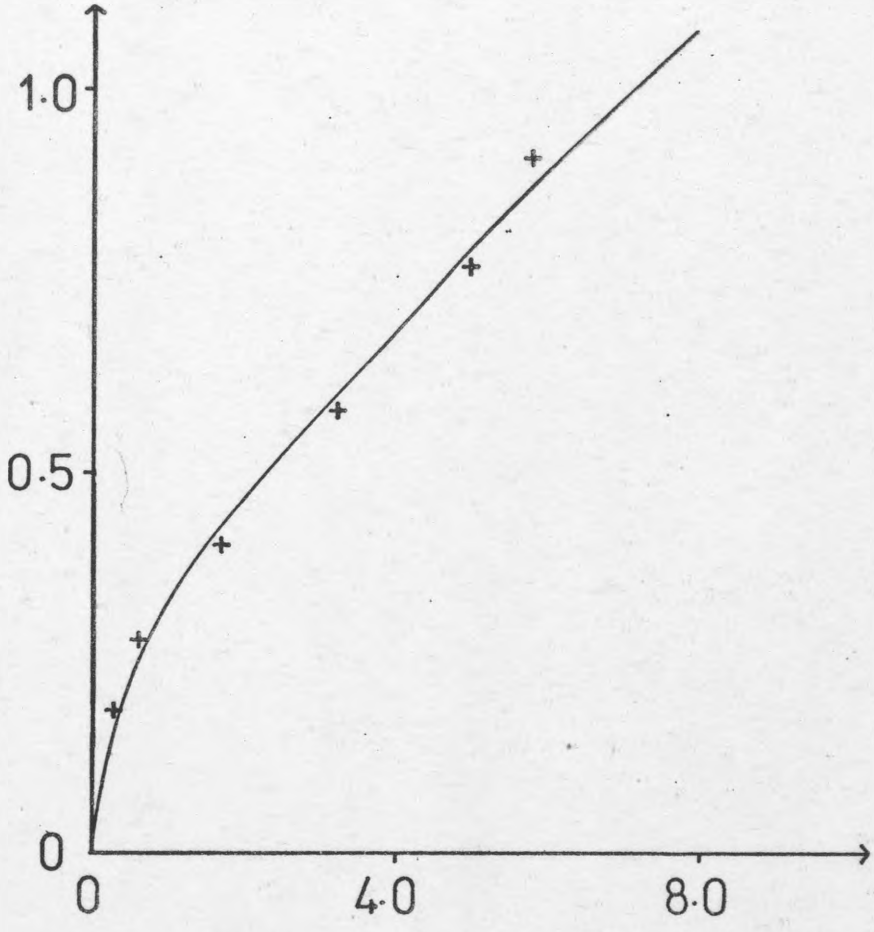

Graph 3.12

θ v P plot for Sn-Sb/O_2 at T=100°C

P cm.oil	Propene 'adsorbed' (mg)	
0.30	0.065	T=200°C
1.00	0.130	
3.80	0.227	
6.10	0.292	
9.00	0.390	
1.20	0.130	
2.60	0.162	
5.00	0.260	
6.10	0.292	

TABLE 3.21

0.90	0.097	T=250°C
2.20	0.162	
3.70	0.195	
6.10	0.227	
8.40	0.292	
0.40	0.065	
1.50	0.130	
3.40	0.195	
5.40	0.227	
8.0	0.292	

TABLE 3.22

The key for the following tables is as described in section 3.5.

Tables 3.23 - 3.31 from Appendix II Tables 2 - 4

BLOCK 1 T = 225°C

Run 1

P_1	P_2	A (mg)	B (mg)	C (mg)	D ($^{mg}/_{g\text{-catalyst}}$)	E
0.20	0.158	0.485	0.030	0.455	0.787	0.322
0.70	0.553	0.705	0.083	0.623	1.077	0.441
1.00	0.790	0.926	0.106	0.820	1.418	0.580
1.30	1.027	1.058	0.123	0.935	1.617	0.661
1.60	1.264	1.234	0.140	1.094	1.892	0.774
2.00	1.580	1.411	0.157	1.254	2.169	0.887
2.40	1.896	1.587	0.173	1.414	2.446	1
2.60	2.053	1.587	0.180	1.407	2.433	1

TABLE 3.23

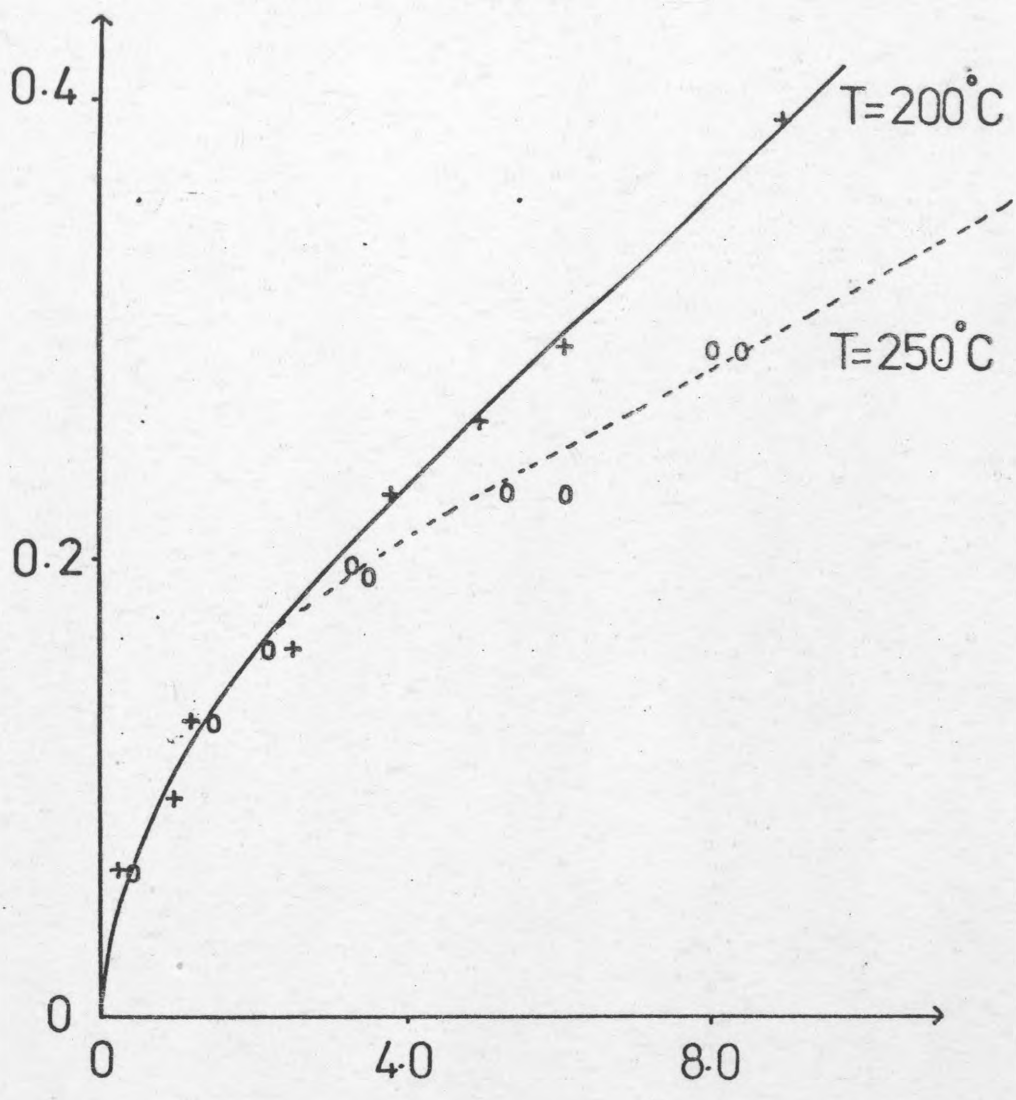

Graph 3.13

Correction curve for Sn-Sb/C_3H_6

Run 2

0.10	0.079	0.265	0.017	0.248	0.429	0.175
0.30	0.237	0.617	0.043	0.574	0.993	0.406
0.50	0.395	0.750	0.063	0.687	1.188	0.486
0.90	0.711	0.882	0.100	0.782	1.352	0.553
1.20	0.948	1.058	0.120	0.938	1.622	0.663
1.70	1.343	1.278	0.145	1.133	1.960	0.801
2.00	1.580	1.411	0.157	1.254	2.169	0.887
2.40	1.896	1.587	0.173	1.414	2.446	1
2.60	2.054	1.587	0.180	1.407	2.433	1

TABLE 3.24

Run 3

0.10	0.079	0.265	0.017	0.248	0.429	0.175
0.30	0.237	0.573	0.043	0.530	0.917	0.375
0.90	0.711	0.838	0.100	0.738	1.276	0.522
1.20	0.948	1.058	0.120	0.938	1.622	0.663
1.60	1.264	1.278	0.140	1.138	1.968	0.805
2.20	1.734	1.543	0.165	1.378	2.383	0.976
2.40	1.896	1.587	0.173	1.414	2.446	1
2.60	2.054	1.587	0.180	1.407	2.443	1

TABLE 3.25

BLOCK 2 T = 250°C

Run 1

0.20	0.158	0.132	0.030	0.102	0.176	0.230
0.50	0.395	0.265	0.063	0.202	0.349	0.455
0.70	0.553	0.353	0.145	0.208	0.360	0.468
1.00	0.790	0.485	0.106	0.379	0.656	0.854
1.30	1.335	0.573	0.129	0.444	0.768	1
1.60	1.264	0.573	0.140	0.433	0.749	1

TABLE 3.26

Run 2

0.10	0.079	0.088	0.017	0.061	0.106	0.137
0.40	0.316	0.220	0.053	0.167	0.289	0.376
0.80	0.632	0.353	0.093	0.260	0.450	0.586
0.90	0.711	0.441	0.100	0.341	0.590	0.768
1.20	0.948	0.529	0.120	0.409	0.707	0.921
1.50	1.185	0.573	0.135	0.438	0.758	1
1.90	1.501	0.573	0.150	0.423	0.732	1

TABLE 3.27

Run 3

0.10	0.079	0.088	0.017	0.061	0.106	0.137
0.30	0.237	0.176	0.043	0.133	0.230	0.300
0.50	0.395	0.265	0.063	0.202	0.349	0.455
0.60	0.474	0.309	0.073	0.236	0.408	0.532
1.00	0.790	0.441	0.106	0.335	0.579	0.755
1.20	0.948	0.529	0.120	0.409	0.707	0.921
1.50	1.185	0.573	0.135	0.438	0.758	1
1.70	1.343	0.573	0.145	0.428	0.740	1

TABLE 3.28

BLOCK 3 T = 200°C

Run 1

0.20	0.158	0.220	0.030	0.190	0.329	0.266
0.50	0.395	0.529	0.063	0.466	0.806	0.652
0.70	0.553	0.617	0.083	0.534	0.924	0.747
1.10	0.869	0.705	0.113	0.592	1.024	0.828
1.50	1.185	0.838	0.135	0.703	1.216	1
1.80	1.422	0.838	0.150	0.688	1.190	1

TABLE 3.29

Run 2

0.20	0.158	0.265	0.030	0.235	0.406	0.329
0.50	0.395	0.529	0.063	0.466	0.806	0.652
0.60	0.474	0.573	0.073	0.500	0.865	0.699
1.00	0.790	0.661	0.106	0.555	0.960	0.776
1.20	0.948	0.793	0.120	0.673	1.164	0.942
1.60	1.264	0.838	0.140	0.698	1.207	1
1.80	1.422	0.838	0.150	0.688	1.190	1

TABLE 3.30

Run 3

0.10	0.079	0.132	0.017	0.115	0.199	0.278
0.40	0.316	0.441	0.053	0.388	0.671	0.543
0.90	0.711	0.661	0.100	0.561	0.970	0.785
1.10	0.869	0.749	0.113	0.636	1.100	0.890
1.30	1.027	0.838	0.123	0.715	1.237	1
1.40	1.106	0.838	0.130	0.708	1.225	1

TABLE 3.31

Graphs 3.14 - 3.16 represent the amount of gas adsorbed per gramme of catalyst at 200, 250 and 225°C. Graphs 3.17 - 3.19 represent coverage against pressure which will be referred to in the section concerning heats of adsorption.

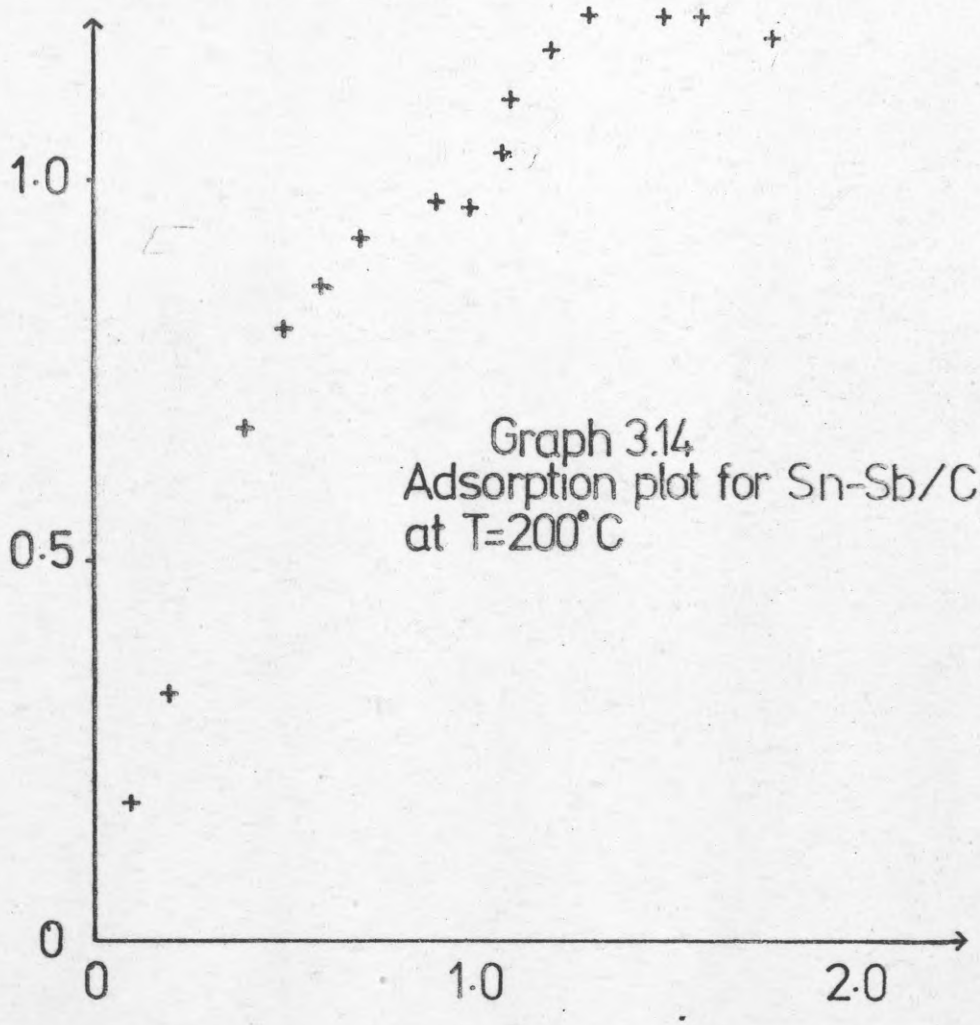

Graph 3.14
Adsorption plot for Sn-Sb/C_3H_6
at T=200°C

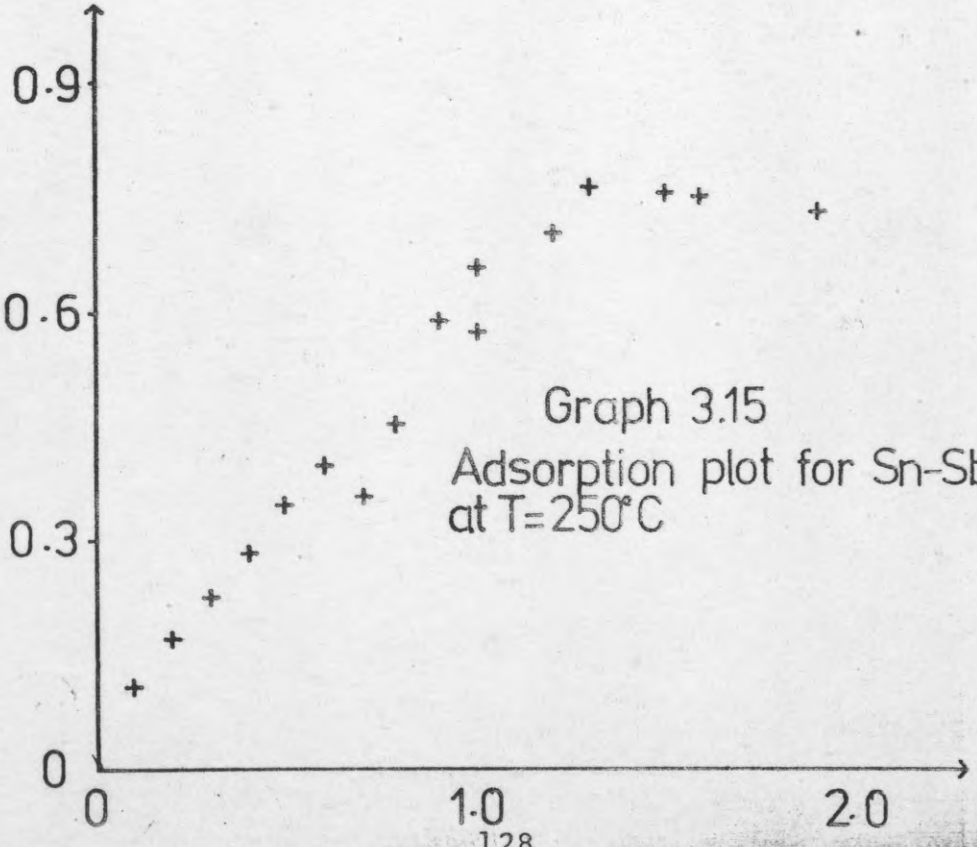

Graph 3.15
Adsorption plot for Sn-Sb/C_3H_6
at T=250°C

ORDINATE mg adsorbate per g adsorbent
ABSCISSA Pressure /cm.oil

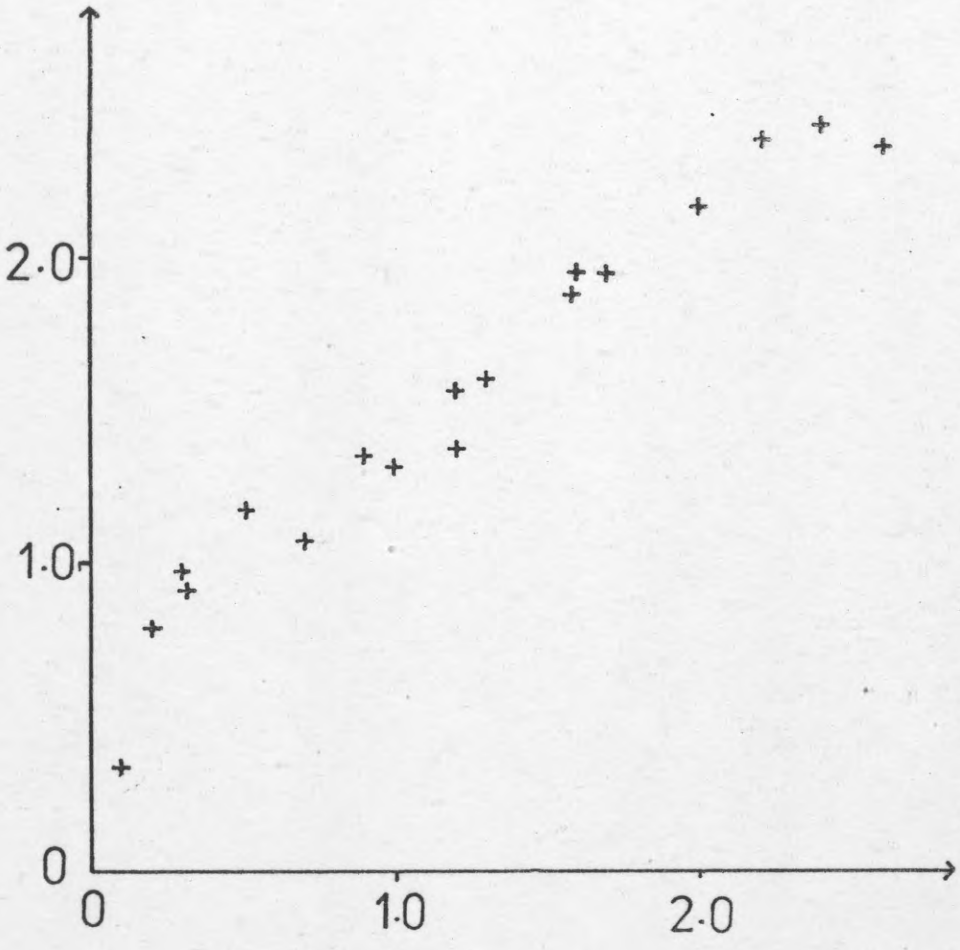

Graph 3.16

Adsorption plot for Sn-Sb/C_3H_6
at T= 225°C

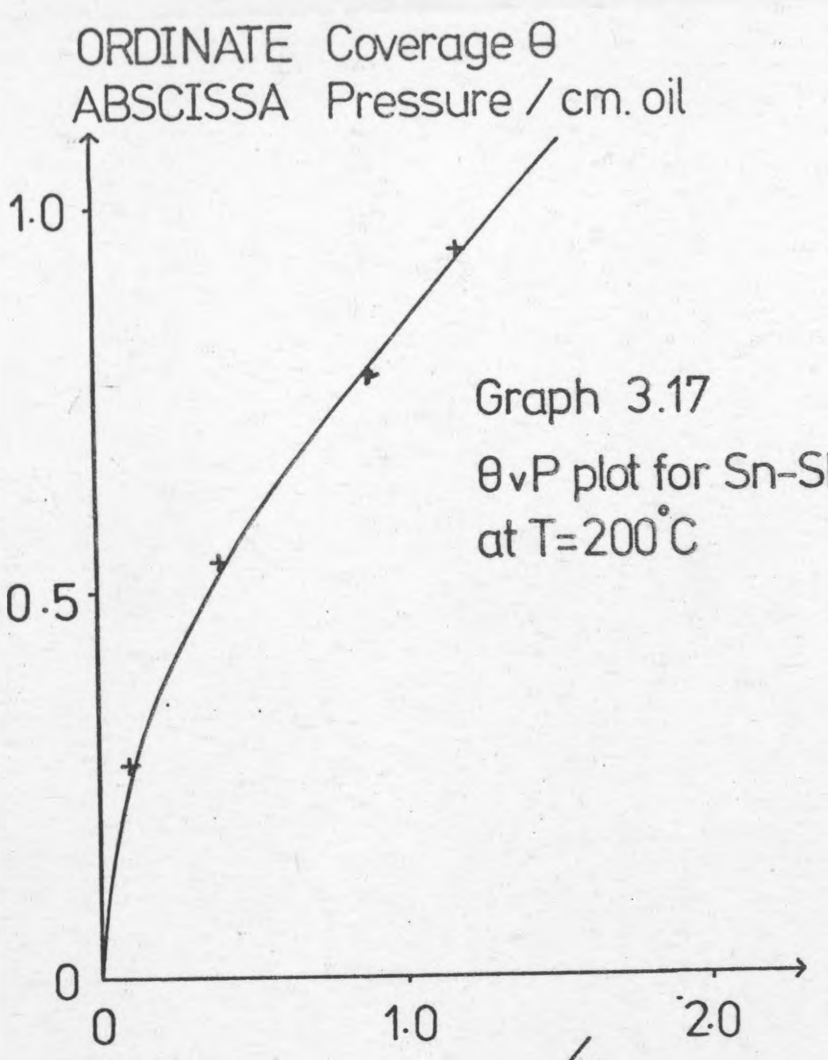

Graph 3.17

θ v P plot for Sn-Sb/C_3H_6 at T=200°C

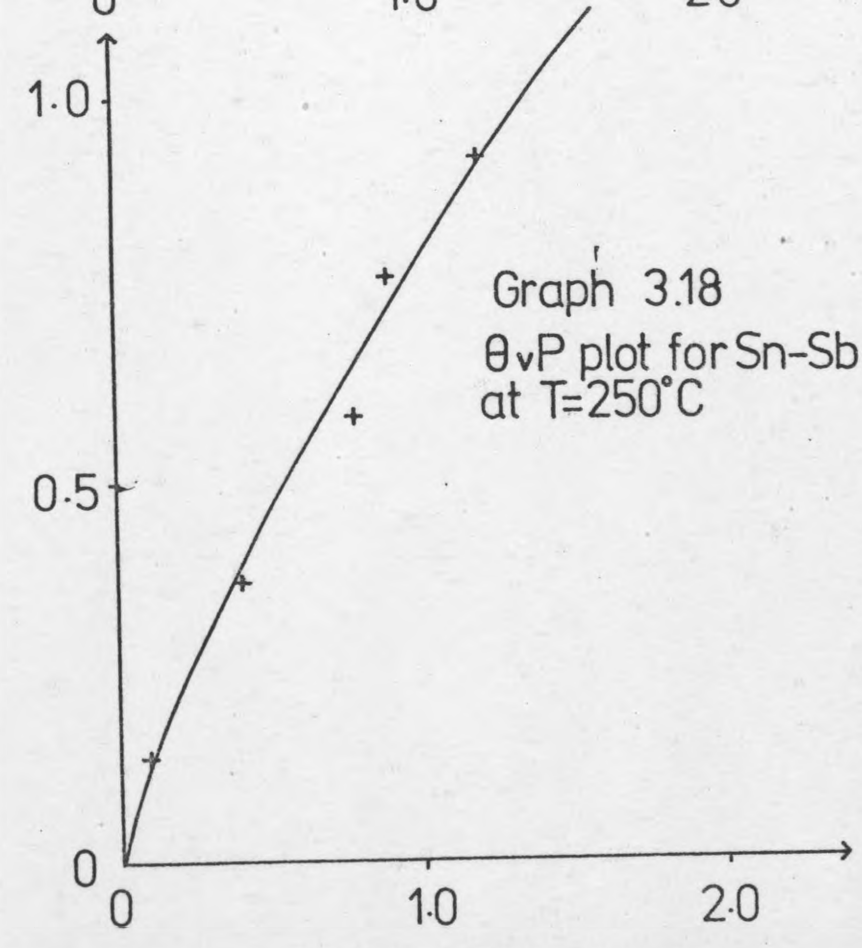

Graph 3.18

θ v P plot for Sn-Sb/C_3H_6 at T=250°C

ORDINATE Coverage θ
ABSCISSA Pressure / cm.oil

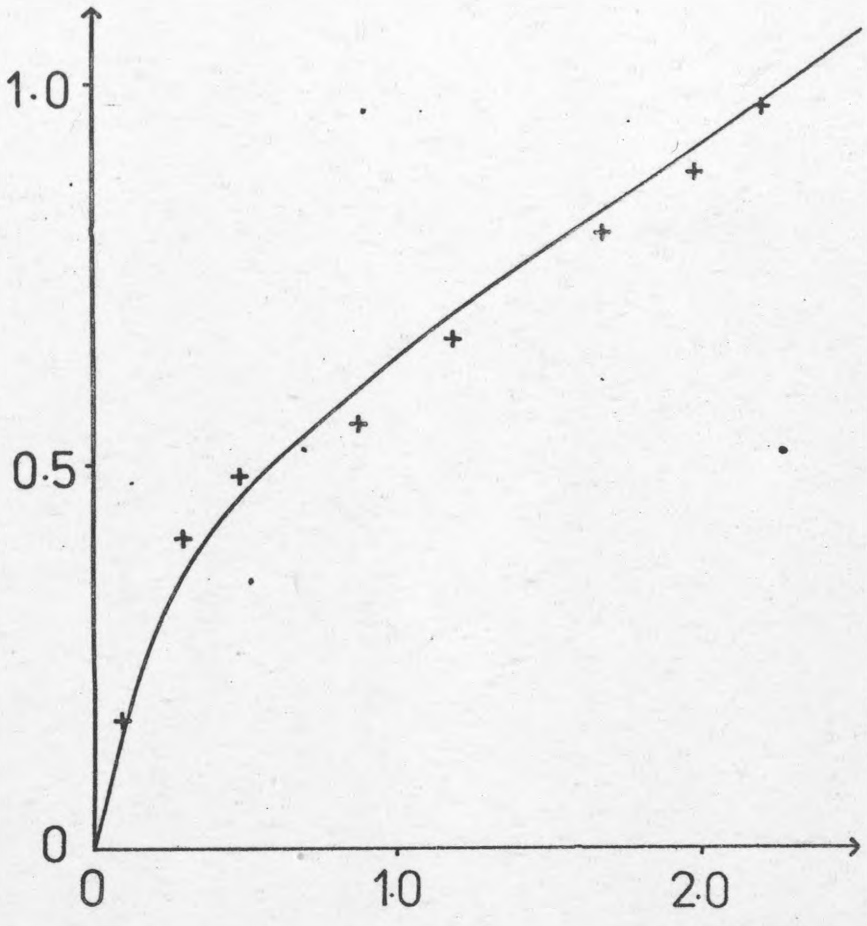

Graph 3.19

θ v P. plot for Sn-Sb/C_3H_6
at T=225°C

3.8 Adsorption Plots for Sn-Sb/1-C_4H_8 at 170, 150 and 130°C

The buoyancy/thermal convection correction was made exactly as described in section 3.5 from data values obtained from Appendix IV Table 1 and tabulated below. The results are shown in Graph 3.20.

P cm.oil	Butene 'adsorbed' (mg)	
2.00	0	T=170°C
14.60	0.130	
26.00	0.260	
39.00	0.389	
2.70	0	
6.10	0.086	
18.90	0.173	
29.80	0.260	

TABLE 3.32

7.20	0.086	T=130°C
15.20	0.130	
25.00	0.216	
34.40	0.303	
2.60	0.043	
14.00	0.130	
18.80	0.173	
27.80	0.260	

TABLE 3.33

The key for the following tables is as described in section 3.5.

Tables 3.34 to 3.42 are from Appendix IV Tables 2-4.

BLOCK 1 T = 170°C

Run 1

P_1	P_2	A (mg)	B (mg)	C (mg)	D ($^{mg}/_{g\text{-catalyst}}$)	E
0.10	0.079	0.062	0.001	0.061	0.105	0.136
0.80	0.632	0.278	0.011	0.267	0.462	0.597
1.10	0.869	0.432	0.015	0.417	0.721	0.933
1.20	0.948	0.463	0.016	0.447	0.773	1
1.40	1.106	0.463	0.019	0.444	0.768	1

TABLE 3.34

ORDINATE Apparent amount C_4H_8 adsorbed / mg
ABSCISSA Pressure / cm. oil

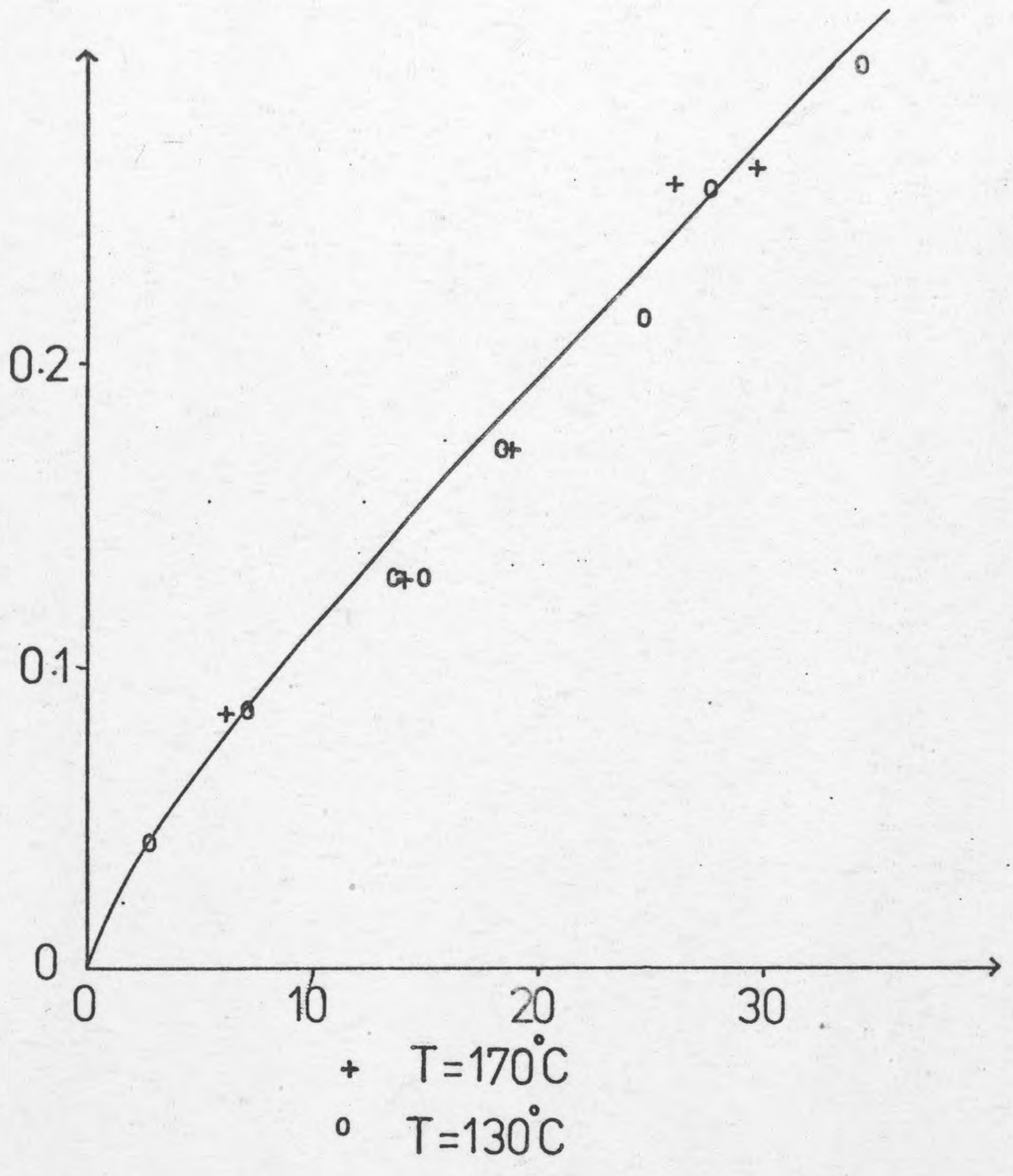

Graph 3.20

Correction curve for Sn-Sb / C_4H_8

Run 2

0.10	0.079	0.093	0.001	0.092	0.159	0.206
0.20	0.158	0.124	0.003	0.121	0.209	0.271
0.70	0.553	0.309	0.010	0.299	0.517	0.669
1.00	0.790	0.402	0.014	0.388	0.671	0.868
1.10	0.869	0.433	0.015	0.418	0.723	0.935
1.20	0.948	0.463	0.016	0.447	0.773	1
1.30	1.027	0.463	0.018	0.445	0.770	1

TABLE 3.35

Run 3

0.20	0.158	0.154	0.003	0.151	0.261	0.338
0.40	0.316	0.216	0.006	0.210	0.363	0.470
0.70	0.553	0.309	0.010	0.299	0.517	0.669
0.90	0.711	0.371	0.013	0.358	0.619	0.801
1.00	0.790	0.402	0.014	0.388	0.671	0.868
1.20	0.948	0.463	0.016	0.447	0.773	1
1.40	1.106	0.463	0.019	0.444	0.768	1

TABLE 3.36

BLOCK 2 T = 150°C

Run 1

P_1	P_2	A (mg)	B (mg)	C (mg)	D (^{mg}/g-catalyst)	E
0.10	0.079	0.185	0.001	0.184	0.318	0.322
0.30	0.237	0.278	0.004	0.274	0.474	0.480
0.60	0.474	0.402	0.008	0.394	0.681	0.690
1.00	0.790	0.525	0.014	0.511	0.884	0.895
1.20	0.948	0.587	0.016	0.571	0.988	1
1.40	1.106	0.587	0.019	0.568	0.982	1

TABLE 3.37

Run 2

0.20	0.158	0.247	0.003	0.244	0.422	0.427
0.50	0.395	0.371	0.007	0.364	0.630	0.637
0.60	0.474	0.432	0.008	0.424	0.733	0.743
1.00	0.790	0.494	0.014	0.480	0.830	0.841
1.20	0.948	0.587	0.016	0.571	0.988	1
1.50	1.185	0.587	0.020	0.567	0.981	1

TABLE 3.38

Run 3

0.10	0.079	0.185	0.001	0.184	0.318	0.322
0.20	0.158	0.247	0.003	0.244	0.422	0.427
0.40	0.316	0.309	0.006	0.303	0.524	0.531
0.90	0.711	0.463	0.013	0.450	0.778	0.788
1.20	0.948	0.587	0.016	0.571	0.987	1
1.40	1.106	0.587	0.019	0.568	0.982	1

TABLE 3.39

BLOCK 3 T = 130°C

Run 1

P_1	P_2	A (mg)	B (mg)	C (mg)	D (^{mg}/g-catalyst	E
0.10	0.079	0.185	0.001	0.184	0.318	0.383
0.20	0.158	0.247	0.003	0.244	0.422	0.508
0.70	0.553	0.432	0.010	0.422	0.730	0.880
1.00	0.790	0.494	0.014	0.480	0.830	1
1.10	0.869	0.494	0.015	0.479	0.828	1

TABLE 3.40

Run 2

0.10	0.079	0.155	0.001	0.154	0.266	0.321
0.30	0.237	0.278	0.004	0.274	0.474	0.571
0.40	0.316	0.371	0.006	0.365	0.631	0.760
0.70	0.553	0.433	0.010	0.423	0.732	0.881
1.00	0.790	0.494	0.014	0.480	0.830	1
1.20	0.948	0.494	0.016	0.478	0.827	1

TABLE 3.41

Run 3

0.20	0.158	0.216	0.003	0.213	0.368	0.444
0.40	0.316	0.340	0.006	0.334	0.578	0.696
0.60	0.474	0.402	0.008	0.394	0.681	0.821
0.90	0.711	0.463	0.013	0.450	0.778	0.937
1.10	0.869	0.494	0.015	0.479	0.828	1
1.30	1.027	0.494	0.018	0.476	0.823	1

TABLE 3.42

Tables 3.20 - 3.22 show the amount of gas adsorbed per gramme of catalyst at 170, 150 and 130°C. Graphs 3.23 - 3.25 represent the coverage against pressure which will be referred to in the section concerning heats of adsorption.

3.9 Heats of Adsorption

From section 1.3.1.1 it has been shown that heats of adsorption may be calculated from the Clapeyron-Clausius type of equation

$$\ln P = \frac{-q_{st}}{RT} + \text{constant of integration}$$

ORDINATE mg adsorbate per g adsorbent
ABSCISSA Pressure /cm.oil

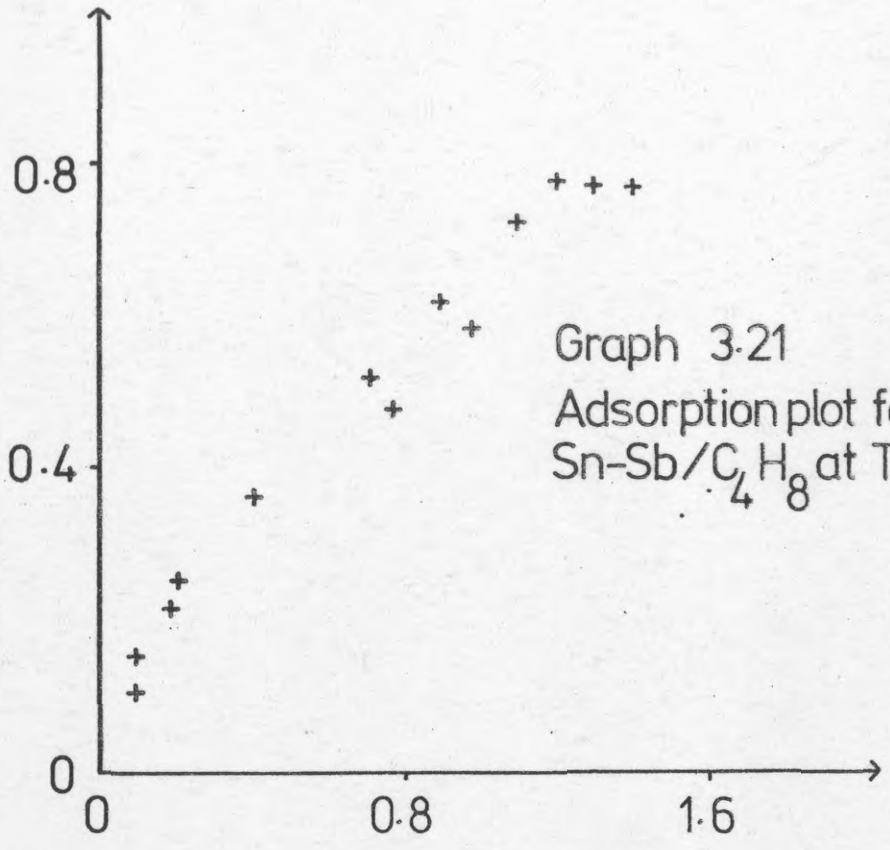

Graph 3.21
Adsorption plot for
Sn-Sb/C_4H_8 at T= 170°C

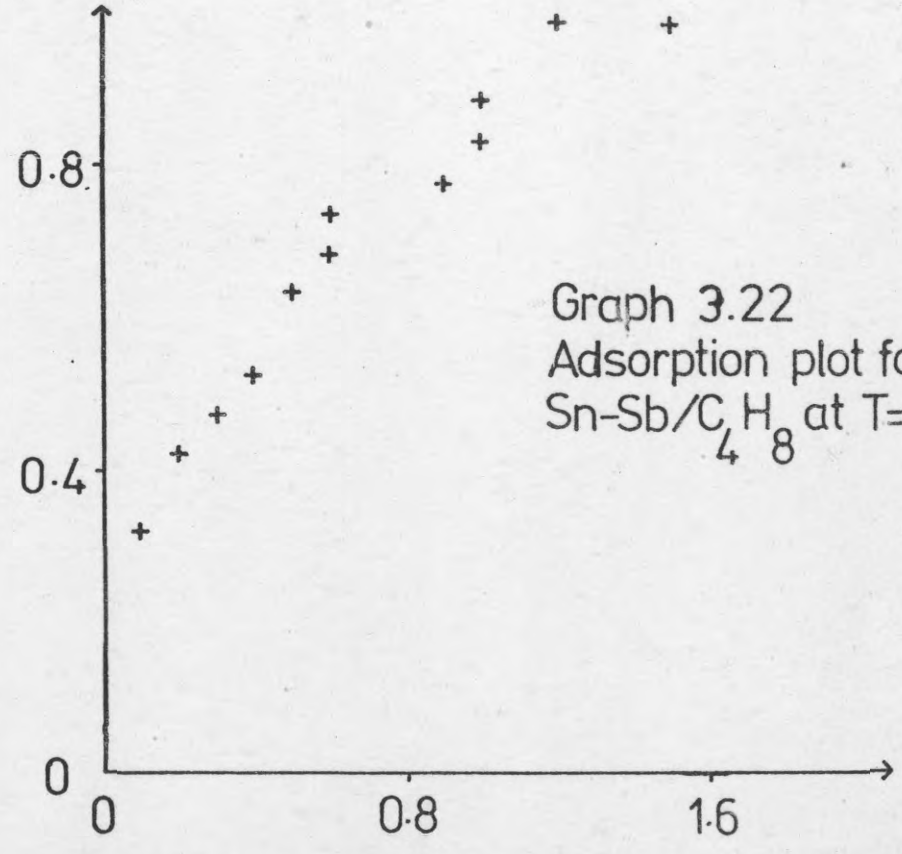

Graph 3.22
Adsorption plot for
Sn-Sb/C_4H_8 at T=150°C

ORDINATE mg adsorbate per g adsorbent
ABSCISSA Pressure/cm. oil

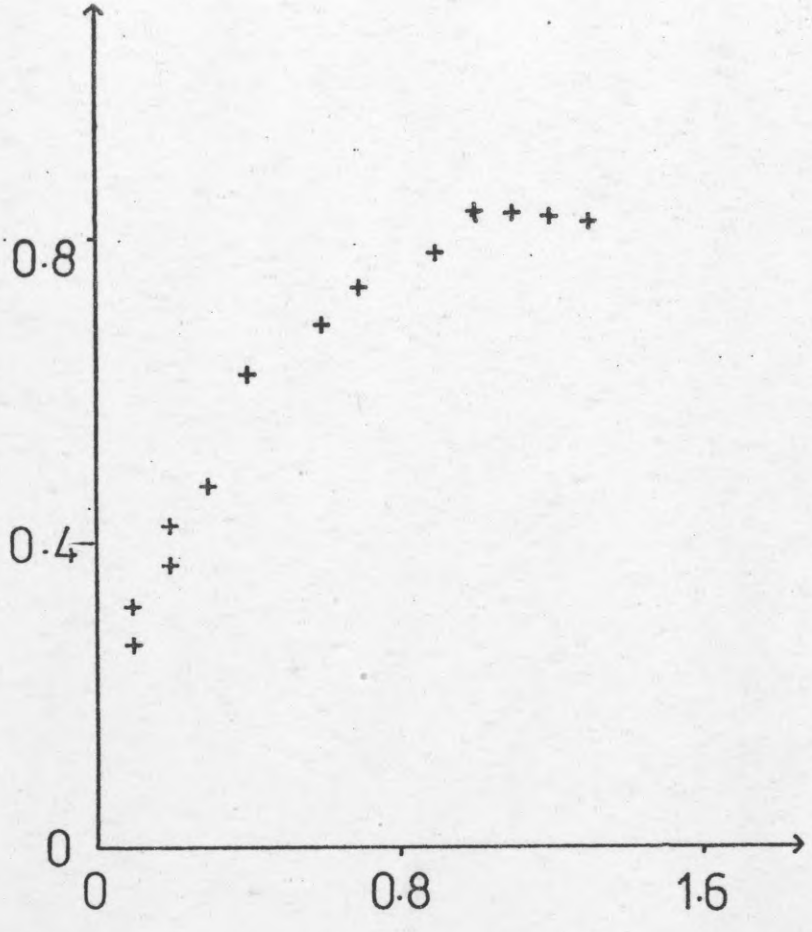

Graph 3.23

Adsorption plot for Sn-Sb/C_4H_8 at T=130°C

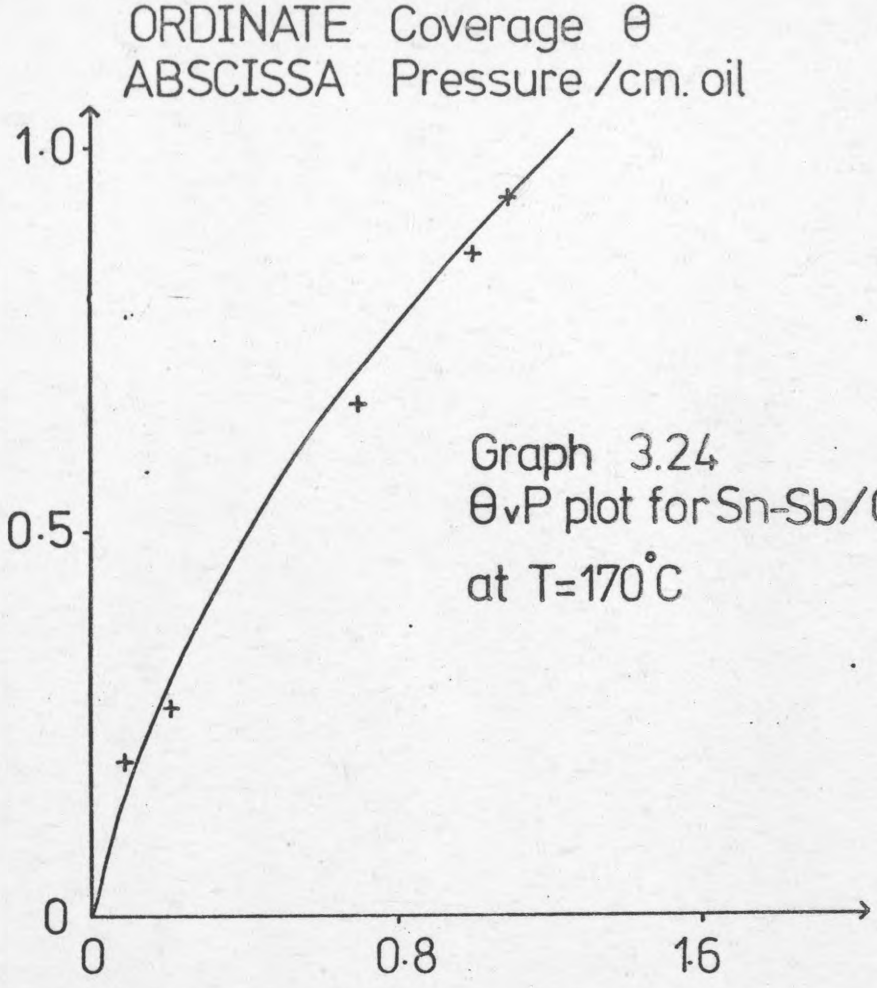

Graph 3.24
θvP plot for Sn-Sb/C_4H_8
at T=170°C

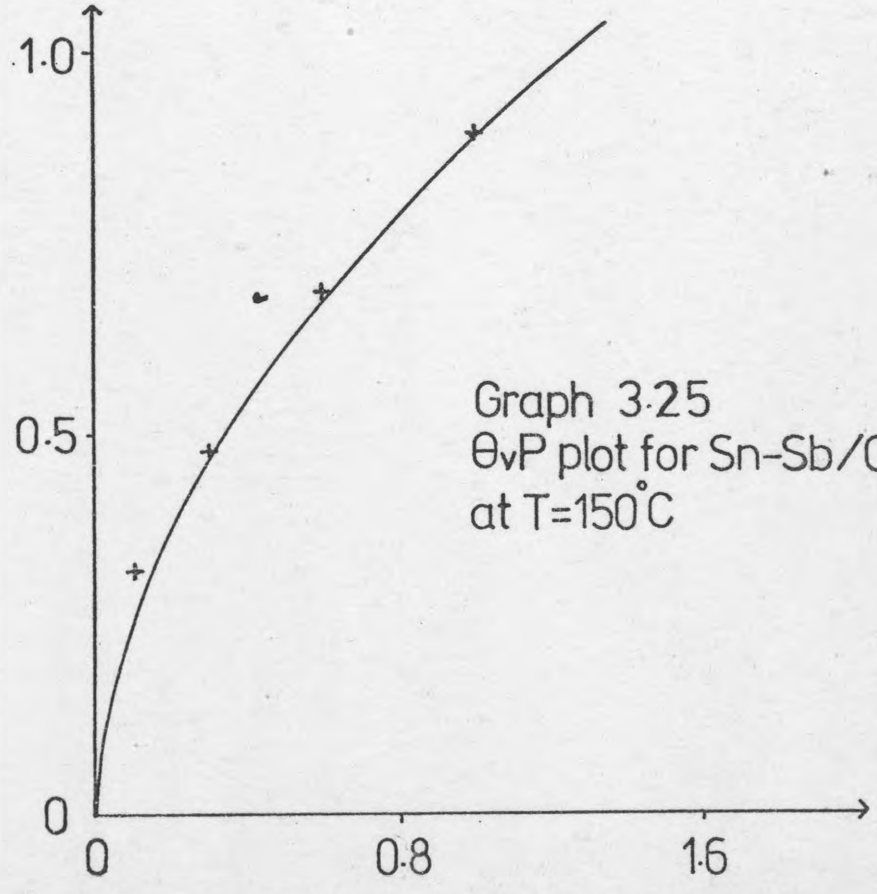

Graph 3·25
θvP plot for Sn-Sb/C_4H_8
at T=150°C

ORDINATE Coverage θ
ABSCISSA Pressure/cm. oil

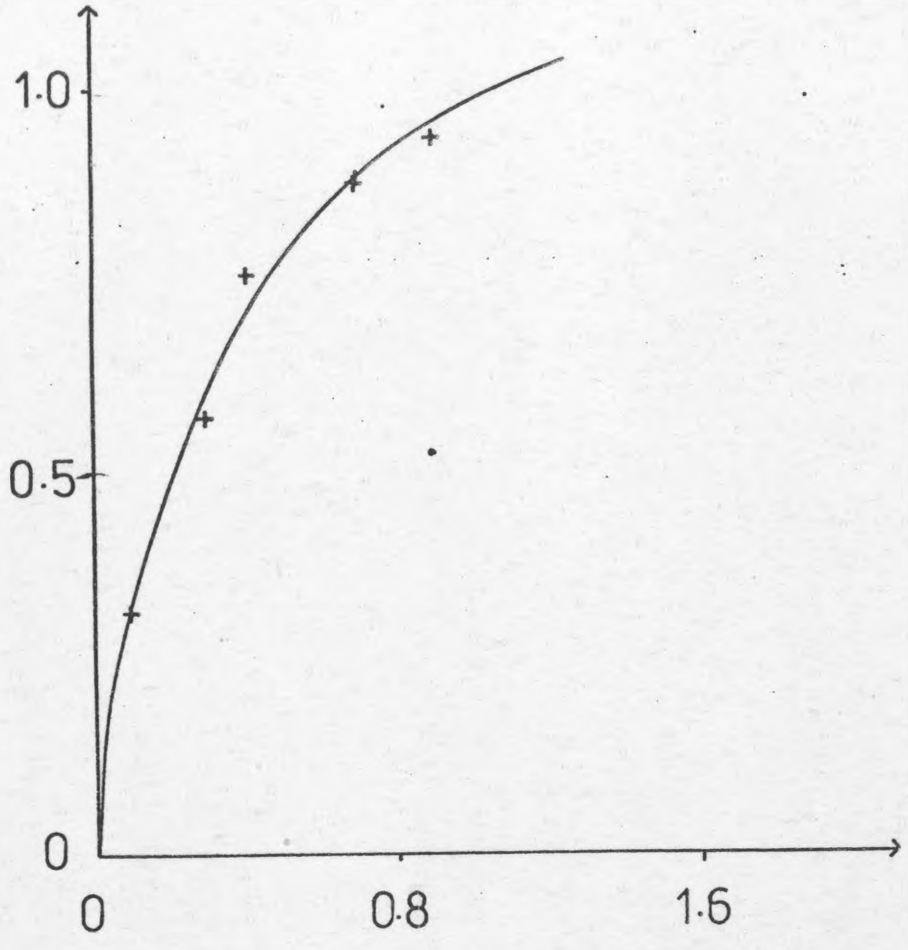

Graph 3.26

θ v P plot for Sn-Sb/C_4H_8 at T = 130°C

where,

P - pressure (torr)

q_{st} - isosteric heat of adsorption ($kJmol^{-1}$)

R - universal gas constant ($J\ K^{-1}mol^{-1}$)

T - temperature (Kelvin)

From plots of pressure against coverage it is possible to obtain a set of data of T^{-1} and ln P, the slope of which is equal to $^{-q_{st}}/_{R}$. (If $\log_{10}$ P were used in place of ln P the slope would be $^{-q_{st}}/_{2.303R}$.) A worked example follows.

From graphs 3.10 - 3.12 for a coverage of 0.5, the following table was produced.

$T^{o}C$	100	90	80
T^{-1} K	2.681×10^{-3}	2.755×10^{-3}	2.833×10^{-3}
P_1	2.250	1.350	1.350
P_2	1.777	1.066	1.066
log P_2	0.249	0.026	0.026

Slope = -1454

$$\therefore -1454 = \frac{-q_{st}}{2.303R}$$

$$\underline{q = 27.82\ kJ\ mol^{-1}}$$

3.9.1 q v θ for Sn-Sb/O_2

T (°C)	100		90		80			
$T^{-1}(K^{-1})$	2.681×10^{-3}		2.755×10^{-3}		2.833×10^{-3}			
θ	P_1	log P_2	P_1	log P_2	P_1	log P_2	Slope	q kJ mol^{-1}
0.2	0.42	-0.479	0.25	-0.704	0.25	-0.704	-1467	28.08
0.3	0.91	-0.143	0.55	-0.362	0.55	-0.362	-1429	27.33
0.4	1.43	0.052	0.86	-0.167	0.86	-0.167	-1428	27.36
0.5	2.24	0.247	1.35	0.026	1.35	0.026	-1441	27.58
0.6	3.12	0.391	1.97	0.192	1.97	0.192	-1297	24.83
0.7	4.20	0.521	2.70	0.329	2.70	0.329	-1252	23.96
0.8	5.17	0.611	4.20	0.520	4.20	0.520	- 593	11.35
0.9	6.35	0.700	5.80	0.661	5.80	0.661	- 254	4.87
1	7.50	0.772	7.37	0.765	7.37	0.765	- 46	<1

Graph 3.27 shows the variation of the heats of chemisorption with coverage.

TABLE 3.43

ORDINATE Isosteric heat of adsorption/kJ mol^{-1}
ABSCISSA Coverage

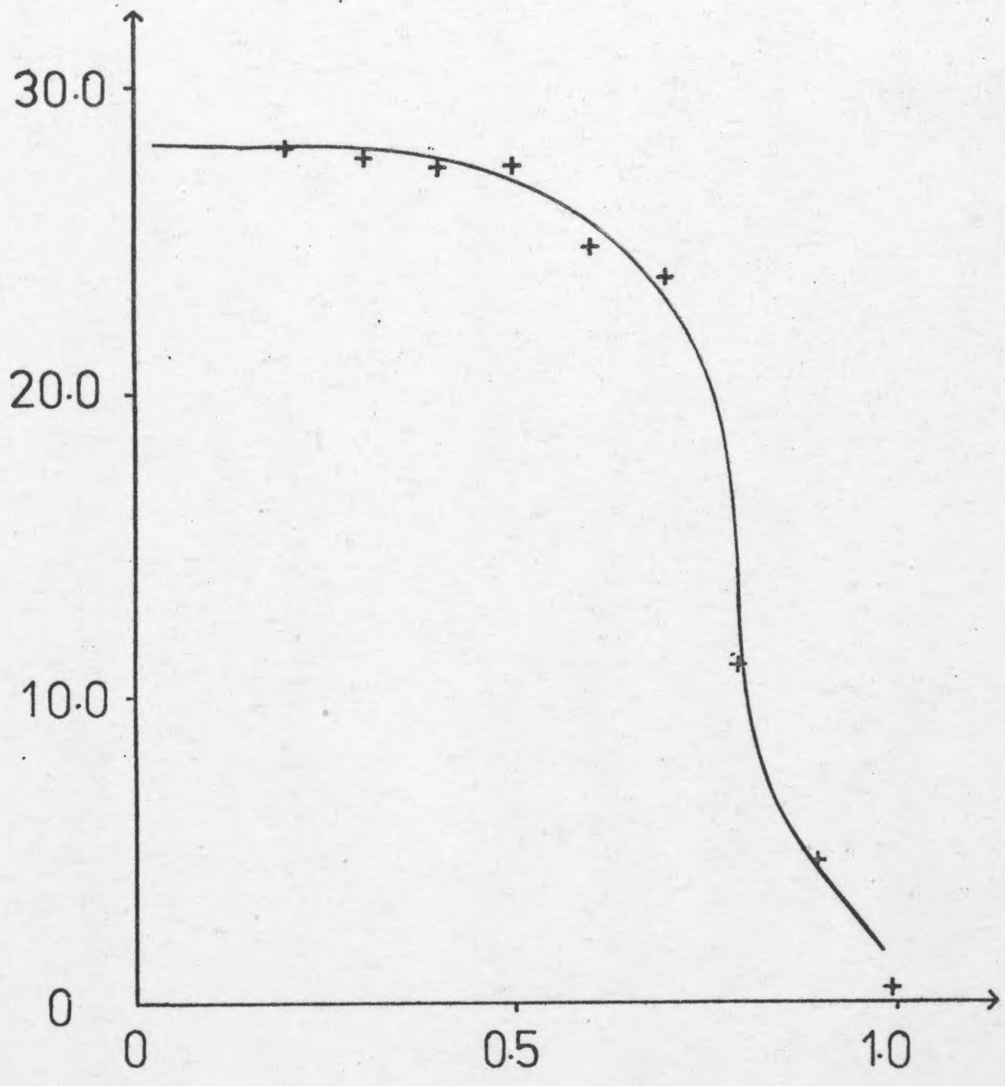

Graph 3.27

Variation of isosteric heat of adsorption with coverage for Sn-Sb/O_2

3.9.2 q v θ for Sn-Sb/C_3H_6

T (°C)	250		225		200			
T^{-1} (Kelvin)	1.912×10^{-3}		2.008×10^{-3}		2.114×10^{-3}			
θ	P_1	log P_2	P_1	log P_2	P_1	log P_2	Slope	q kJ mol^{-1}
0.1	0.10	-1.102	0.05	-1.404	0.01	-2.100	-4968	95.09
0.2	0.21	-0.801	0.13	-0.972	0.06	-1.324	-2601	49.80
0.3	0.32	-0.597	0.26	-0.687	0.12	-1.006	-2041	39.08
0.4	0.44	-0.459	0.42	-0.474	0.21	-0.780	-1611	30.83
0.5	0.56	-0.354	0.62	-0.307	0.34	-0.571	-1098	21.01
0.6	0.68	-0.270	0.83	-0.181	0.50	-0.403	- 683	13.08
0.7	0.82	-0.186	1.10	-0.061	0.68	-0.267	- 428	8.18
0.8	0.97	-0.116	1.41	-0.047	0.88	-0.158	- 222	4.26
0.9	1.13	-0.049	1.77	0.147	1.11	-0.057	- 72	1.38
1.0	1.31	0.015	2.20	0.239	1.31	0.015	- 37	<1

Graph 3.28 shows the variation of the heat of chemisorption with coverage.

TABLE 3.44

ORDINATE Isosteric heat of adsorption/ kJ mol^{-1}
ABSCISSA Coverage

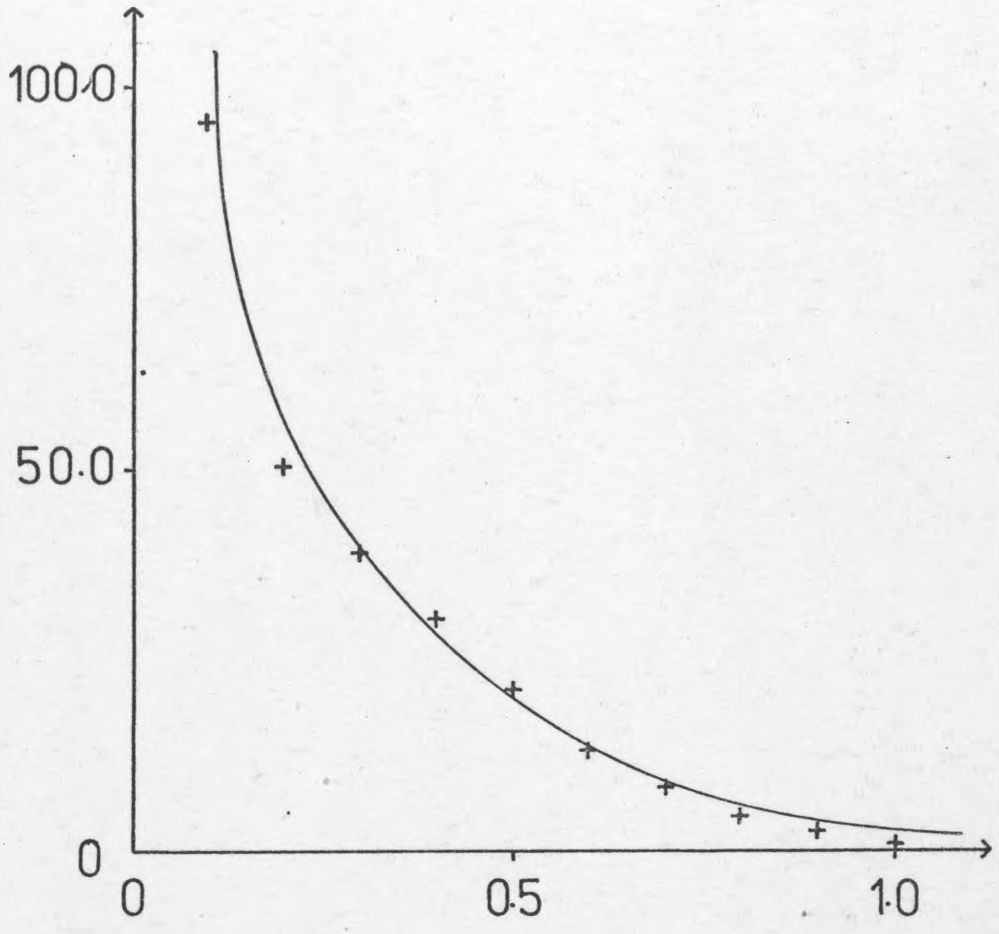

Graph 3.28

Variation of isosteric heat of adsorption with coverage for Sn-Sb/C_3H_6

3.9.3 q v θ for Sn-Sb/l-C_4H_8

T (°C)	170		150		130			
T^{-1}(Kelvin)	2.257×10^{-3}		2.364×10^{-3}		2.481×10^{-3}			
θ	P_1	log P_2	P_1	log P_2	P_1	log P_2	Slope	q_{st} kJ/mol
0.1	0.06	-1.324	0.03	-1.625	0.01	-2.102	-3483	66.65
0.2	0.13	-0.988	0.06	-1.324	0.04	-1.500	-2274	43.51
0.3	0.22	0.760	0.11	-1.061	0.08	-1.199	-1947	37.28
0.4	0.30	-0.625	0.19	-0.824	0.14	-0.956	-1472	28.18
0.5	0.41	-0.490	0.32	-0.597	0.21	-0.780	-1298	24.86
0.6	0.53	-0.378	0.47	-0.430	0.27	-0.671	-1320	25.26
0.7	0.68	-0.270	0.65	-0.289	0.37	-0.534	-1193	22.83
0.8	0.85	-0.173	0.85	-0.173	0.53	-0.378	- 928	17.76
0.9	1.02	-0.094	1.04	-0.085	0.80	-0.199	- 476	9.12
1.0	1.20	-0.023	1.24	-0.009	1.08	-0.069	- 210	4.02

Graph 3.29 shows the variation of the heat of chemisorption with coverage

TABLE 3.45

ORDINATE Isosteric heat of adsorption/kJ mol^{-1}
ABSCISSA Coverage

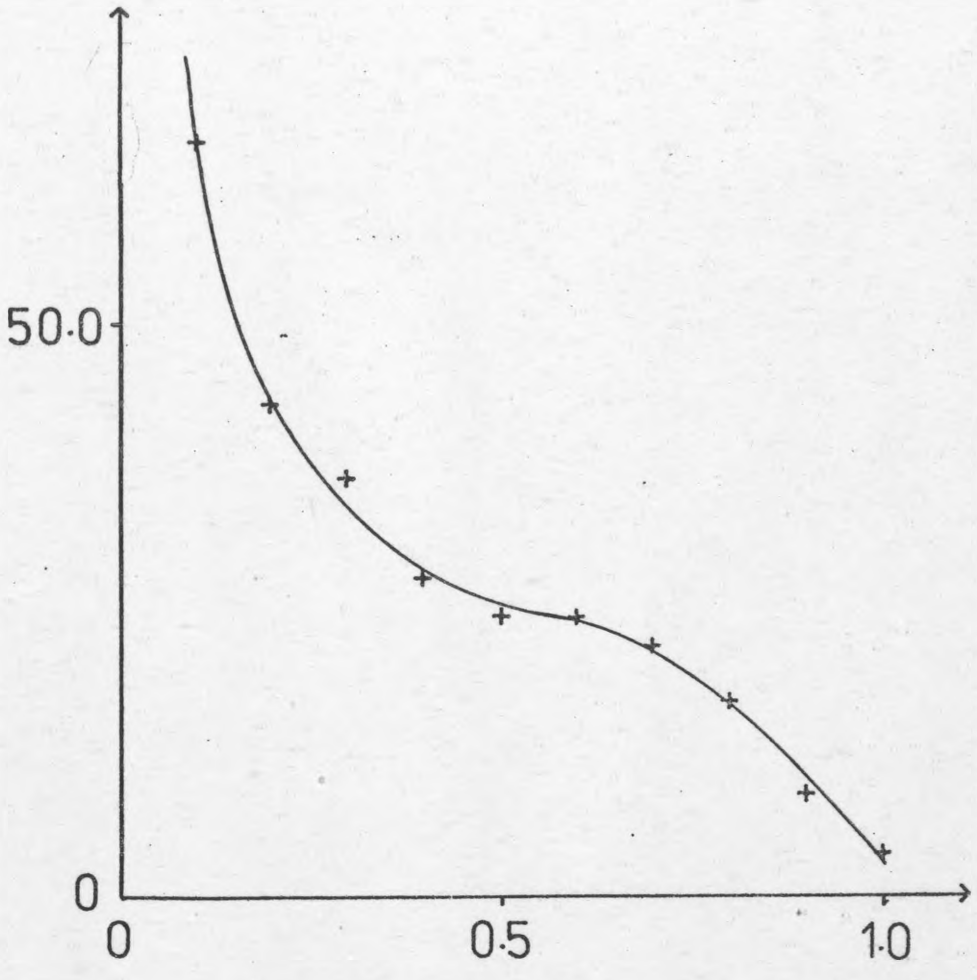

Graph 3.29

Variation of isosteric heat of adsorption with coverage for Sn-Sb/C_4H_8

3.10 Entropies of Adsorption

As has been described in section 1.3.2 it is possible to evaluate the entropy of adsorption from P, q_{st} and T data. For comparative purposes the differential molar entropy of adsorption is used, and is evaluated from the following relationship

$$\bar{s}_s = s_{m,g} - R \ln P_3 - {}^{q_{st}}/_{T} \qquad JK^{-1}mol^{-1}$$

As can be seen from the above relationship it is necessary to evaluate the molar entropy of the gas phase. This may be done by taking into account translational and rotational effects as described in Appendix VI. The calculated values for oxygen, propene and butene are also in Appendix VI.

The above has been used for the systems Sn-Sb/O_2, Sn-Sb/C_3H_6 and Sn-Sb/C_4H_8 at the temperature corresponding to maximum coverage, due to negligible variation of $\bar{S}_s$ with T. Graphs 3.30 - 3.32 illustrates the variation of $\bar{S}_s$ with θ from the tables below.

3.10.1 Sn-Sb/O_2

$s_{m,g}$ = 195.42 $JK^{-1}mol^{-1}$

θ	P_1	$RlnP_3$	$q_{st}/_T$	$\bar{s}_s (JK^{-1}mol^{-1})$
0.2	0.42	31.488	75.282	88.65
0.3	0.91	37.913	73.271	84.24
0.4	1.43	41.669	73.351	80.40
0.5	2.24	45.339	73.941	76.14
0.6	3.12	48.152	66.568	80.70
0.7	4.20	50.622	64.236	80.56
0.8	5.17	52.349	30.429	112.64
0.9	6.35	54.058	13.056	128.31
1.0	7.50	55.441	2.681	137.30

TABLE 3.46

3.10.2 Sn-Sb/C_3H_6

$s_{m,g}$ = 256.79 $JK^{-1}mol^{-1}$

θ	P_1	$RlnP_3$	$q_{st}/_T$	$\bar{s}_s(JK^{-1}mol^{-1})$
0.1	0.05	13.802	190.944	52.04
0.2	0.13	21.743	100.000	135.05
0.3	0.26	27.503	78.474	150.81
0.4	0.42	31.488	61.908	163.39
0.5	0.62	34.724	42.189	179.88
0.6	0.83	37.149	26.265	193.38
0.7	1.10	39.489	16.426	200.88
0.8	1.41	41.552	8.554	206.68
0.9	1.77	43.442	2.771	210.58
1.0	2.20	45.249	2.008	209.53

TABLE 3.47

3.10.3 Sn-Sb/C_4H_8

θ	P_1	$RlnP_3$	$q_{st}/_T$	$\bar{s}_s(JK^{-1}mol^{-1})$
0.1	0.03	9.557	157.565	93.06
0.2	0.06	15.318	102.861	142.00
0.3	0.11	20.355	88.132	151.69
0.4	0.19	24.896	66.619	168.66
0.5	0.32	29.228	58.771	172.18
0.6	0.47	32.422	59.716	168.04
0.7	0.65	35.117	53.972	171.09
0.8	0.85	37.346	41.986	180.85
0.9	1.04	39.023	21.560	199.60
1.0	1.24	40.485	9.504	210.19

TABLE 3.48

3.11 Actual Surface Coverage

From BET calculations the surface area of the Sn-Sb catalyst was 7.40 m^2g^{-1}. The actual weight of the catalyst used was 0.5782g. Therefore the total area available for adsorption to take place was $4.279 \times 10^4 cm.^2$

Below a sample calculation is given for the adsorption of O_2 on Sn-Sb at 100°C

ORDINATE Diff. molar entropy $\bar{s}_s / JK^{-1}mol^{-1}$
ABSCISSA Coverage θ

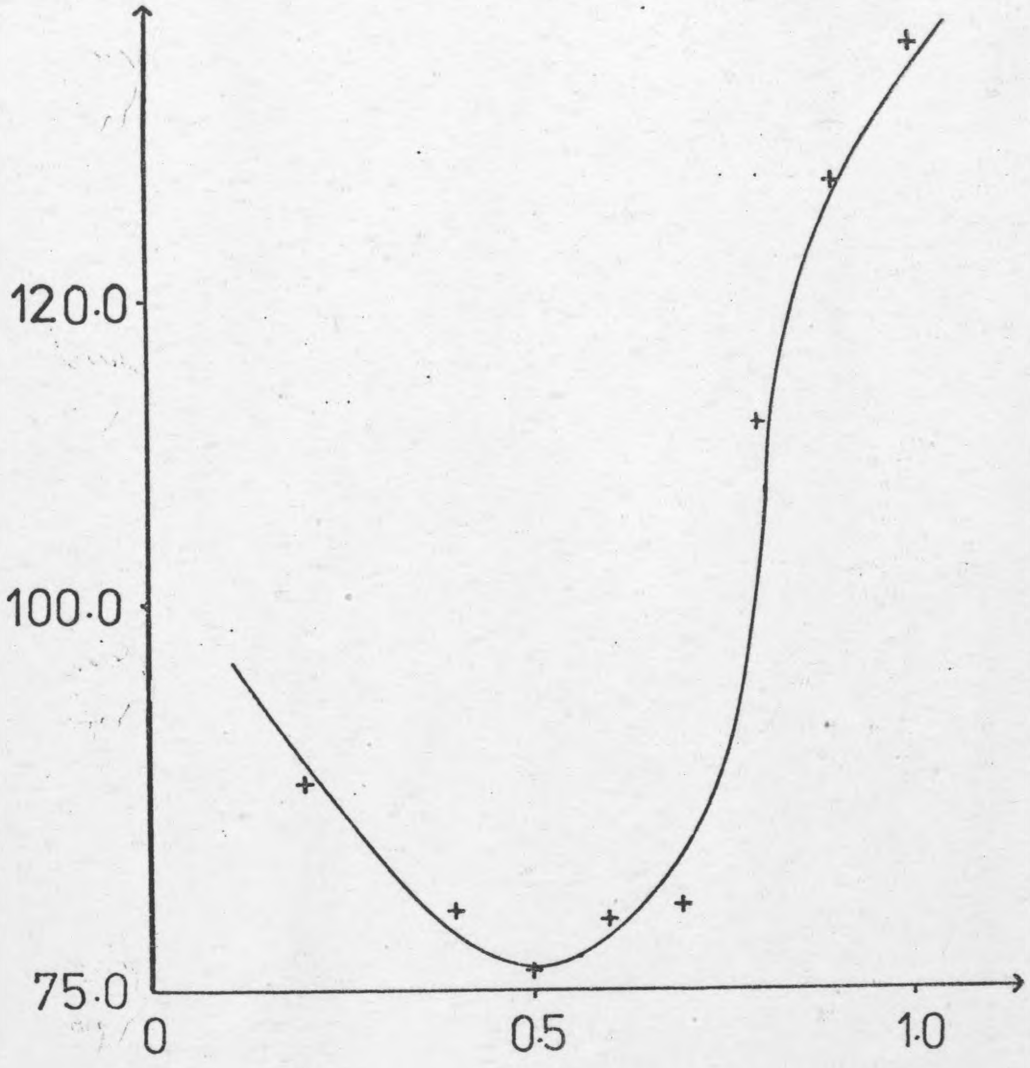

Graph 3.30

Variation of $\bar{s}_s$ with θ for Sn-Sb/O_2

ORDINATE Diff. molar entropy $\bar{s}_s / JK^{-1}mol^{-1}$
ABSCISSA Coverage θ

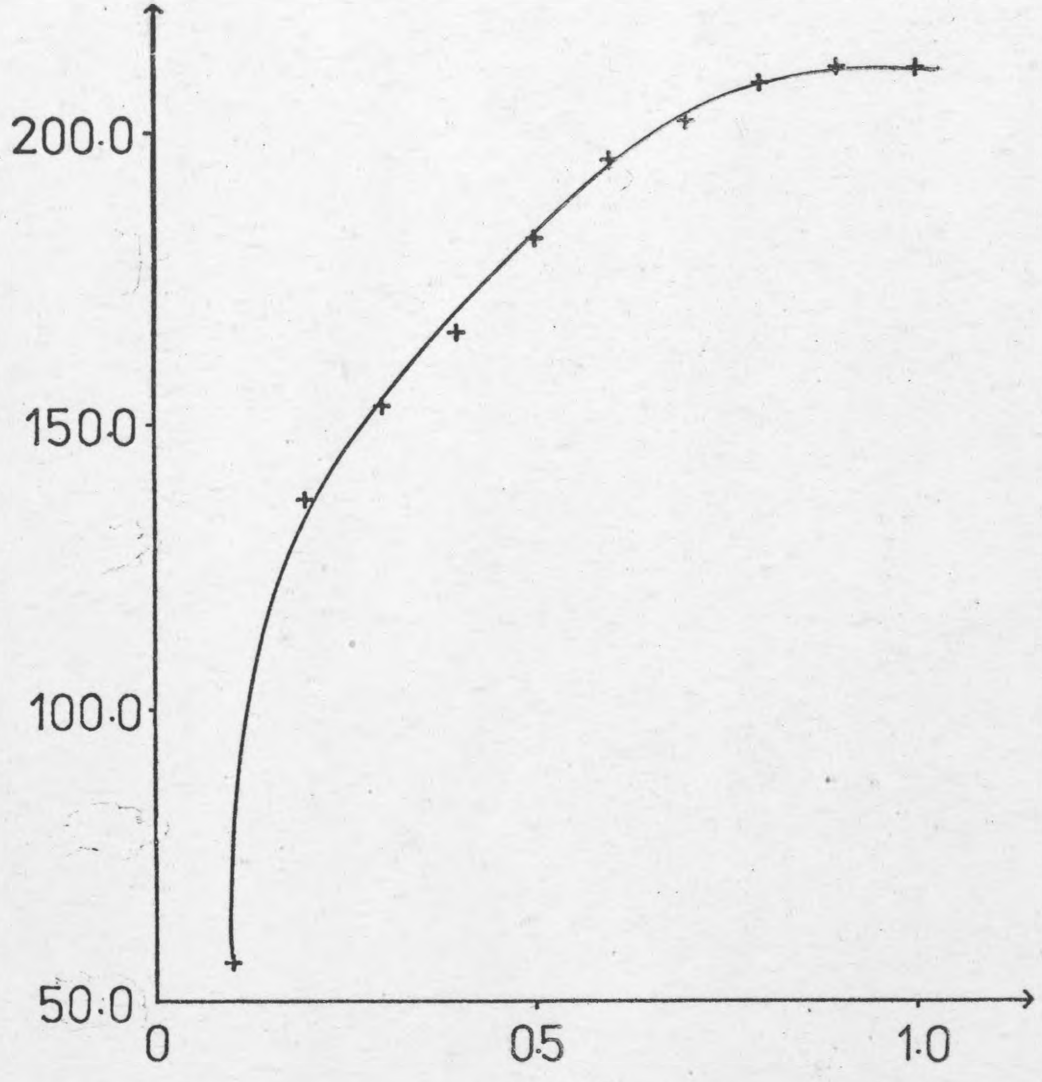

Graph 3.31

Variation of $\bar{s}_s$ with θ for Sn-Sb/C_3H_6

ORDINATE Diff. molar entropy $\bar{s}_i / JK^{-1}mol^{-1}$

ABSCISSA Coverage θ

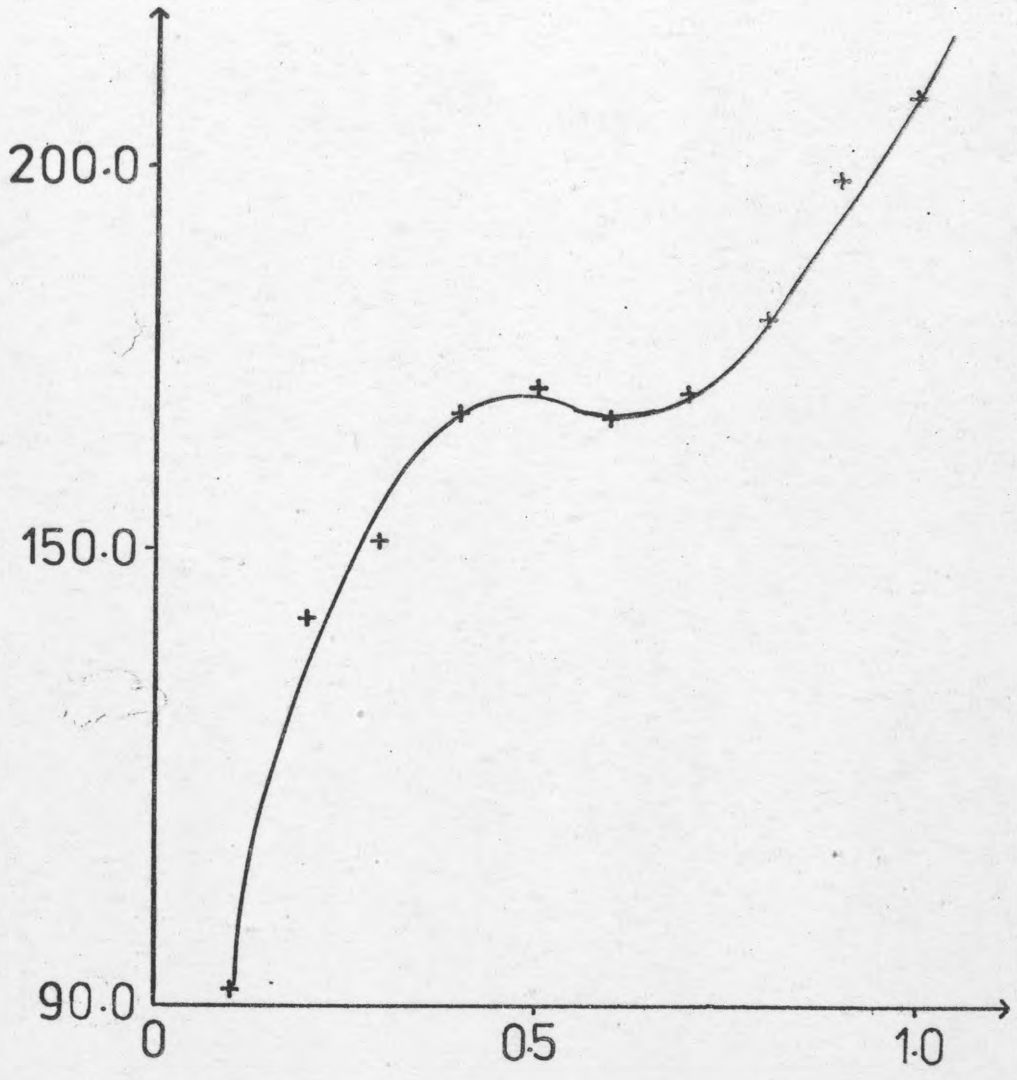

Graph 3.32

Variation of $\bar{s}_i$ with θ for Sn-Sb/C_4H_8

Weight of one molecule of oxygen = $\frac{\text{mol.wt}}{6.023 \times 10^{23}}$

$= 5.313 \times 10^{-23}$ g./molecule

Weight adsorbed at 100°C = 1.666×10^{-3}g.

No. of molecules adsorbed = $\frac{1.666 \times 10^{-3}}{5.313 \times 10^{-23}} = 3.136 \times 10^{19}$

From section 3.1 diameter of an oxygen molecule is 3.467×10^{-10}m.

The area covered by one molecule = $\frac{\pi d^2}{4}$

$= \pi . \frac{(3.467 \times 10^{-8})^2}{4}$ cm^2

$= 9.441 \times 10^{-16}$ cm^2.

Total area covered = $(3.136 \times 10^{19}) \times (9.441 \times 10^{-16})$

$= 2.961 \times 10^4$ cm^2

$\therefore$ surface area covered = $\frac{2.961 \times 10^4}{4.279 \times 10^4} \times 100 = 69.20\%$

3.11.1 Sn-Sb/O_2 at 100, 90 and 80°C

T (°C)	Surface Coverage (%)
100	38.29
90	63.62
80	69.20

TABLE 3.49

3.11.2 Sn-Sb/C_3H_6 at 250, 225 and 200°C

T (°C)	Surface Covered (%)
250	25.57
225	81.45
200	41.18

TABLE 3.50

3.11.3 Sn-Sb/C_4H_8 at 170, 150 and 130°C

T (°C)	Surface Covered (%)
170	24.13
150	30.82
130	25.86

TABLE 3.51

3.12 Experimental Variance

Two types of errors have been identified[69]. They are determinate and indeterminate errors. The former type of errors are defined as those that can be avoided once recognized, e.g. improper calibration of glassware or instruments. The latter type of errors cannot be eliminated, they exist by the very nature of measurement data and it is those errors that are known as the experimental error. In order to judge the reliability of the experimental results, they must be compared with the estimated experimental error.

Normally experimental error is based on the use of replicate experiments[69]. In this case it was not possible to

precisely replicate any one adsorption run. The reason for this was the doser system. The doser taps (see Fig. 2.1) had to be operated manually and it was found impossible to admit exactly the same dosage of gas in different experiments. The only practical way to overcome this problem would be to use an expensive electronic gas injection system.

In this work variances have been used to give an estimate of experimental errors. The only way to calculate the experimental variances and standard deviations was by the use of linear interpolation to convert similar pairs of readings from two runs of a particular experimental block into ones effectively taken at the same pressure of adsorbate.

Consequently, similar pairs of readings from two runs were taken (a typical set of pairs being given below), and the extension value of the lower pressure reading was altered by linear interpolation (linear interpolation being used as the increase in the amount adsorbed with pressure over a small range was virtually linear) and the percentage

$Sn\text{-}Sb/O_2$	Block 3	T = 100°C	
P	Δ	P	Δ
0.30	0.004	0.30	0.004
0.70	0.006	0.80	0.006
1.70	0.009	1.90	0.010
3.20	0.013	3.40	0.014
5.00	0.017	5.80	0.020
6.90	0.022	7.60	0.022

difference (X) between the unchanged extension value and the corrected extension value for a pair of readings calculated. If the pressure readings were equal the percentage difference between extension values (if any) was calculated directly. The mean difference ($\bar{X}$) could be calculated by summing all

the individual differences and dividing by the number of pressure readings (N). The calculation of variance (σ^2) and the standard deviation σ was carried out by using the following equation

$$\sigma^2 = \frac{\sum_{1}^{N}(X-\bar{X})^2}{N-1}$$

and the relationship $\sigma = \sqrt{\sigma^2}$.

The experimental variances calculated in this section are of great importance, as not only do they give an indication of the experimental errors involved but also of goodness of fit when used in the subsequent sections of data fitting to various models.

The complete computer programme is presented in Appendix V.

Adsorbate	Temperature (°C)	Experimental Variance σ_e^2	Experimental Std. Dev. σ %
C_3H_6	200	57.992	± 7.526
C_3H_6	225	16.601	± 4.074
C_3H_6	250	15.789	± 3.974
O_2	80	92.202	± 9.602
O_2	90	91.012	± 9.540
O_2	100	30.528	± 5.525
C_4H_8	130	15.338	± 3.916
C_4H_8	150	21.701	± 4.658
C_4H_8	170	100.000	± 10.000

TABLE 3.52

Computed values of experimental variances and standard deviations.

3.13 Data Fitting Tables

As discussed in section 1.2.1 it is possible to linearise the Langmuir isotherm for single site adsorption by taking reciprocals. This form should have unit slope. The above was carried out by using a linear regression program and the goodness of fit was defined as the ratio of the variance from the linear regression analysis to that of the experimental variance calculated as in the previous section.

In the case of oxygen, it has often been found that the oxygen molecule dissociates and double site adsorption takes place. In the Langmuir isotherm this should lead to a linear relationship between $P^{\frac{1}{2}}$ and $P^{\frac{1}{2}}/\theta$, this was carried out and variances compared.

By inspection of the heat of chemisorption against coverage plot for the Sn-Sb/C_3H_6 system the relationship can be seen to be exponential. This is the type of heat of adsorption and coverage relationship described by the Freundlich isotherm. From the Freundlich equation a linear relationship between ln V and ln P should exist.

Data fitting was also carried out on two other isotherms. Firstly that of Misra which under certain conditions yields the Langmuir and Jovanovic isotherms; secondly on a modified Langmuir equation of the form $\theta = \frac{K_1 P}{1+K_2 P}$, for both single and double site adsorption with $K_1 > K_2$ to give $\theta=1$ at finite values of P. This also gives the minimum saturation pressure $P_{min} = \frac{1}{k_1-k_2}$.

3.13.1 Fit to Langmuirs Isotherm for Single Site Adsorption

3.13.1.1 $Sn-Sb/O_2$

T	σ^2	σ_e^2	σ^2/σ_e^2	
80	418.80	92.20	4.54	
90	100.00	91.01	1.10	(s=0.63)
100	1451.00	30.53	47.53	

TABLE 3.53

3.13.1.2 $Sn-Sb/C_3H_6$

200	72.60	57.99	1.25	(s=0.56)
225	144.40	16.60	8.70	
250	171.00	15.79	10.83	

TABLE 3.54

3.13.1.3 $Sn-Sb/C_4H_8$

130	61.69	15.34	4.02	
150	93.49	21.70	4.31	
170	96.20	100.00	0.96	(s=0.56)

TABLE 3.55

3.13.2 Fit to Langmuirs Isotherm for Double Site Adsorption

3.13.2.1 $Sn-Sb/O_2$

80	4483.00	92.20	48.62
90	964.50	91.01	10.60
100	243.10	30.53	7.96

TABLE 3.56

3.13.3 Fit to Misras Isotherm

3.13.3.1 Sn-Sb/O_2

T	σ^2	σ_e^2	σ^2/σ_e^2
80	195.18	92.20	2.12
90	129.54	91.01	1.42
100	133.00	30.53	4.36

TABLE 3.57

3.13.3.2 Sn-Sb/C_3H_6

200	59.83	57.99	1.03
225	126.23	16.60	7.61
250	103.46	15.79	6.55

TABLE 3.58

3.13.3.3 Sn-Sb/C_4H_8

130	97.77	15.34	6.37
150	115.33	21.70	5.32
170	286.98	100.00	2.87

TABLE 3.59

3.13.4 Fit to Freundlich's Isotherm

3.13.4.1 Sn-Sb/C_3H_6

200	1932.00	57.99	33.32
225	1596.00	16.60	96.15
250	310.30	15.79	19.63

TABLE 3.60

3.13.5 Fit to the Modified Langmuir Equation

3.13.5.1 Sn-Sb/O_2

T (°C)	σ^2	σ_e^2	σ^2/σ_e^2	Sat.Press. (mmHg)	K_1	K_2
Single Site						
80	190.41	92.20	2.06	-	0.742	0.762
90	79.42	91.01	0.88	18.302	1.000	0.945
100	71.02	30.53	2.33	12.121	0.923	0.841
Double Site						
80	27.66	115.27	0.24	2.365	0.353	0.069
90	176.21	91.01	1.94	2.344	0.482	0.055
100	30.24	38.16	0.79	2.402	0.544	0.128

TABLE 3.61

3.13.5.2 Sn-Sb/C_3H_6

Single Site						
200	74.94	57.99	1.29	1.176	2.419	1.569
225	141.54	19.70	7.18	19.336	2.169	2.118
250	21.85	19.73	1.11	1.133	1.475	0.529
Double Site						
200	135.70	57.99	2.34	1.019	0.681	-0.301
225	59.37	19.70	3.01	1.479	0.724	0.047
250	18.07	19.73	0.92	0.999	0.484	-0.517

TABLE 3.62

3.13.5.3 Sn-Sb/C_4H_8

Single Site						
130	23.21	14.98	1.55	0.862	4.457	3.297
150	38.87	18.81	2.07	2.091	3.775	3.297
170	38.52	100.00	0.39	1.085	2.149	1.227
Double Site						
130	42.94	14.98	2.87	0.859	1.227	0.063
150	21.22	18.81	1.13	1.091	1.155	0.239
170	13.72	100.00	0.13	0.982	0.715	-0.303

4.1 Initial Work

The physisorption of nitrogen on carbon-black at liquid nitrogen temperature (77K) was carried out to test the apparatus. This also gave the opportunity to discover any shortcomings of the design, e.g. in the vacuum system. A BET specific surface area determination was carried out on carbon-black as well as the tin-antimony oxide catalyst. No accurate BET data could be produced from the bismuth-molybdate catalyst due to its very low specific surface area quoted as 0.25 m^2g^{-1}(82).

To determine whether the apparatus could be used for chemisorption studies, scouting experiments were carried out on the tin-antimony oxide and bismuth-molybdate catalysts. These used different adsorbates and various temperature ranges. The conclusion was that the apparatus did not have sufficient sensitivity to study chemisorption on the bismuth-molybdate catalyst.

However, adequate spring extensions were given by the tin-antimony oxide catalyst when adsorbing oxygen, propene and 1-butene. These adsorptions were found at temperature ranges of 80-100°C, 200-250°C and 130-170°C respectively, and occurred with convenient pressure changes.

4.2 Data Correction

Before any information could be gained from the adsorption data it was important to make corrections for buoyancy and thermal effects. From the correction data for nitrogen on Sn-Sb catalyst at liquid nitrogen temperature (Table 3.2) no

noticeable change of the datum value was found until a large relative pressure had been reached (≈0.75), much above that required in the experiments (0.30). This was either because the above mentioned effects were not present or the apparatus was not sensitive enough to detect them. Thus no correction was required to the observed amount adsorbed. This was also found to be the case for the carbon-black/N_2 system. In both cases, however, a pressure correction was required when the pressure of gas in the balance case was greater than 50cm. of oil. Larger manometer arms could have been used, but this would have made reading the oil levels very difficult.

In the case of the chemisorption runs a correction to the amount adsorbed was required. The correction data produced (Tables 3.10, 3.11, 3.21, 3.22, 3.32 and 3.33) was a mixture of buoyancy and thermal effects. If buoyancy alone was significant we would expect the datum value to decrease as an inert gas was being admitted, due to the increasing upthrust exerted by the gas on the catalyst and basket. This was not the case. In fact the datum increased with increasing pressure of gas as if the gas were adsorbed. This indicated that thermal effects were dominant. The causes were thermal gradients along the hang-down wire and also the existence of convection currents, due to the lower part of the balance case being at a higher (and in some cases appreciably higher) temperature than the rest of the case. (The thermal effects could have worked in the opposite direction, leading to an exaggerated buoyancy effect.) No pressure corrections were required as the largest pressure required for complete site coverage was in

the region of 12cm. of oil.

If at low pressures the adsorbent were maintained at a temperature different to that of the manometer, then there would be an associated pressure gradient. This is known as the thermal transpiration effect and must be taken into account. Should the mean free path (λ) of the gas be larger than the diameter of any part of the glass tubing from the adsorbent to the manometer, the pressure shown on the manometer would be different to that existing in the vicinity of the adsorbent. Complicated empirical formulas are necessary to correct for this effect[88].

In fact from section 3.1 the λ values for the gases used, at the lowest pressure at which a reading was taken (0.1 cm.oil) was always much smaller than the diameter of the smallest tubing. Consequently with the use of wide bore tubing, the pressure throughout the apparatus was assumed to be constant. Also no thermal transpiration correction was necessary.

When the temperature of the lower half of the balance case was approximately 200K below that of the thermostated region, no appreciable change in datum was noted till high pressures ($\approx$57cm.Hg) had been reached (see Graph 3.1). Yet when the temperature of the lower region of the balance case was 200K above the thermostated region, datum changes were first noticed at appreciably lower pressures ($\approx$0.08cm. Hg). Also the larger the positive temperature difference between the oven region and the thermostated region the larger was the correction. This was simply due to rising hot gases leading to effects not present when the gases

were cold.

4.3 Physisorption Study (BET)

The basic data for the physisorption studies consist of changes in datum values (Δ) with pressure (cm.oil). The amount adsorbed being the product of Δ and the spring sensitivity. It was found that no correction to this weight was required to compensate for thermal or buoyancy effects. However, as large pressures were used, a pressure correction was required and this was given in the previous section.

Physical adsorption on non-porous adsorbents (those without internal surfaces) will give isotherms of Types II and III from the BET classification, and also step-wise isotherms. Should the adsorbent be macro-porous then the thickness of the adsorbed layer is limited by the pore diameter and adsorption may give a Type IV or V isotherm. With macro-porous solids there may also be a hysterisis loop because the adsorption and desorption paths were different. This may be caused by condensation within the pores or other reasons. The situation becomes much more complicated if the adsorbent is microporous giving a Type I isotherm with a hysterisis loop.

In the case of the tin-antimony oxide and carbon-black adsorbents Graph 4.1 shows a typical plot of amount adsorbed against relative pressure. This is clearly a Type II isotherm, which is given by non-porous or macro-porous adsorbents. Surface area calculations can only be made from this type of isotherm.

ORDINATE Amount adsorbed / mg

ABSCISSA Relative pressure

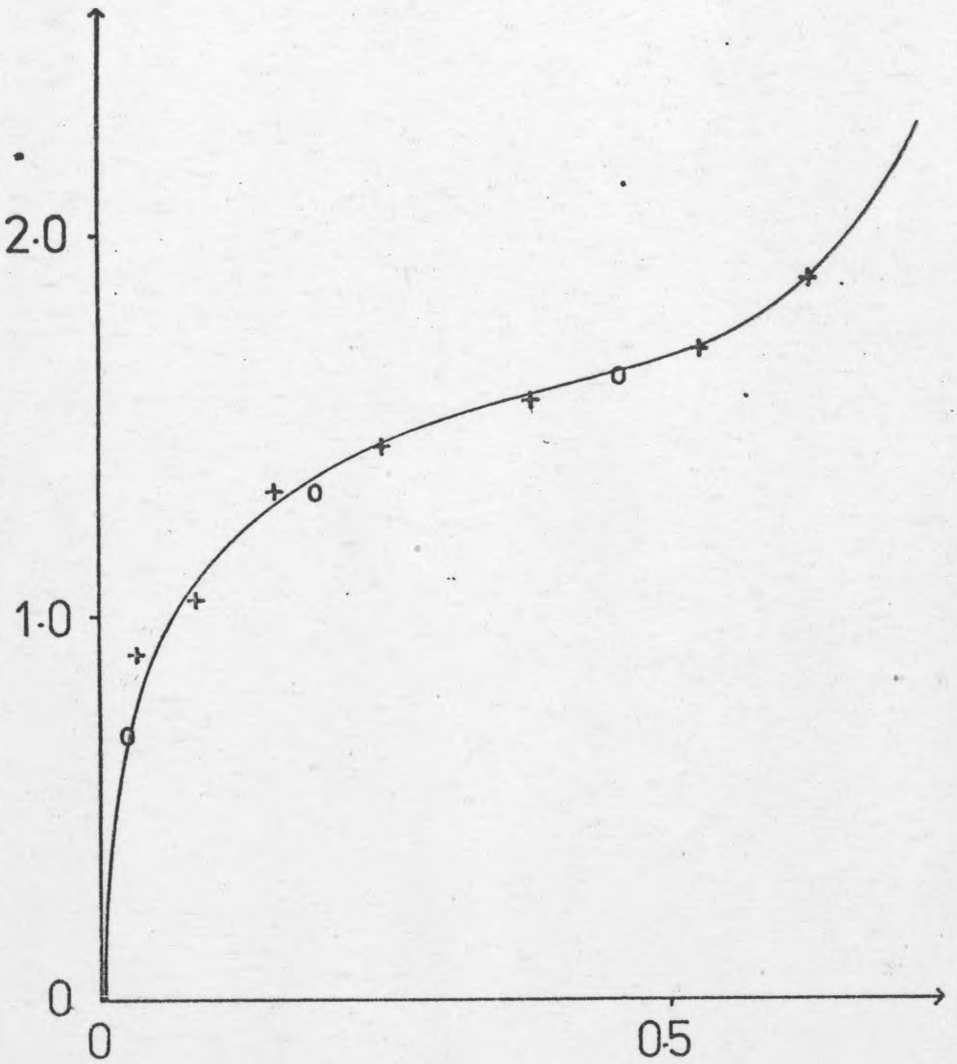

+ adsorption o desorption

Graph 4.1

Characteristic data plot

This is because a sharp kink is required to define the monolayer capacity (x_m) which when used in the following equation provides the specific surface area (S).

$$S = \frac{x_m . N . A_m}{M} \times 10^{-20} \; m^2 g^{-1}$$

Whether such a kink exists or not is indicated by the numerical value of the BET constant in the BET equation (see section 1.2.5). Values of C greater than 2 indicate a Type II isotherm, the larger the value the more pronounced is the kink in the isotherm. Should the value of C be 2 or less the isotherm will be a Type III, which cannot be used to calculate specific surface areas as already stated. The reason for this can be found from the Type II and Type III isotherms (Fig. 1.3). x_m may be determined by extrapolating the linear portion of the curve to the ordinate, (on the assumption that the monolayer is complete at this point). The point of intersection is the monolayer capacity; this is known as the point B method. If this extrapolation is carried out on a Type III isotherm the value for the monolayer capacity will be negative and thus have no physical significance. It can be seen from the C values of the carbon-black adsorbent (400-600) and the tin-antimony oxide adsorbent (30-70) that the isotherm kink is much more obvious with the former, as shown in Graph 4.2.

However, there is some uncertainty over the precise position of point B, especially if the isotherm kink is not sharp (i.e. the C value is low). Consequently the monolayer capacity was determined by using the BET formula as described in sections 3.4 and 3.5. As can be seen from Graphs 3.2-3.5 of the BET equation, these were non-linear at relative

ORDINATE Amount adsorbed / mg
ABSCISSA Relative pressure

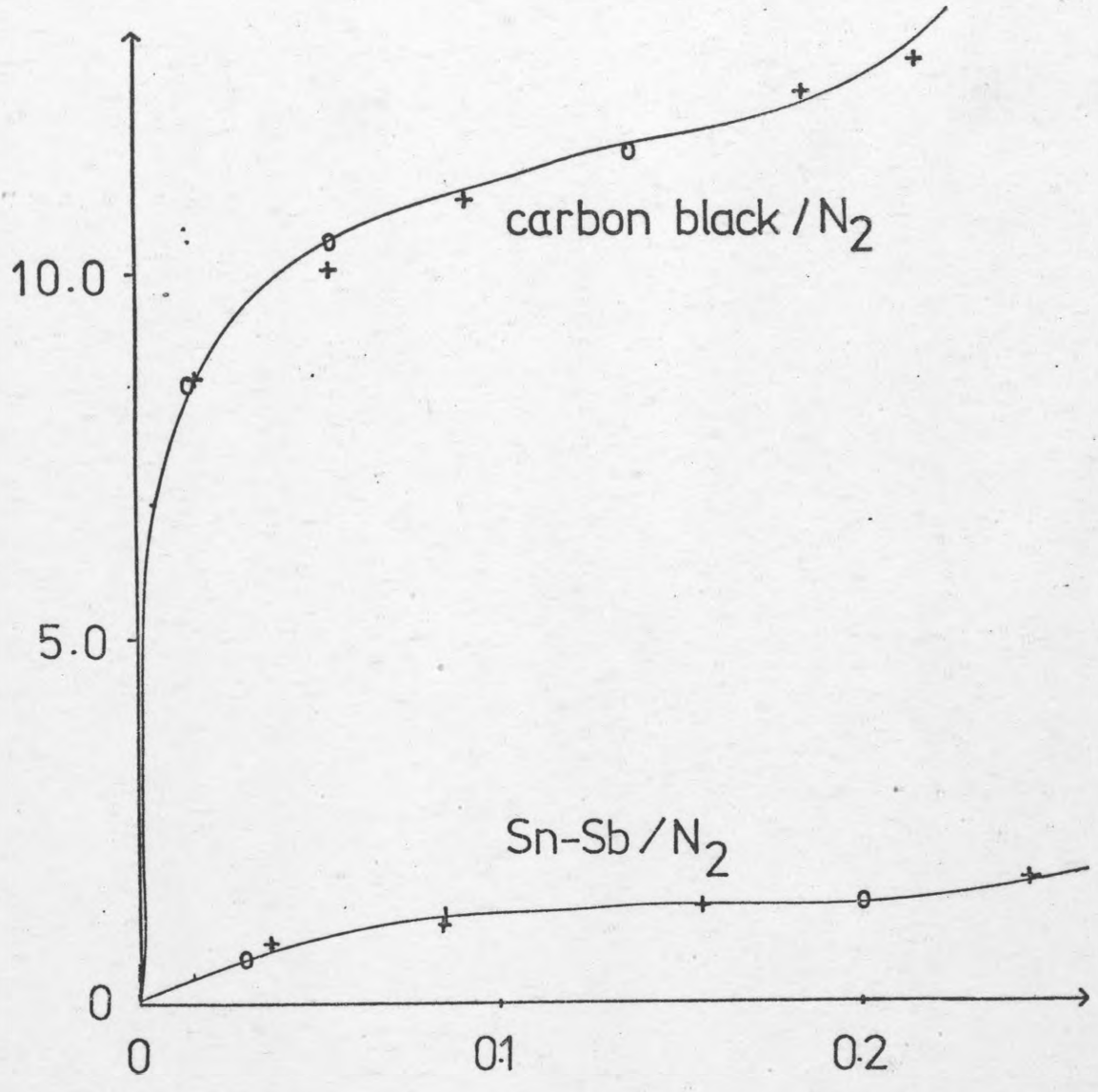

+ adsorption o desorption

Graph 4.2

Comparative data plots

pressures below approximately 0.03 and above 0.3. The divergence at low relative pressures was probably due to the non-uniformity of the surface (the BET theory, as with the Langmuir theory assumes a homogeneous surface). At higher relative pressures the divergence was presumably caused by lateral interaction of adsorbate molecules due to physisorbed molecules being closer packed with increasing coverage (another phenomenon ignored by both the BET and Langmuir models). Therefore data within the range of relative pressures 0.03 to 0.30 were used to calculate the surface areas.

The reason for using the BET rather than any refined theories, such as Huttigs[20], was that the BET surface area, in spite of some of its theoretical weaknesses, was the most quoted in the literature. As can be seen there was good agreement between the quoted areas and those determined experimentally. However, the method of determination by the supplier was not known. The value determined experimentally for the carbon-black adsorbent was $65.89 \pm 1.69 m^2 g^{-1}$, the quoted value by 'CABOT CARBON LTD.' was 65.05 ± 0.5 $m^2 g^{-1}$[83]. The experimentally determined value for the tin-antimony oxide adsorbent was 7.45 ± 0.34 $m^2 g^{-1}$ as compared to the value 7.40 $m^2 g^{-1}$ quoted by 'B.P. LTD.'[82].

4.4 Chemisorption Study

The basic data from the chemisorption of Sn-Sb/O_2, Sn-Sb/C_3H_6 and Sn-Sb/1-C_4H_8 consist of change in datum values (Δ) with equilibrium pressure (cm.oil). The amount adsorbed (in mg.) was the product of the Δ values and the spring

sensitivity with possible corrections for thermal and buoyancy effects as previously described. In these adsorption studies there was no need for pressure corrections (unlike the case of physisorption), due to the low pressures at which maximum adsorption took place. For each system the necessary data were collected at three different temperatures. It was found that a temperature of between 10 to 25°C was required to produce noticeable differences in the maximum amount of gas adsorbed. Three complete sets of data were taken at each temperature for each adsorbate to allow a critical estimate to be made of the reproducibility of the results. This also allowed a quantitative estimate of experimental error to be made for each adsorbate at each temperature.

The adsorption plots (Graphs 3.7-3.9, 3.14-3.16 and 3.21-3.23) indicated chemisorption, showing the Type I isotherm of the BET classification. A gradual increase in adsorption with increasing pressure (in some cases virtually linear) occurred to a point where all the active sites were presumably occupied, i.e. saturation. After this there was no further adsorption with increased pressure (i.e. the plateau region).

At saturation it was found that the amount adsorbed decreased in the series oxygen, propene and butene. Also in all three cases the amount adsorbed went through a maximum as the temperature was varied (Tables 3.49-3.51). The lack of adsorption at low temperatures indicated that an activated adsorption had occurred (the activation energy theory was also verified by the solid-gas stirred reactor work done

by previous researchers[4]). The increasing amount of adsorption with increasing temperature, up to the maximum could probably be due to the activation of otherwise inactive sites by collisions of adsorbate molecules having a higher kinetic energy than the average value for the gaseous molecules. The subsequent decreases of the amount adsorbed with increased temperature (very marked with oxygen and propene) was much more difficult to explain. Possibly at higher temperatures the average time the adsorbate molecule spent on the surface may be too short for chemisorption to take place, leading to an overall decrease in the amount adsorbed. This could be verified by kinetic studies which were not possible, due to the limited sensitivity of the apparatus. It was also not possible to measure the rate of adsorption for the same reason.

With both olefins it was found that the amount of olefin removed from the surface by evacuating the system at the adsorption temperature was negligible. Consequently it was decided that it would be pointless to carry out any prolonged desorption investigation. On outgassing at elevated temperatures (≈300°C) for several hours, most, though not all, of the species held on the surface could be removed. It was found necessary to heat the catalyst to 200°C in oxygen for several hours and then outgas under vacuum to restore the initial state as indicated by a return to the original datum.

Furthermore, if after removing most of the surface species, at high temperatures (300°C), and carrying out another adsorption, it was found that the amount adsorbed was less

in the second case than the first. When this was repeated for a third time the amount adsorbed was found to be less than the second. This has also been reported by other researchers[70].

The explanation is thought to be due to the fact that two types of adsorption occurred, reversible and irreversible. The major part was irreversibly adsorbed. From the literature[71,72] it is generally accepted that reversible adsorption leads to partial oxidation products and the irreversible adsorption to complete oxidation products.

The importance of lattice oxygen in the oxidation of olefins is well known[73], and the removal of this source of oxygen without replenishment is thought to be the reason for the apparent deactivation. Also heating the catalyst in oxygen not only helps the oxidation of the irreversibly adsorbed olefin, but also replenishes the lattice oxygen. It was not possible within the scope of this work to test for oxidation products.

The reversibly adsorbed layer is considered to be held as an allylic complex leading to the production of selective oxidation products. The irreversibly held major part gives completely oxidised products and is probably the olefin held as a carbonate-carboxylate type intermediate. It was found, as described above, to be dislodged at high temperatures in the presence of oxygen[87].

4.5 Heats and Entropies of Adsorption

The theory behind the calculations of the isosteric heats

and differential molar entropies of adsorption are given in section 1.3 and the Appendices. The variation of isosteric heats of adsorption (q_{st}) with coverage (θ) are given in Graphs 3.27-3.29, and those of the variation of differential molar entropy ($\bar{s}_s$) with coverage are given in Graphs 3.30-3.32.

The heats of adsorption were calculated from a Clapeyron-Clausius equation. The plot being that of $\log_{10} P$ v T^{-1} at constant coverage the slope of which was equal to $-q_{st}/2.303R$, R being the universal gas constant.

A typical example of a calculation being that of Sn-Sb/C_3H_6 at 200-250°C as follows:-

From Graphs 3.17-3.19 the corresponding pressure reading to a particular surface coverage may be read for the different temperatures, e.g. at 50% coverage the pressure reading (in cm.oil) are 0.56, 0.62 and 0.34 at 250, 225 and 200°C respectively (Table 3.44). By plotting $\log_{10} P$ against T^{-1} the slope of the best straight line through the data points may be obtained which when equated to the theoretical slope of $-q_{st}/2.303R$ will yield the isosteric heat of adsorption. In this example the slope was -1098 giving a value for the heat of adsorption of 21.01 kJ/mol.

The best straight line through the data points was found by linear regression analysis, i.e. the sum of the squares of the distances from the data points to a fitted line is an algebraic minimum.

In all three cases the data showed that there was a fall

with increasing surface coverage from some maximum q_{st} value. This indicated a dependence of q_{st} on θ (clearly opposing the assumption of Langmuir that q_{st} and θ are independent), showing the surface to be heterogeneous. The q_{st} v θ plots of Sn-Sb/O_2 and Sn-Sb/1-C_4H_8 showed a complex relationship. The first showed a gradual decrease to approximately 50% coverage followed by a sharp decrease. The second had a point of inflexion, once again at approximately 50% coverage. The Sn-Sb/C_3H_6 showed an exponential type of decrease typical of the Freundlich isotherm.

In general the progressively decreasing q_{st} value with θ was as expected, from a surface assumed to be made up of sites of differing activity. The most active sites would be occupied first followed by the gradual occupation of the less active sites. The situation being made more complex in the case of propene and butene by the intermediate oxidation complexes presumably formed by the active lattice oxygen.

It is possible to compare theoretical and experimental heats of chemisorption at low coverages (so that adsorbate-adsorbate interactions on the surface may be ignored) for simple systems such as W/H_2 and Fe/H_2. Theoretical models to describe the chemisorption process have two extreme cases, namely purely ionic or purely covalent bonding. The energy associated with the bonding is the heat of chemisorption.

The ionic bond is regarded theoretically as occurring in two steps[74]. The molecule loses an electron to the adsorbent followed by the adsorbate ion approaching the

equilibrium separation distance. A typical example of the covalent case could be the formation of a hydride

$$2Me\text{-}H_2 \rightarrow 2Me\text{-}H$$

where Me represents the metal. However, this equation could be somewhat misleading as it implies the breaking of the Me-Me bond. It is much more accurate to write

$$q_s(\text{heat of adsorption}) = 2E_{Me\text{-}H} - 2E_{H\text{-}H}$$

with $E_{Me\text{-}H}$ representing the energy to form the Me-H bond and $E_{H\text{-}H}$ the energy to break the H-H bond. $E_{Me\text{-}H}$ may normally be found from the Pauling relationship[86].

Most of the work in this field has been carried out on metal surfaces[9]. Attempting to apply this to olefin adsorption on metal oxides is not justified for two main reasons. First, there is still much that is unknown about the surface processes and, second, the different reaction pathways complicate the calculation of the energetics of the various surface species.

The differential molar entropies ($\bar{s}_s$) were calculated from the following equation

$$\bar{s}_s = s_{m,g} - R\ln P - {}^{q_{st}}/_{T}$$

Consequently with q_{st} (see above), T and P data $\bar{s}_s$ may be calculated once the molar gas entropy $s_{m,g}$ is known at standard conditions, R being the universal gas constant.

$s_{m,g}$ is theoretically made up of four components, they are entropies of translation, rotation, vibration and electronic effects. The latter two may be assumed to be negligible. The entropy of vibration because the relevant factor $e^{-h\nu/kT}$

is significant at high temperatures only, and the electronic effect because the difference between energy levels is assumed to be too great for electrons to migrate from one level to another. The translational contribution may be calculated from the Sackur-Tetrode equation[48] and the rotational contribution is described in Appendix VI.

The differential molar entropy is a measure of the entropy of a mole of adsorbate when adsorbed onto a partially covered surface from the gas phase.

The Sn-Sb/O_2 $\bar{s}_s$ v θ plot shows a decreasing $\bar{s}_s$ value up to the minimum at approximately fifty per cent coverage followed by a marked increase in $\bar{s}_s$ up to maximum coverage. The decreasing part of the curve showed a gradual ordered chemisorption with fewer degrees of freedom for the molecules on the surface. This was due presumably to loss of translational motion and also in the case of oxygen adsorption with dissociation. The increasing part of the curve indicated some compensation for the previous loss of degrees of freedom, perhaps due to adsorbate-adsorbate interactions and also the possibility of some surface mobility.

In the case of the olefins both show different types of curve but in general $\bar{s}_s$ increased with coverage, the butene curve, as does that for oxygen, showing a possible change in adsorption mechanism at fifty per cent coverage. A possible reason for this general loss of surface order may be formation of the previously discussed allylic and carbonate-carboxylate intermediates. Pre-oxidation product complexes formed on the surface by interaction of the lattice

oxygen with the above allylic complex may also explain this effect. There may be further complications if these species were mobile on the surface as sites could now be occupied that could have been appropriate for olefin adsorption. (This latter point is not of great importance in actual oxidation experiments as the reduced sites are thought to be re-oxidised by the gaseous oxygen to allow olefin adsorption once again[4,86].)

There is a possibility that oxidation products desorbed from the surface without either evacuating the system or increasing the temperature. There was no evidence of this by spurious weight losses indicated by the spring balance but it is possible that this effect was obscured by the lack of spring sensitivity. Gas analysis immediately after evacuation might have shown oxidation products.

The propene $\bar{s}_s$ v θ curve shows a gradual increase with coverage, butene was much more complex passing through a point of inflexion with a maximum at approximately fifty per cent coverage.

In statistical mechanical derivations of isotherms the factor used to describe the maximum number of different ways that adsorbed molecules may be distributed among the available adsorption sites (C_N) is as follows

$$C_N = \frac{N_S!}{(N_S-N_A)!N_A!}$$

where N_S is the number of sites and N_A the number of adsorbed molecules. C_N reaches a maximum at fifty per cent coverage, hence at this point the probability that a 1-butene

molecule approaching a site with an available oxygen is at its lowest. This effect loses importance after fifty per cent coverage and other factors become important. It is also possible that the point of inflexion is the barrier at which there is a change in the mechanism of adsorption.

In general a gas molecule being adsorbed will (assuming immobile adsorption) lose its rotational and translational degrees of freedom which will be replaced by vibrational ones. This will lead to a substantial nett loss of entropy. However, as can be seen from the large positive values of the entropies, this is not the case, clearly the situation is much more complex than the simple immobile framework put forward and appears to indicate an increasing liquid-like adsorbed layer with increasing coverage.

From the basic Gibbs free energy relationaship $\Delta G = \Delta H - T\Delta S$ we have, with increasing coverage, a decreasing negative value, i.e. towards zero, because both q_{st} and ΔS become smaller with increasing coverage, indicating the decreasing favourability of the chemisorption with coverage. (It is interesting to note that if the Langmuir hypothesis of constant heat of adsorption with coverage is accepted, i.e. q_{st} = constant, then the above equation is of the form $y = mx + c$ and a linear relationship between ΔG and ΔS would be expected.)

Making some simplifying assumptions it is possible to estimate the probability of a molecule colliding on the surface and then being chemisorbed. Taking the case of the

minimum amount of C_3H_6 adsorbed on Sn-Sb at 200°C and assuming a hypothetical equilibration time of one second, the number of collisions per square metre (Z) may be derived from

$$Z = p/(2\pi mkT)^{\frac{1}{2}}$$

and is equal to 1.788×10^{23}. The total surface area of the catalyst from BET measurements (see section 3.4) was $7.40 m^2 g^{-1}$, knowing the weight of catalyst used (0.5782g), the total number of collisions on the surface may be estimated from

$$Z \quad \frac{7.40}{0.5782} = 2.288 \times 10^{24} \text{ collisions}$$

From Graph 3.14 the amount adsorbed in mg. is 0.8, that is a total of 2.583×10^{18} molecules have been adsorbed. Consequently the probability that a molecule will be adsorbed is the ratio of the number of molecules adsorbed to the total number colliding with the surface, that is $2.583 \times 10^{18}/2.288 \times 10^{24}$ which is equal to 1.129×10^{-6}. Thus the chances of a molecule hitting the surface and then being chemisorbed are in the region of a million to one. Clearly the longer the equilibrium time the larger the total number of collisions on the surface leading to a further decrease in the probability. We would also expect a decreasing probability with coverage because not only are the sites available becoming less energetic, but the proportion of molecules with sufficient energy to chemisorb on these sites will also diminish.

4.6 Data Fitting

An attempt was made to fit all the experimental data to

various isotherms. Three sets of results were taken at each temperature for each adsorbate, the three sets of results were then combined to give one block of data for fitting. Thus nine blocks of data in all were fitted to the isotherms to be discussed. The measure of goodness of fit used was the ratio of the fitting variance to the experimental variance. The fitting variance being calculated from the differences between 'observed' and 'fitted' values for a given isotherm. The experimental variance was that calculated by using linear interpolation[85], described in section 3.12. The variance (σ^2) was used in preference to the standard deviation (σ), because the latter may take positive or negative values as it is = $\sqrt{\sigma^2}$, this was the reason for minimising the sum of squares of differences between observed and fitted values.

The first isotherm to be fitted was Langmuir's, the most widely used model in gas adsorption studies which still generates discussion[86]. From the data fitting tables it can be seen that the fitting variance from the regression analysis (the linear form of Langmuir's equation was used which is described in section 1.2.1) when compared with the experimental variance gave ratios which were all greater than one. A ratio approaching one would be expected for a perfect fit. In several cases Sn-Sb/O_2 at T = 90°C, Sn-Sb/C_3H_6 at T = 200°C and Sn-Sb/1-C_4H_8 at T = 170°C the fitting ratio was found to be in the region of one, due to high experimental variances, but the values of the slope, 0.63, 0.56 and 0.56 respectively was well outside the value of one that would be expected from theoretical considerations (section 1.2.1). In the case of the Sn-Sb/O_2 system the

data was fitted to the linearised form of the Langmuir equation modified for double site adsorption ($p^{\frac{1}{2}}/\theta$ v $p^{\frac{1}{2}}$) as oxygen adsorption is generally thought to go through a dissociative step[74]. As with the single site adsorption it was generally found that the variance ratios were greater than one.

By inspection of the variation of heats of adsorption with coverage for the Sn-Sb/C_3H_6 system, it can be seen that there is an exponential type of decay as postulated by Freundlich in his isotherm. A fit was attempted to the linearised form of the Freundlich equation (lnx v lnp see section 1.2.6) but once again large variance ratios were found.

A non-linear regression fit[85] (as with most of the computer work carried out by Dr. J. Cartlidge on a 'CROMEMCO' Z2 microcomputer) was attempted to the Misra equation. This takes the form

$$P = \frac{1}{(1-K)C}\left|1-(1-\theta)^{1-K}\right|$$

where

P	pressure
θ	coverage
C,K	constants

The significance of this equation is that for K values of 1 and 2 the Jovanovic and Langmuir isotherms are generated. However, for other values of K no kinetic models have as yet been proposed (although the true significance of K is not as yet established it is thought to be related to the adsorption process). As can be seen from the tabulated data large variance ratios were found showing that the

experimental data does not fit the proposed isotherm.

At present most work done on generating a formula to describe adsorption is based on the Langmuir equation, as it generates nearly all known synthetic isotherms providing the appropriate energy distribution function of the surface is chosen. One such example is that proposed by Wojciechowski[3], where a Maxwell-Boltzmann energy distribution (normally associated with molecular velocities) is assumed. However such equations tend to have several unknown parameters requiring the use of numerical integration in conjunction with non-linear fitting techniques. It is also possible that such complex functions may disguise other processes occurring on the surface such as adsorbate-adsorbate interactions.

The obvious failure of the Langmuir isotherm is that $\theta = 1$ only when $P \to \infty$. Consequently, an empirically modified Langmuir isotherm was used which took the form $\theta = \frac{K_1 P}{1+K_2 P}$ with $K_1 > K_2$. The advantage of such an isotherm is that when $\theta = 1$ a finite saturation pressure is obtained given by $\frac{1}{(K_1-K_2)}$. The closeness of this calculated minimum saturation pressure to the observed one was a further indication of the goodness of fit of any block of data to this particular isotherm. In comparing the actual and experimental variances, a modification was necessary to the latter, as extensions corresponding to only two or three vernier divisions of the cathetometer scale were left out as these generated the greatest inaccuracies. For double site adsorption the isotherm was modified to $\theta = K_1 P^{\frac{1}{2}} / 1+K_2 P^{\frac{1}{2}}$ which is analagous to that of Langmuir for double site

adsorption.

As previously stated the isotherm is empirical, and the significance of K_1 and K_2 is not understood, but it is thought that K_1 and K_2 may be related to adsorption and desorption rates respectively.

By comparing the variance ratios in section 3.13 it can be seen that the best ratios were found with the modified Langmuir isotherm.

In the case of oxygen the better fit was found with the double site isotherm, but the experimental saturation pressures are about twice that of the fitted values, e.g. at 80°C the fitted value was 2.37 mm.Hg and the experimental value was in the region 5.23-5.29 mm.Hg. (All pressures will now be stated in units of mm.Hg.) In the case of the olefins not only were good variances found but also the correlation between experimental and fitted saturation pressures was good, but there were complications because the above two points held for both the single and double site isotherms as shown in the table below.

	Single Site		Double Site		
	σ^2/σ_e^2	Sat. P	σ^2/σ_e^2	Sat. P	Experimental P. Range
$Sn-Sb/C_3H_6$					
200	1.29	1.18	2.34	1.02	0.95-1.03
225	7.18	-	3.01	1.48	1.73-1.90
250	1.11	1.13	0.92	1.00	0.95-1.34
$Sn-Sb/C_4H_8$					
130	1.55	0.86	2.87	0.86	0.71-0.79
150	2.07	2.09	1.13	1.09	0.79-0.95
170	0.39	1.09	0.13	0.98	0.87-0.95

For both systems there was one temperature at which a good fit was found which appears to indicate that qualitative as well as quantitative changes of surface properties with temperature occurred. From the results of fitting it was difficult to distinguish between the modified isotherms put forward for single site and double site adsorption.

However, the single site adsorption was thought to be of greater validity than the double site model as in the latter case only the pressure has been changed, as in the original Langmuir isotherm, but other factors not considered here may also need altering. The single site model is an improvement on the Langmuir because of the fact that a finite saturation pressure is obtained at complete adsorption site coverage.

It is interesting to note that whilst no model could be found to fit the apparently simpler Sn-Sb/O_2 system, the modified Langmuir was found to give a good fit to the much more complex (as indicated by the calculated entropy data) olefin systems.

The fact that 3.44×10^{19} molecules of propene are adsorbed per gramme of catalyst as compared to 1.05×10^{19} of butene at maximum coverage was thought to indicate a stereo specific adsorption such that the larger butene molecule on adsorption makes sites in close vicinity inaccessible to other adsorbing olefin molecules, to a greater extent than the propene.

The experimental variance as calculated by linear interpolation not only gave a measure of the goodness of fit, but by taking the square root of the variance, i.e. the standard deviation, gives a quantitative value for the experimental error which was found to be between 4-10%, the mean error being 6%.

The two sources of error were the measurement of the amount of gas adsorbed, read off a vernier scale and the pressure of gas as indicated on an oil manometer, the greatest source of error being the former.

The largest errors were found when the first dose of gas was admitted to the system leading to a 2-3 vernier division change, the accuracy of the reading being to one vernier division.

5. Conclusions

The apparatus was found in general to be easy to handle. The only equipment likely to be damaged was the fragile quartz springs. However during the course of the experimental work only one spring was broken.

The balance was found to be appropriate for BET surface area measurements with samples of surface areas of $1 m^2 g^{-1}$ or greater. Although still being the most widely used treatment for data from surface area measurements, the BET model was found to be valid only between the relative pressure range of 0.03-0.30.

The adsorption of oxygen, propene and 1-butene on the tin-antimony oxide catalyst led to the following conclusions: In all three cases chemisorption was clearly taking place, indicated by a gradual rise in the amount adsorbed up to a maximum after which no adsorption took place (also indicated by the heats of adsorption values), also the majority of the adsorbed species was irreversibly held on the surface and could only be removed at high temperature and, as in the case of the olefins, in the presence of an oxygen atmosphere. Chemisorption was found in all three cases to take place within a limited temperature range indicating an activation process. In the case of olefin adsorption the importance of lattice oxygen was found by the gradual deactivation of the catalyst between adsorptions, also indicating a redox mechanism in olefin oxidation.

The heats of adsorption calculations quite clearly indicated the heterogeneity of the surface towards the adsorbates by the decreasing variation of these values with coverage from

a maximum of 28.1, 95.1 and 66.7 kJ mol^{-1} for oxygen, propene and 1-butene respectively to less than one. The importance of the interactions of surface complexes with lattice oxygen and mobility of the surface species in a liquid-like adsorbed layer appeared to be indicated by the variation of the entropies of adsorption with coverage (this approach has not been previously used with mixed oxide catalysts). What was clearly shown by this data was the complex nature of the mechanism of adsorption of olefins onto the tin-antimony catalyst which as yet is not fully understood. Further evidence of this was the previous unsuccessful attempt to fit accurate data from Sn-Sb catalysed reactions in the gas-solid stirred reactor work[4].

Using the variance ratio as the main criterion of the measure of goodness of fit of the data to an isotherm, of those models used only the empirically modified Langmuir isotherm for single site adsorption was a satisfactory fit to only some of the olefin data. No reasonable fit was found for the more accurate oxygen data.

There is still a need for a relatively simple model which when fitted to adsorption data will yield parameters that may be used to characterize a system, i.e. that are of real physical significance.

Further Work

The main drawback to this work has been the insensitivity of the spring balance. Increased sensitivity could have been achieved by using specially made quartz springs. This, however, must necessarily mean longer springs leading to

associated handling problems. Consequently, the only way to increase the sensitivity of the apparatus is to replace the spring by an expensive vacuum microbalance; if such a balance had been available then work could have been carried out on the bismuth-molybdate catalyst. Another, but not as vital change, is to replace the oil manometer with a pressure transducer (which was bought but not used). Overall such improvements described would be beyond available means.

Having increased the sensitivity of the apparatus it would be possible to carry out kinetic studies of the catalytic systems and information such as variation of the sticking probability with coverage, rates of adsorption and activation energies could be measured, which was not possible in this work.

It may be possible to analyse the gases present within the balance case during the adsorption to examine the importance of lattice oxygen; there is no evidence in the literature that this has been done.

Appendices

Appendix I

Table 1

Sn-Sb weight correction data

Uncorrected catalyst weight	0.5791g	
Loss in weight due to evacuation and degassing	Δ_1	Δ_2
	0.031	0.036
Buoyancy correction using Ar.	Δ_1	Δ_2
	0.008	0.008

Spring II used

Table 2

Correction data using He at liquid N_2 temperature

Pressure (cm.oil)	Head (cm.)	Δ (cm.)
52.70	59.30	0
107.20	60.20	0
165.10	61.90	0
220.30	60.00	0
275.60	60.50	0
329.60	59.85	0.001
383.10	59.60	0.002
431.30	57.00	0.003
12.60	8.80	0.003
60.20	4.60	0.003
116.30	6.60	0.003
168.30	6.55	0.003
220.50	6.30	0.003
272.80	5.50	0.003
326.60	4.70	0.002
382.60	7.80	0.001

Table 3

Sn-Sb/N_2 BET data

	Pressure cm.oil	Level of Head cm.	Δ cm.
RUN 1	45.00	55.40	0.032
	95.80	58.40	0.044
	151.40	60.80	0.048
	203.20	58.95	0.059
RUN 2	32.80	49.30	0.022
	71.60	52.35	0.031
	117.50	55.90	0.042
	154.10	51.65	0.046
	210.60	61.20	0.052
	243.10	49.10	0.057
	296.70	59.75	0.063
RUN 3	34.40	50.10	0.027
	74.70	53.10	0.034
	121.30	56.25	0.043
	168.80	56.80	0.047
	221.30	59.20	0.051
	270.40	57.55	0.055
	303.70	49.70	0.060
	246.30	3.90	0.053
	193.50 }	6.00 }	0.043
	137.80 }	4.60 }	
	84.00 }	5.05 }	0.021
	29.90 }	5.60 }	

Spring II used

Table 4

Carbon black weight correction data

Uncorrected catalyst weight	0.5317g		
Loss in weight due to evacuation and degassing (Spring I)	Δ_1	Δ_2	Δ_3
	0.137	0.137	0.136
Buoyancy correction using Ar. (Spring II)	Δ_1	Δ_2	Δ_3
	0.011	0.011	0.011

Springs I and II used

Table 5

Carbon black /N_2 BET data

	Pressure cm.oil	Level of Head cm.	Δ cm.
RUN 1	13.80	39.80	0.204
	39.60	45.80	0.227
	68.70	47.50	0.250
	99.70	48.50	0.267
	126.70	46.40	0.282
	143.00	41.00	0.293
	100.10	11.20	0.265
	58.80	12.00	0.241
	39.40	23.00	0.224
RUN 2	23.70	44.65	0.200
	44.90	55.40	0.230
	71.40	46.00	0.238
	92.50	56.70	0.262
	120.10	46.60	0.274
RUN 3	33.10	49.50	0.204
	81.30	57.00	0.236
	123.20	53.90	0.266
	162.10	52.40	0.286
	192.10	47.85	0.312
	140.00	6.25	0.279
	119.90 }	22.50 }	0.243
	78.60 }	11.85 }	

Spring I used

Appendix II

Table 1

Sn-Sb/C_3H_6 correction data (using Argon)

	Pressure cm.oil	Δ cm.
T = 200°C	0.30	0.002
	1.00	0.004
	3.80	0.007
	6.10	0.009
	9.00	0.012
	1.20	0.004
	2.60	0.005
	5.00	0.008
	6.10	0.009
T = 250°C	0.90	0.003
	2.20	0.005
	3.70	0.006
	6.10	0.007
	8.40	0.009
	0.40	0.002
	1.50	0.004
	3.40	0.006
	5.40	0.007
	8.00	0.009

Table 2

Sn-Sb/C_3H_6 adsorption data at T = 225°C

Block 1

RUN 1		RUN 2		RUN 3	
P	Δ	P	Δ	P	Δ
0.20	0.011	0.10	0.006	0.10	0.006
0.70	0.016	0.30	0.014	0.30	0.013
1.00	0.021	0.50	0.017	0.90	0.019
1.30	0.024	0.90	0.020	1.20	0.024
1.60	0.028	1.20	0.024	1.60	0.029
2.00	0.032	1.70	0.029	2.20	0.035
2.40	0.036	2.00	0.032	2.40	0.036
2.60	0.036	2.40	0.036	2.60	0.036
		2.60	0.036		

Table 3

Sn-Sb/C_3H_6 adsorption data at T = 250°C
Block 2

RUN 1		RUN 2		RUN 3	
P	Δ	P	Δ	P	Δ
0.20	0.003	0.10	0.002	0.10	0.002
0.50	0.006	0.40	0.005	0.30	0.004
0.70	0.008	0.80	0.008	0.50	0.006
1.00	0.011	0.90	0.010	0.60	0.007
1.30	0.013	1.20	0.012	1.00	0.010
1.60	0.013	1.50	0.013	1.20	0.012
		1.90	0.013	1.50	0.013

Table 4

Sn-Sb/C_3H_6 adsorption data at T = 200°C
Block 3

RUN 1		RUN 2		RUN 3	
P	Δ	P	Δ	P	Δ
0.20	0.005	0.20	0.006	0.10	0.003
0.50	0.012	0.50	0.012	0.40	0.010
0.70	0.014	0.60	0.013	0.90	0.015
1.10	0.016	1.00	0.015	1.10	0.017
1.50	0.019	1.20	0.018	1.30	0.019
1.80	0.019	1.60	0.019	1.40	0.019
		1.80	0.019		

Spring I and II used

Appendix III

Table 1

Sn-Sb/0_2 correction data (using Argon)

	Pressure cm.oil	Δ cm.
T = 80°C	6.80	0.002
	15.80	0.003
	20.50	0.004
	49.30	0.006
	2.10	0.001
	13.00	0.003
	28.90	0.005
	38.70	0.005
T = 100°C	6.80	0.002
	19.90	0.004
	28.90	0.005
	11.30	0.003
	32.90	0.005
	44.30	0.006

Table 2

Sn-Sb/0_2 adsorption data at T = 80°C

Block 1

RUN 1		RUN 2		RUN 3	
P	Δ	P	Δ	P	Δ
0.20	0.003	0.20	0.003	0.10	0.002
0.40	0.009	0.50	0.012	0.40	0.008
0.80	0.018	0.70	0.014	0.90	0.015
1.70	0.022	1.50	0.023	2.50	0.024
3.50	0.029	2.60	0.026	4.30	0.031
5.80	0.036	3.60	0.030	6.70	0.038
7.80	0.039	4.50	0.033	8.00	0.039
9.00	0.039	6.60	0.037	9.00	0.039
		8.80	0.039		
		9.00	0.039		

Table 3

Sn-Sb/0_2 adsorption data at T = 90°C
Block 2

RUN 1		RUN 2		RUN 3	
P	Δ	P	Δ	P	Δ
0.50	0.011	0.40	0.008	0.10	0.003
1.10	0.017	0.70	0.016	0.30	0.006
1.50	0.019	1.80	0.020	0.70	0.015
2.00	0.020	3.10	0.025	1.10	0.018
3.50	0.028	4.70	0.029	2.90	0.024
5.80	0.033	6.40	0.032	4.70	0.029
8.20	0.036	8.30	0.036	7.30	0.034
10.20	0.036	8.70	0.036	9.50	0.036
				11.50	0.036

Table 4

Sn-Sb/0_2 adsorption data at T = 100°C
Block 3

RUN 1		RUN 2		RUN 3	
P	Δ	P	Δ	P	Δ
0.30	0.004	0.10	0.003	0.30	0.004
0.70	0.006	0.50	0.005	0.80	0.006
1.70	0.009	1.80	0.010	1.90	0.010
3.20	0.013	3.40	0.015	3.40	0.014
5.00	0.017	5.60	0.021	5.80	0.020
6.90	0.022	7.10	0.022	7.60	0.022
8.90	0.022	9.40	0.022	9.40	0.022

Spring I used throughout

Appendix IV

Table 1

Sn-Sb/C_4H_8 correction data (using Argon)

	Pressure cm.oil	Δ cm.
T = 170°C	2.00	0.000
	14.60	0.003
	26.00	0.006
	39.00	0.009
	2.70	0.000
	6.10	0.002
	18.90	0.004
	29.80	0.006
T = 130°C	7.20	0.002
	15.20	0.003
	25.00	0.005
	34.40	0.007
	2.60	0.001
	14.00	0.003
	18.80	0.004
	27.80	0.006

Table 2

Sn-Sb/C_4H_8 adsorption data at T = 170°C

Block 1

RUN 1		RUN 2		RUN 3	
P	Δ	P	Δ	P	Δ
0.10	0.002	0.10	0.003	0.20	0.005
0.50	0.009	0.20	0.004	0.40	0.007
0.80	0.012	0.70	0.010	0.70	0.010
1.10	0.014	1.00	0.013	0.90	0.012
1.20	0.015	1.10	0.014	1.00	0.013
1.40	0.015	1.20	0.015	1.20	0.015
		1.30	0.015	1.40	0.015

Table 3

Sn-Sb/C_4H_8 adsorption data at T = 150°C
Block 2

RUN 1		RUN 2		RUN 3	
P	Δ	P	Δ	P	Δ
0.10	0.006	0.20	0.008	0.10	0.006
0.30	0.009	0.50	0.012	0.20	0.008
0.60	0.013	0.60	0.014	0.40	0.010
1.00	0.017	1.00	0.016	0.90	0.015
1.20	0.019	1.20	0.019	1.20	0.019
1.40	0.019	1.50	0.019	1.40	0.019

Table 4

Sn-Sb/C_4H_8 adsorption data at T = 130°C
Block 3

RUN 1		RUN 2		RUN 3	
P	Δ	P	Δ	P	Δ
0.10	0.006	0.10	0.005	0.20	0.007
0.20	0.008	0.30	0.009	0.40	0.011
0.70	0.014	0.40	0.012	0.60	0.013
1.00	0.016	0.70	0.014	0.90	0.015
1.10	0.016	1.00	0.016	1.10	0.016
		1.20	0.016	1.30	0.016

Spring II used throughout

Appendix V

Computer programme for calculating the experimental variance and standard deviation by linear interpolation.

Computer programme for calculating the experimental variance and standard deviation by linear interpolation (pp.204-205) has been removed for copyright reasons

Appendix VI

Evaluation of the Molar Entropy of a Gas from Statistical Mechanical Considerations.

Evaluation of the Molar Entropy of a Gas from Statistical Mechanical Considerations[45,75]

From statistical mechanical considerations the molar entropy of a gas is described by

$$S_{m,g} = k\, d/dT\left(\frac{T \ln (p.f.)_t^N}{N!}\right) + R\, d/dT\,(T \ln (p.f.)_e) + R\, d/dT\,(T \ln (p.f.)_v) + R\, d/dT\,(T \ln (p.f.)_r) \quad 1$$

where,

$(p.f.)_t$ - translational partition function

$(p.f.)_e$ - electronic partition function

$(p.f.)_v$ - vibrational partition function

$(p.f.)_r$ - rotational partition function

The electronic and vibrational effects may normally be ignored; the former because the energy difference between levels is too great for electrons to migrate from one level to another, and the latter because the important relation in $(p.f.)_v$ is $e^{-h\nu/kT}$, (where ν is the vibrational frequency and h is Plancks' constant) and is normally significant at high temperatures.

Consequently the important contributory factors to the molar gas entropy are the rotational and translational effects.

Rotational Entropy

From equation 1 it follows that

$$S_{m,g}(rot) = R\frac{d}{dT}\, T \ln (p.f.)_r \quad 2$$

For a diatomic molecule the partition function is

$$(p.f.)_r = \frac{8\pi^2 AkT}{\sigma h^2} = (\text{constant}).T \qquad 3$$

where,

A - moment of inertia $kg.m^2$

k - Boltzmann constant JK^{-1}

T - temperature K

h - Planck constant Js

σ - symmetry factor

In the case of oxygen $\sigma = 2$. Substituting 3 into 2 and carrying out the differentiation we have

$$S_{m,g}(rot) = R(\ln(p.f.)_r + 1) \qquad 4$$

A non-linear molecule, such as propene and butene, will be characterized by three principle moments of inertia A, B and C, in this case the partition function is more complex

$$(p.f.)_r = \frac{\pi^{\frac{1}{2}}(8\pi^2 kT)^{3/2}(A.B.C)^{\frac{1}{2}}}{\sigma h^3} \qquad 5$$

The symmetry number being equal to one for propene and butene. Substituting 5 into 2 and carrying out the differentiation the rotational entropy becomes

$$S_{m,g}(rot) = R(\ln (p.f.)_r + {}^3/2) \qquad 6$$

Data from Landold and Bernstein[76] gives the following values for the moments of inertia (M.O.I.) of oxygen, propene and butene molecules

Gas	M.O.I. ($g.cm^2$)
O_2	1.934×10^{-39}
$C_3 H_6$	A 1.816×10^{-38} B 9.019×10^{-39} C 1.032×10^{-38}
$C_4 H_8$	A 5.484×10^{-39} B 1.506×10^{-38} C 1.950×10^{-38}

The subsequent calculations, from the above equations, give rise to the following rotational entropies

Gas	$S_{m,g}(rot)$ $JK^{-1}mol^{-1}$
O_2	43.820
$C_3 H_6$	101.804
$C_4 H_8$	101.604

Translational Entropy

The translational contribution to the gas entropy is given by the Sackur-Tetrode[48] equation, which is

$$S_{m,g}(trans) = N\,k\left({}^5/_2 \ln T - \ln P + \ln\left(\frac{2\pi m}{h^2}\right)^{3/2} k^{5/2} + {}^5/_2 \right) \qquad 7$$

This equation can be simplified to

$$S_{m,g}(trans) = R \ln \left(\frac{T^{5/2}.(2\pi m)^{3/2}.\, k^{5/2}.\, e^{5/2}}{P.\ h^3} \right) \qquad 8$$

where,

S entropy $J\,K^{-1}mol^{-1}$

R gas constant $J\,K^{-1}mol^{-1}$

T	temperature	K
m	mass	Kg
k	Boltzmann const.	JK^{-1}
P	pressure	Nm^{-2}
h	Planck constant	Js

It is important that the correct units are used when substituting for the standard state in equation 7. To ensure this a dimensional analysis must be carried out. This was done for the expression within the brackets of equation 2, which should be dimensionless.

Substituting the units into the bracketed expression of equation 8 the following is found

$$\frac{(K^{5/2})\ (Kg^{3/2})\ (J^{5/2}\ K^{-5/2})}{(Nm^{-2})\ (J^{3}\ s^{3})} \qquad 9$$

By definition 1J = 1Nm, substituting

$$\frac{(K^{5/2})\ (Kg^{3/2})\ (J^{5/2}\ K^{-5/2})}{(Nm^{-2})\ (N^{3}m^{3}\ s^{3})} \qquad 10$$

Once again, by definition, a force of one Newton is required to accelerate a mass of one Kg. by one ms^{-2}. The units of N are therefore $Kg.m.s^{-2}$, substituting into 4

$$\frac{(k^{5/2})\ (Kg^{3/2})\ (Kg^{5/2}m^{5/2}s^{-5}m^{5/2}K^{-5/2})}{(Kg.m.s^{-2}\ m^{-2})\ (Kg^{3}m^{3}s^{-6}\ m^{3}s^{3})} \qquad 11$$

Collecting like terms in the denominator and numerator

$$\frac{(Kg^{4})\ (m^{5})\ (s^{-5})}{(Kg)^{4}\ (m^{5})\ (s^{-5})} \qquad 12$$

As all the units cancel the correct pressure units are Nm^{-2} and the mass in Kg.

In the standard state T = 298.1K and P = 1.013 Nm^{-2}, also $m = M/10^3L$ where M is the molecular weight in g.

Therefore

$$S = R\ln M^{3/2} T^{5/2} - R\ln P + R\ln\left(\frac{2\pi}{10^3 Lh^2}\right) + R\ln K^{5/2} + {}^5/_2R \qquad 13$$

which simplifies to

$$S = R \ln M^{3/2} T^{5/2} - 10.04\ JK^{-1}mol^{-1} \qquad 14$$

Substituting the values for oxygen, propene and butene into 14 gives

Gas	$S_{m,g}$(trans) $JK^{-1}mol^{-1}$
O_2	151.600
C_3H_6	154.986
C_4H_8	158.574

Finally the molar gas entropy, assuming negligible values for the electronic and vibrational effects, is as follows

Gas	$S_{m,g}$ $JK^{-1}mol^{-1}$
O_2	195.420
C_3H_6	256.790
C_4H_8	260.178

Appendix VII

Derivation of master equations for surface thermodynamic properties.

Derivation of Master Equations for Surface Thermodynamic Properties[77-79]

Simplifying Notations

1. Subscript x refers to the adsorbent in the presence of adsorbed gas.
2. Subscript s refers to the surface.
3. Subscript x' refers to the adsorbent in the presence of a negligible amount of adsorbed gas.
4. Subscript (o) refers to a property in the absence of a surface.
5. No subscript implies a property of the thermodynamic system.

The thermodynamic system in equilibrium with the unadsorbed gas is defined as the combination of adsorbed gas plus adsorbent enclosed by an imperfectly defined surface. The change in the internal energy, U of the thermodynamic system, for n_x molecules of adsorbent and n_s molecules of adsorbed gas at a temperature T, pressure P and enclosed by a volume V, may be described by

$$dU = TdS - PdV + \mu_x dn_x + \mu_s dn_s \qquad 1$$

where dS represents the entropy change and μ_x and μ_s represent the chemical potentials (the intrinsic molar energy function) of the adsorbent and adsorbed gas respectively.

On removal of the adsorbed gas equation 1 may be modified to

$$dU_x' = TdS_x' - PdV_x' + \mu_x' dn_x \qquad 2$$

This assumes that the removal of the gas from the surface has some effect on the chemical potential of the surface.

From 1 and 2 it is now possible to produce a formula for dU_s, defined previously

$$dU_s = dU - dU_x'$$

$$= TdS_s - PdV_s + (\mu_x - \mu_x')dn_x + \mu_s dn_s \qquad 3$$

The chemical potential of a solid in the absence of gas is made up of two components

$$\mu_x' = \mu_{x',(o)} + \gamma_x' A_{m,x} \qquad 4$$

where $\mu_x'(o)$ is a hypothetical chemical potential of a solid in the absence of adsorbed gas and surface with $\gamma_x' A_{m,x}$ representing the surface contribution. γ_x' is the surface tension in the absence of adsorbed gas and $A_{m,x}$ the molar surface area of the adsorbent.

In the presence of adsorbed gas 4 may be modified to

$$\mu_x = \mu_{x,(o)} + \gamma_x A_{m,x} \qquad 5$$

where, once again, $\mu_{x,(o)}$ is a hypothetical chemical potential, this time in the presence of adsorbed gas but absence of surface. The surface contribution being $\gamma_x A_{m,x}$. It follows that

$$\mu_x - \mu_x' = (\mu_{x,(o)} - \mu_{x,(o)}) + (\gamma_x - \gamma_x')A_{m,x} \qquad 6$$

Assuming the solid to be inert then $(\mu_x'(o) - \mu_x'(o)) = 0$ and by definition the surface pressure $(\pi) = \gamma_x' - \gamma_x$. Equation 3 may now be modified to

$$dU_s = TdS_s - PdV_s - (\pi)A_{m,x}dn_x + \mu_s dn_s \qquad 7$$

$A_{m,x}dn_x$ represents the change in area dA due to a very small increase in the number of adsorbed molecules, equation 7 can be further modified to

$$dU_s = TdS_s - PdV_s - \pi dA + \mu_s dn_s \qquad 8$$

From this other master equations may be derived, such as

the Gibbs free energy of an adsorbed gas on a solid, i.e.

$$dG_s = V_s dP - S_s dT - \pi_s dA + \mu_s dn_s \qquad 9$$

Appendix VIII

Entropies of adsorption.

Entropies of Adsorption

It is important to define exactly which entropy of adsorption is being used as either the molar entropy of the adsorbed layer ($s_{m,s}$) or the differential molar entropy ($\bar{s}_s$) may be used.

(i) Molar Entropy of the Adsorbed Layer

From the master equation 9 in Appendix VII and with T and P constant, the Gibbs free energy function of the surface may be described by

$$dG_s = -\pi dA + \mu_s dn_s \qquad 1$$

integration w.r.t. n_s and A gives

$$G_s = -\pi A + \mu_s n_s + 2 \text{ constants of integration} \qquad 2$$

differentiating w.r.t. A, π, μ_s and n_s gives

$$dG_s = \mu_s dn_s + n_s d\mu_s - \pi dA - A d\pi \qquad 3$$

Since 3 above and equation 9 from Appendix VII both equal dG_s, it follows that subtraction of 9 from 3 gives

$$S_s dT - V_s dP - A d\pi + n_s d\mu_s = 0 \qquad 4$$

rearranging and dividing by n_s - the number of moles adsorbed on the surface, to give molar properties

$$d\mu_s = V_{m,s} dP - s_{m,s} dT + A_{m,s} d\pi \qquad 5$$

Considering the gas phase, keeping P and T constant in the following equation

$$dG_g = V_g dP - S_g dT + \mu_g dn_g \qquad 6$$

gives

$$dG_g = \mu_g dn_g \qquad 7$$

Integrating 7 w.r.t. n_g gives

$$G_g = \mu_g n_g + \text{constant of integration} \qquad 8$$

which when differentiated w.r.t. μ_g and n_g gives

$$dG_g = \mu_g dn_g + n_g d\mu_g \qquad 9$$

When this equation is subtracted from 6 and then divided by n_g and rearranged, the chemical potential of the gas phase is described

$$d\mu_g = V_{m,g}dP - s_{m,g}dT \qquad 10$$

At equilibrium there is no change in the chemical potential, therefore $d\mu_{(g)} = d\mu_{(s)}$ equating 10 and 5 we have

$$V_{m,g}\,dP - s_{m,g}dT = V_{m,s}dP - s_{m,s}dT + A_{m,s}d\pi \qquad 11$$

with constant surface pressure, $d\pi = 0$, and rearranging the above

$$(V_{m,g} - V_{m,s})dP = (s_{m,g} - s_{m,s})dT \qquad 12$$

Assuming $V_{m,g} \gg V_{m,s}$ and also that $V_{mg} = {}^{RT}/P$ we have

$$\frac{RTdP}{P} = (s_{m,g} - s_{m,s})dT \qquad 13$$

or

$$\left(\frac{\partial \ln P}{\partial T}\right)_\pi = \frac{(s_{m,g} - s_{m,s})}{RT} \quad \text{at constant surface pressure} \qquad 14$$

$s_{m,g}$, the molar gas entropy may be evaluated from statistical mechanical considerations (see Appendix VI).

(ii) Differential Molar Entropy of the Adsorbed Layer

Starting with the master equation

$$dG_s = V_s dP - s_s dT - \pi dA + \mu_s dn_s \qquad 15$$

and differentiating w.r.t. n_s 15 becomes

$$\frac{\partial}{\partial n_s}(dG)_s = \left(\frac{\partial V_s}{\partial n_s}\right)_{P,T,A} dP - \left(\frac{\partial S_s}{\partial n_s}\right)_{P,T,A} dT - \left(\frac{\partial \pi}{\partial n_s}\right)_{P,T,A} dA + \left(\frac{\partial \mu_s}{\partial n_s}\right)_{P,T,A} dn_s$$

where symbol "-" indicates a molar property then

$$\frac{\partial}{\partial n_s}(dG)_s = \bar{V}_s dP - \bar{s}_s dT - \left(\frac{\partial \pi}{\partial n_s}\right)_{P,T,A} dA + \left(\frac{\partial \mu_s}{\partial n_s}\right)_{P,T,A} dn_s \qquad 16$$

For a constant amount adsorbed ($dn_s = 0$) and adsorbent of fixed area ($dA = 0$) i.e. at constant coverage, 16 becomes

$$d\mu_s = \bar{V}_s dP - \bar{s}_s dT \qquad 17$$

Once again assuming equilibrium and that the chemical potential of the surface can be equated to the chemical potential of the gas, which is

$$d\mu_g = V_{m,g} dP - s_{m,g} dT$$

we have

$$(V_{m,g} - \bar{V}_s)dP = (s_{m,g} - \bar{s}_s)dT \qquad 18$$

Again, assuming $V_{m,g} \gg \bar{V}_s$ and that $V_{m,g} = {}^{RT}/_{P}$

$$\frac{RTdP}{P} = (s_{m,g} - \bar{s}_s)dT \qquad 19$$

or

$$\left(\frac{\partial \ln P}{\partial T}\right)_\theta = \frac{(s_{m,g} - \bar{s}_s)}{RT} \quad \text{at constant coverage} \qquad 20$$

The molar entropy for the gas phase being calculated by use of statistical mechanics.

Consequently, the molar entropy of adsorption is measured from P v T plots at constant surface pressure and the differential molar entropy of adsorption by similar plots at constant surface coverage.

Appendix IX

Heats of adsorption.

Heats of Adsorption

As with entropies of adsorption, it is important to identify the different heats of adsorption; they are

(i) The Equilibrium Heat of Adsorption

This corresponds to the molar entropy of adsorption and is defined as

$$\Delta H = T(s_{m,g} - s_{m,s}) \qquad 1$$

Substitution into equation 14 of Appendix VIII i.e.

$$\left(\frac{\partial \ln P}{\partial T}\right)_{\pi} = \frac{(s_{m,g} - s_{m,s})}{RT} \quad \text{at constant surface pressure}$$

as

$$\frac{\Delta H}{T} = s_{m,g} - s_{m,s}$$

$$\left(\frac{\partial \ln P}{\partial T}\right)_{\pi} = \frac{\Delta H}{RT^2} \qquad 2$$

(ii) The Isosteric Heat of Adsorption

This heat of adsorption q_{st} is derived from

$$q_{st} = T(s_{m,g} - \bar{s}_s) \qquad 3$$

which when substituted into equation 20 of Appendix VIII i.e.

$$\left(\frac{\partial \ln P}{\partial T}\right)_{\theta} = \frac{(s_{m,g} - \bar{s}_s)}{RT} \quad \text{at constant coverage}$$

yields

$$\left(\frac{\partial \ln P}{\partial T}\right)_{\theta} = q_{st}/RT^2 \quad \text{again at constant coverage} \qquad 4$$

(iii) The Differential Heat of Adsorption

This heat of adsorption (q_d) is found only by calorimetric

methods and is defined in a similar manner to q_{st}, but applies to constant volume conditions.

The relationship between the isosteric and differential heats of adsorption is

$$q_{st} = q_d + RT \qquad 5$$

Appendix X

Number of collisions on a surface from kinetic considerations.

Derivation of Collision Frequency[80]

Consider a wall of area A perpendicular to the x-axis. If a molecule has a velocity V_x in the x direction, lying between 0 and $+\infty$ it will strike the wall in time Δt if it lies at a distance of $V_x \Delta t$ (if its velocity is between 0 and $-\infty$ it is moving in the opposite direction) from the wall. Therefore any molecule in the volume $AV_x \Delta t$ will strike the wall in a time Δt providing it has the appropriate velocity. The total number of collisions is therefore

$$Z = C.\ A.\ \Delta t. \int_0^{\infty} V_x \ f(V_x) dV_x \qquad 1$$

where,

Z - number of collisions

C - concentration i.e. the number of molecules/unit volume

$f(V_x)$ - velocity distribution, undefined at present

To solve the above equation the explicit form of the velocity distribution must be known.

Consider the mean velocity of a particle

$$\langle V_x \rangle = \int_{-\infty}^{+\infty} V_x f(V_x) dV_x \qquad 2$$

The function $f(V_x)$ gives the probability of the x-component of velocity lying in range V_x to $V_x + dV_x$. The probability that a molecule has a velocity component V_x in the above range, a velocity component V_y in the range V_y and $V_y + dV_y$ and a component V_z in the range V_z and $V_z + dV_z$ is $f(V_x)f(V_y)f(V_z)dV_x dV_y dV_z$, since these velocities are independent of each other

i.e. $$F(V_x, V_y, V_z)dV_x dV_y dV_z$$
$$= f(V_x)f(V_y)f(V_z)dV_x dV_y dV_z \qquad 2$$

Assuming that the velocity distribution is independent of orientation, but dependent only on speed V, where $V^2 = V_x^2 + V_y^2 + V_z^2$ equation 2 becomes

$$F(V_x^2 + V_y^2 + V_z^2) = f(V_x)f(V_y)f(V_z) \qquad 3$$

It is found that $f(V_x) = K \exp(-\zeta V_x^2)$ satisfies equation 3 where K and ζ are constants.

Therefore,

$$f(V_x)f(V_y)f(V_z) = K^3 \exp(-\zeta(V_x^2 + V_y^2 + V_z^2)) \qquad 4$$

The probability that the velocity lies between $-\infty$ and $+\infty$ must be unity

$$\int_{-\infty}^{\infty} f(V_x)dV_x = 1 \qquad 5$$

Substituting 5 into the equation for $f(V_x)$

$$\int_{-\infty}^{\infty} f(V_x)dV_x = K \int_{-\infty}^{\infty} \exp(-\zeta V_x^2)dV_x$$

$$= K (\pi/\zeta)^{\frac{1}{2}} = 1 \qquad 6$$

where, π is the geometric π

Therefore

$$K = (\zeta/\pi)^{\frac{1}{2}}$$

To evaluate ζ

$$\langle V_x^2 \rangle = \int_{-\infty}^{\infty} V_x^2 f(V_x)dV_x$$

$$= (\zeta/\pi)^{\frac{1}{2}} \int_{-\infty}^{\infty} V_x^2 \exp(-\zeta V_x^2)dV_x \qquad 7$$

The integral on the right hand side is a standard one and has the value $\frac{1}{2}(\pi/\zeta^3)^{\frac{1}{2}}$.

Therefore

$$v_x^2 = (\zeta/\pi)^{\frac{1}{2}} \tfrac{1}{2}(\pi/\zeta^3)^{\frac{1}{2}} = \tfrac{1}{2}\zeta \qquad 8$$

The mean square speed U is

$$U = \langle v^2 \rangle = \langle v_x^2 + v_y^2 + v_z^2 \rangle \qquad 9$$

and therefore

$$U = \frac{3}{2}\zeta \qquad 10$$

Also, from kinetic theory,

$$pV = \frac{1}{3}N.m.U \qquad 11$$

where N is the actual number of molecules present and m is the mass of one molecule.

In addition

$$pV = NkT \qquad 12$$

Equating 11 and 12 and substituting for U the following is obtained

$$\frac{Nm}{2\zeta} = NkT$$

$$\zeta \simeq \frac{m}{2kT}$$

Hence the velocity distribution is

$$f(V_x) = \left(\frac{m}{2\pi kT}\right)^{\frac{1}{2}} \exp\left(\frac{-mV_x^2}{2kT}\right) \qquad 13$$

The integral in equation 1 may now be evaluated

$$Z = C.A.\ \Delta t \int_0^\infty V_x\, f(V_x)\, dV_x \qquad 1$$

Therefore

$$\int_0^\infty V_x f(V_x)\, dV_x = \left(\frac{m}{2\pi kT}\right)^{\frac{1}{2}} \int_0^\infty V_x \exp\left(\frac{-mV_x^2}{2kT}\right) dV_x$$

The integral on the right hand side is again a standard one, viz:

$$\int_0^\infty x.e^{-ax^2}\,dx = \tfrac{1}{2}a$$

whence

$$\int_0^\infty V_x\, f(V_x)\,dV_x = \left(\frac{kT}{2\pi m}\right)^{\frac{1}{2}}$$

Therefore the number of collisions per unit area per unit time is

$$Z = \left(\frac{kT}{2\pi m}\right)^{\frac{1}{2}} C. \qquad 14$$

If there are N molecules in a volume V then $C = N/V$ and 14 becomes

$$Z = \left(\frac{kT\ N^2}{2\pi m V^2}\right)^{\frac{1}{2}} \qquad 15$$

Furthermore $pV = NkT$, substituting into 15

$$Z = \left(\frac{k\ T\ p^2}{2\pi m\ k^2 T^2}\right)^{\frac{1}{2}} = \left(\frac{p^2}{2\pi m k T}\right)^{\frac{1}{2}}$$

i.e.

$$Z = \left(\frac{p}{(2\pi m k T)^{\frac{1}{2}}}\right) \text{ collisions/unit time/unit area} \qquad 16$$

Appendix XI

Calculation of the mean free path (λ).

The Mean Free Path λ (80)

If a molecule is travelling with a speed U and collides at a frequency Z, it spends a time Z^{-1} in free flight between collisions, and therefore travels a distance U/Z between collisions. Therefore the mean free path may be described as

$$\lambda = U/Z \qquad 1$$

Z, the number of intermolecular collisions may be accounted for as follows.

A collision is said to occur when two molecules come to within some distance d of each other (since we are assuming only one gas, d may be taken as the molecular diameter). If we now 'freeze' the positions of all atoms except the one of interest, in travelling at an average speed U in time Δt a 'collision tube' of area $\sigma = \pi d^2$ and volume $\sigma U \Delta t$ is swept out (σ is the collision cross section). The number of molecules with centres inside this volume is N/V where N represents the number of molecules in a volume V. Consequently the number of collisions per unit time is $\sigma U N/V$.

There is an error in calculation arising from the assumption that the molecules are 'frozen'. There are two limiting cases of collision. Firstly there is the head on collision of relative velocity 2U and then there is the grazing collision of relative velocity $\sqrt{2}U$. The latter is thought to be predominant, consequently

$$Z = \sqrt{2}\ \sigma\ U\ N/V \qquad 2$$

Substituting into 1

$$\lambda = \frac{V}{\sqrt{2}\ \sigma\ N} \qquad 3$$

From the relationships N = nL and pV = nRT 3 may be modified by substitution to

$$\lambda = \frac{k\,T}{\sqrt{2}\ \sigma\ p} \qquad 4$$

and from $\sigma = \pi d^2$ we finally have

$$\lambda = \frac{k\,T}{\sqrt{2}\pi d^2 p} \qquad 5$$

Therefore a knowledge of T, p and d will yield the value of λ.

Appendix XII

Extension of a spiral spring.

Extension of a Spiral Spring[81]

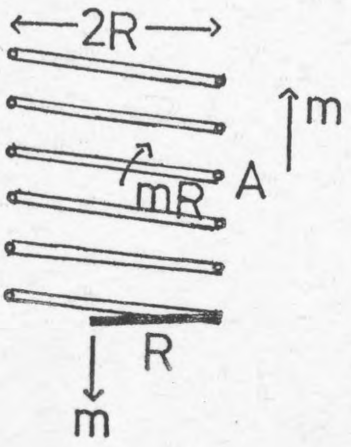

Imagine a spiral spring formed by winding a wire of radius r on a cylinder of radius R, the plane of the wire being practically perpendicular to the axis of the cylinder (i.e. a flat spiral spring).

Suppose a weight m is attached to the free end. Then considering the equilibrium of the part of the spring below a section A in the above diagram, there must be a shearing force equal to m acting vertically over the section and couple of moment mR. The effect of the latter is to produce a uniform twist, ϕ, per unit length of spring, and this is balanced by the torsional resistance (t.r.)

$$\text{t.r.} = \tfrac{1}{2} Z\pi r^4 \phi \qquad 1$$

where

Z - torsional modulus

For equilibrium,

$$mR = \frac{Z\pi r^4 \phi}{2} \qquad 2$$

Adopting the terms stress and strain, Hooke's Law may be stated as; the ratio of stress to strain is constant. This constant is called the elastic modulus. In the case

of a body under a linear stress, the ratio of stress to strain is known as Youngs modulus; while for a shear effect the constant is known as the modulus of rigidity Z. Consequently the shearing strain at A in the diagram is $^{m}/_{Z\pi r^2}$. If the length of the spring is ℓ, the total extension will be $^{m\ell}/_{Z\pi r^2}$. The extension due to twist is $\ell R\phi$ and from equation 2 assuming this extension to be x then

$$x = \frac{2mR^2\ell}{\pi Z r^4} \qquad 3$$

Furthermore,

$$\frac{\text{extension due to vertical shear}}{\text{extension due to torsion (twist)}} = \frac{r^2}{2R^2} \qquad 4$$

and, in general, this ratio is very small. In fact for the spring used in this study the ratio was found to be 8.9×10^{-5}.

REFERENCES

1. A.V. Krylova, Prob. Kinet. i Katal, 1970, 14, 180.

2. Y. Kubokawa and T. Ono, Bull. Chem. Soc. Jap., 1973, 51, 3435.

3. B. Wojciechowski, R.A. Pachovsky, B.A. Spencer, and B. Kindl, J.C.S. Faraday I, 1973, 69, 1162.

4. Dr. G. Jamieson, Private Communication.

5. F. London, Z. Physik, 1930, 63, 245.

6. J.G. Kirkwood, Phys. Zeits., 1932, 33, 57.

7. A. Muller, Proc. Roy. Soc., 1936, 154A, 624.

8. S.J. Gregg and K.S.W. Sing, "Adsorption, Surface Area and Porosity", Academic Press, 1967.

9. G. Wedler, "Chemisorption: An Experimental Approach", Butterworths, 1976.

10. S. Brunauer, L.S. Deming, W.S. Deming, and E. Teller, J. Amer. Chem. Soc., 1940, 62, 1723.

11. J.T. Kummer and P.H. Emmett, J. Phys. Chem., 1951, 55, 337.

12. H.S. Taylor, Disc. Faraday Soc., 1950, 8, 9.

13. R.M. Barrar, J. Chem Soc., 1934, 378.

14. R.M. Barrar and E.K. Rideal, Proc. Roy. Soc, 1935, 149A, 231.

15. I. Langmuir, J. Amer. Chem. Soc., 1912, 34, 1310.

16. H.S. Taylor, J. Amer. Chem. Soc., 1931, 53, 578.

17. M. Volmer, Z. Phys. Chem., 1925, 115, 253.

18. R.H. Fowler, Proc. Camb. Phil. Soc., 1935, 31, 260,

19. I. Langmuir, J. Amer. Chem. Soc., 1918, 40, 1361.

20. D.M. Young and D. Crowell, "Physical Adsorption of Gases", Butterworths, 1962.

21. A.M. Williams, Proc. Roy. Soc., 1919, A96, 287, 298.

22. D.C. Henry, Phil. Mag., 1922, 44(B), 689.

23. A. Boutaric, J. Chim. Phys., 1938, 35, 158.

24. W.L. Bragg and E.J. Williams, Proc. Roy. Soc. 1934, A145, 699.

25. G.S. Rushbrooke, Proc. Camb. Phil. Soc., 1940, 36, 248.

26. S. Brunauer, K.S. Love, and G.R. Keenan, J. Amer. Chem. Soc., 1942, 64, 751.

27. A. Frumkin and A. Slygin, Acta Physicochim.U.R.S.S., 1935, 3, 791.

28. E. Cremer and E. Flugge, Z. Phys. Chem., 1938, B41, 453.

29. S.Z. Roginskii, C.R. Acad. Sci. U.R.S.S., 1944, 45, 61.

30. ibid, 1944, 45, 194.

31. S.Z. Roginskii and O.M. Todes, Acta Physicochim. U.R.S.S., 1946, 21, 519.

32. G.D. Halsey and H.S. Taylor, J. Chem. Phys., 1947, 15, 624.

33. R. Sips, J. Chem. Phys., 1948, 16, 490.

34. ibid, 1950, 18, 1024.

35. G.D. Halsey, J. Chem. Phys., 1948, 16, 931.

36. D.S. Jovanovic, Kolloid-Z., 1969, 235, 1203.

37. D.S. Jovanovic, ibid, 1969, 235, 1214.

38. P. Budrugeac, Rev. Roum. Chim., 1980, 25, 487.

39. D.N. Misra, J. Coll. Interface Sci., 1980, 77, 543.

40. A.W. Adamson, I. Ling, L. Dormant and M. Orem, J. Coll. Interface Sci., 1966, 21, 445.

41. B. Kindl, and B.W. Wojciechowski, J.C.S. Faraday I, 1973, 69, 1926.

42. C.C. Hsu, W. Rudzinski and B.W. Wojciechowski, ibid, 1976, 72, 453.

43. S. Brunauer, P.H. Emmet and E. Teller, J. Amer. Chem. Soc., 1938, 60, 309.

44. H. Freundlich, "Colloid and Capillary Chemistry", Metheun, 1926.

45, E.K.Rideal, "Surface Chemistry", C.U.P. 1930.

46, G. Halsey and H.S. Taylor, J. Chem Phys., 1947, 15, 624.

47. G. Halsey, Adv. Catal., 1952 4, 259.

48. G.S. Rushbrooke, "Statistical Mechanics", Clarendon Press, 1951.

49. R.L. Burwell, Surv. Prog. Chem., 1977, 8, 1.

50. R.G. Pearson, "Hard and Soft Acids and Bases", Dowden, Hutchinson and Ross, 1973.

51. R. N. Pease, J. Amer. Chem. Soc., 1923, 45, 1196.

52. S. Dushman, "Scientific Foundations of Vacuum Technique", Wiley, 1949, pp. 65.

53. J.W. Mc.Bain and A.M. Bakr, J. Amer. Chem. Soc., 1926, 48, 690.

54. D.F. Othmer and F.G. Sawyer, Ind. Eng. Chem., 1944, 36, 894.

55. S. Josefowitz and D.F. Othmer, ibid, 1948, 40, 739.

56. A.V. Kiselev and G.G. Muttik, Kolloidzschr., 1957, 19, 562.

57. M. Dubinin and E.D. Zaverina, Acta Phys-chim., 1936, 4, 647.

58. L. Cahn and H.R. Schutz, "Vacuum Microbalance Techniques", Plenum Press, 1961, 1, 129.

59. T. Gast, Z. Agnew. Physik., 1956, 8, 167.

60. L.S. Burrage, J. Phys. Chem., 1930, 34, 2202.

61. E.C. Williams, J. Soc. Chem. Ind., 1924, 43, 97T.

62. H.L. Gruber, Analyt. Chem., 1962, 34, 1828.

63. A.L. Reimann, "Vacuum Technique", Chapman and Hall, 1952.

64. R.M. Dell and V.J. Wheeler, A.E.R.E. Report No. 3424, 1960.

65. F.M. Ersberger, Rev. Sci. Instrum., 1953, 24, 998.

66. S.H. Wilson, Ph.D. Thesis, 1977, The City University.

67. C. Orr and J.M. Dalla-Valle, "Fine Particle Measurement", Macmillan, 1959, pp. 175.

68. R.C. Reid, J.M. Pravsnitz, and T.K. Sherwood, "The Properties of Gases and Liquids", McGraw-Hill, 1977.

69. E.L. Bauer, "A Statistical Manual for Chemistry", Academic Press, 1971.

70. F. Trifiro, C. Lambri and I. Pasquan, Chim. Ind., 1971, 53, 339.

71. B. Viswanathan, Proc. Indian Acad. Sci., 1978, 87A, 405.

72. E. Rostevanov, Russ. J. Phys. Chem., 1978, 52, 1652.

73. G.W. Keulks, Adv. Catal., 1978, 27, 183.

74. D.O. Hayward and B.M.W. Trapnell, "Chemisorption", Butterworths, 1964, pp. 201.

75. R.F. Fowler and E.A. Guggenheim, "Statistical Thermodynamics", C.U.P., 1948.

76. Landholt-Bornstein, "Numerical Data and Functional Relationships in Science and Technology", Springer-Verlag (Berlin), 1974.

77. T.L. Hill, J. Chem. Phys., 1949, 17, 520.

78. T.L. Hill, Adv. Catal., 1952, 4, 211.

79. D.H. Everett, Trans. Faraday Soc., 1950, 46, 453.

80. P.W. Atkins, "Physical Chemistry", O.U.P., 1978.

81. F.H. Newman and V.H.L. Searle, "The General Properties of Matter", Edward Arnold Ltd., 1957.

82. B.P. Ltd., Research Laboratories. Private Communication.

83. Cabot Carbon Ltd., Manufacturers' Specification.

84. A.A. Dayvdov et al., J. Catal., 1978, 55, 219.

85. J. Cartlidge and L.M. McGrath, Trans. Instn. Chem. Eng., 1974, 52, 222.

86. M. Jaroniec, A. Patrykiejew, M. Borowko, Z. Phys. Chemie, 1979, 260, 221.

87. Rostevanov et al., Zh. Fiz. Khim., 1978, 52, 1652.

88. H. Melville and B.G. Gowenlock, "Experimental Methods in Gas Reactions", 1964, Macmillan.